

T-2408

RESOLUTION OF GEOPHYSICAL SURVEYS  
FOR SHALLOW WORK

by  
Martin Plikk

ProQuest Number: 10782222

All rights reserved

INFORMATION TO ALL USERS

The quality of this reproduction is dependent upon the quality of the copy submitted.

In the unlikely event that the author did not send a complete manuscript and there are missing pages, these will be noted. Also, if material had to be removed, a note will indicate the deletion.



ProQuest 10782222

Published by ProQuest LLC (2018). Copyright of the Dissertation is held by the Author.

All rights reserved.

This work is protected against unauthorized copying under Title 17, United States Code  
Microform Edition © ProQuest LLC.

ProQuest LLC.  
789 East Eisenhower Parkway  
P.O. Box 1346  
Ann Arbor, MI 48106 – 1346

T-2408

A thesis submitted to the Faculty and the Board of Trustees of the Colorado School of Mines in partial fulfillment of the requirements for the degree of Master of Science (Geophysical Engineering).

Golden, Colorado

Date Jan 20, 1981

Signed: Martin Plikk  
Martin Plikk

Approved: Terence K. Young  
Terence K. Young  
Thesis Advisor

Golden, Colorado

Date Jan 20, 1981

George V. Keller  
George V. Keller  
Head of Department  
of Geophysics.

## ABSTRACT

The limits of resolution of various methods of geophysical prospecting, as applied to engineering problems, are investigated using computer modeling. Electrical, seismic, gravity, magnetics and crosshole techniques are examined in the context of void and fracture-zone detection.

The results show that resolution is generally better for wave-field methods than for potential methods. Near-surface screens may negate the general trend in resolving capability. A trade-off always exists between depth of penetration and resolution. Borehole and cross-borehole methods offer best resolution but at considerably greater expense. The study illustrates the enhancement of interpretive insight which can result from the analysis of several different geophysical data sets for a single problem.

## ACKNOWLEDGEMENTS

I would like to express my sincere thanks to my thesis advisor Dr. T.K. Young who has provided assistance and helpful suggestions throughout this work, and to Dr. C.H. Stoyer and Dr. P.R. Romig who also guided me through graduate studies as my committee members.

I am also grateful to Rotary Foundation, which initially sponsored my studies at Colorado School of Mines, and to Integrated Geophysics Project (IGP) and U.S. Army Mobility Equipment Research and Development Command, which sponsored the thesis work.

My thanks also goes to my wife Rigmor, who has given me moral support and encouragement when I needed it.

Last, but not least, I would like to thank my fellow geophysics graduate students who offered constructive criticism and encouragement throughout the work.

## TABLE OF CONTENTS

Abstract .....	iii
Acknowledgements .....	iv
Table of contents .....	v
List of figures and tables .....	vii
	.
1. Introduction .....	1
2. Problems addressed .....	6
3. Methods of investigation .....	12
3.1 Potential methods .....	14
3.1.1.1 Gravity modeling .....	14
3.1.1.2 Gravity modeling program used .....	17
3.1.1.3 Results of gravity modeling .....	19
3.1.2.1 Magnetic modeling .....	33
3.1.2.2 Magnetic modeling program used .....	35
3.1.2.3 Results of magnetic modeling .....	36
3.1.3.1 Direct-current electrical modeling .....	51
3.1.3.2 Direct-current electrical modeling program used .....	54
3.1.3.3 Results of direct-current electrical modeling .....	56

3.2	Wave field methods .....	68
3.2.1.1	Electromagnetic modeling .....	68
3.2.1.2	Electromagnetic modeling program used .....	71
3.2.1.3	Results of electromagnetic modeling .....	71
3.2.2.1	Magnetotelluric modeling .....	84
3.2.2.2	Magnetotelluric modeling program used .....	85
3.2.2.3	Results of magnetotelluric modeling .....	86
3.2.3.1	Reflection seismic modeling .....	91
3.2.3.2	Reflection seismic modeling program used ...	98
3.2.3.3	Results of reflection seismic modeling .....	99
4.	Conclusions .....	115
5.	References .....	121

## LIST OF FIGURES AND TABLES

Table 1.	Methods and models investigated .....	3
Fig 1.	Tunnel model .....	8
Fig 2.	Vertical fracture zone model .....	9
Fig 3.	Horizontal fracture zone model .....	10
Fig 4.	Basement fault model .....	11
Fig 5.	Gravity survey model .....	18
Fig 6.	Gravity over tunnel. Density contrast -2.65 g/cc.....	20
Fig 7.	Gravity over tunnel. Density contrast -2.00 g/cc.....	21
Fig 8.	Gravity over 2-by-2 meter tunnel (shallow)...	22
Fig 9.	Gravity over 2-by-2 meter tunnel (deeper)....	23
Fig 10.	Gravity over vertical fracture zone. Height and length 100 meters.....	24
Fig 11.	Gravity over vertical fracture zone. Height and length 1,000 meters.....	25
Fig 12.	Gravity over vertical fracture zone. Height and length 10 meters.....	26
Fig 13.	Gravity over horizontal fracture zone. Length and width 10 meters.....	28
Fig 14.	Gravity over horizontal fracture zone. Length and width 500 meters.....	29

Fig 15.	Gravity over horizontal fracture zone. Length and width 100 meters.....	30
Fig 16.	Gravity over basement fault. Density contrast $-.5 \text{ g/cc}$ .....	31
Fig 17.	Gravity over basement fault. Density contrast $-.1 \text{ g/cc}$ .....	32
Fig 18.	Magnetic survey model.....	37
Fig 19.	Magnetics over 2-by-2 meter tunnel (shallow).....	40
Fig 20.	Magnetics over 2-by-2 meter tunnel (deeper).....	41
Fig 21.	Magnetics over tunnel.....	42
Fig 22.	Magnetics over vertical fracture zone. Height and length 10 meters.....	43
Fig 23.	Magnetics over vertical fracture zone. Height and length 100 meters.....	44
Fig 24.	Magnetics over vertical fracture zone. Height and length 1,000 meters.....	45
Fig 25.	Magnetics over horizontal fracture zone. Length and width 10 meters.....	46
Fig 26.	Magnetics over horizontal fracture zone. Length and width 100 meters.....	47
Fig 27.	Magnetics over horizontal fracture zone. Length and width 500 meters.....	48

Fig 28.	Magnetics over basement fault.	
	Susceptibility contrast .001 emu.....	49
Fig 29.	Magnetics over basement fault.	
	Susceptibility contrast .005 emu.....	50
Fig 30.	Direct-current electrical survey model.....	55
Fig 31.	Polar-dipole response over tunnel (shallow)..	58
Fig 32.	Polar-dipole response over tunnel (deeper)...	59
Fig 33.	Equatorial-dipole response over tunnel (shallow).....	60
Fig 34.	Equatorial-dipole response over tunnel (deeper).....	61
Fig 35.	Polar-dipole response over vertical fracture zone. Low resistivity contrast.....	62
Fig 36.	Polar-dipole response over vertical fracture zone. High resistivity contrast.....	63
Fig 37.	Equatorial-dipole response over vertical fracture zone. Low resistivity contrast.....	64
Fig 38.	Equatorial-dipole response over vertical fracture zone. High resistivity contrast.....	65
Fig 39.	Polar-dipole response over basement fault....	66
Fig 40.	Polar-dipole response over horizontal fracture zone.....	67
Fig 41.	Electromagnetic survey model.....	72

Fig 42. EM over vertical fracture zone (VMD-source).  
 Low resistivity contrast..... 75

Fig 43. EM over vertical fracture zone (VMD-source).  
 High resistivity contrast..... 76

Fig 44. EM over vertical fracture zone (HMD-source).  
 High resistivity contrast..... 77

Fig 45. EM over vertical fracture zone (HMD-source).  
 Low resistivity contrast..... 78

Fig 46. EM over horizontal fracture zone  
 (HMD-source)..... 79

Fig 47. EM over basement fault (HMD-source)..... 80

Fig 48. Borehole-to-borehole EM survey model..... 81

Fig 49. Borehole-to-borehole EM over tunnel.  
 Complex amplitude..... 82

Fig 50. Borehole-to-borehole EM over tunnel.  
 Real component..... 83

Fig 51. Magnetotelluric survey model..... 87

Fig 52. Magnetotelluric response over vertical  
 fracture zone. High resistivity contrast..... 88

Fig 53. Magnetotelluric response over vertical  
 fracture zone. Low resistivity contrast..... 89

Fig 54. Magnetotelluric response over tunnel..... 90

Fig 55. Exploration scale model..... 92

Fig 56. Engineering scale model..... 93

Fig 57.	Lateral resolution for spherical waves.....	95
Fig 58.	Tunnel versus thin-bed reflection amplitude.	97
Fig 59.	Seismic tunnel model.....	100
Fig 60.	Wave-theory synthetic seismic spike section. 5-by-5 meter tunnel.....	101
Fig 61.	Wave-theory synthetic seismic spike section. 10-by-10 meter tunnel.....	102
Fig 62.	Wave-theory synthetic seismic spike section. 20-by-20 meter tunnel.....	103
Fig 63.	Ray-theory synthetic seismic spike section. 5-by-5 meter tunnel.....	105
Fig 64.	Ray-theory synthetic seismic spike section. 10-by-10 meter tunnel.....	106
Fig 65.	Ray-theory synthetic seismic spike section. 20-by-20 meter tunnel.....	107
Fig 66.	Synthetic seismic section with -36 dB noise. 20-by-20 meter tunnel.....	108
Fig 67.	Synthetic seismic section with -36 dB noise. 10-by-10 meter tunnel.....	109
Fig 68.	Synthetic seismic section with -36 dB noise. 5-by-5 meter tunnel.....	110
Fig 69.	Synthetic seismic section with -24 dB noise. 5-by-5 meter tunnel.....	111

## INTRODUCTION

This thesis is concerned with computer simulation of geophysical methods as applied to engineering problems. Computer simulation can be a very valuable tool in the effort to determine the resolution capabilities of different techniques. Advantages of numerical modeling as compared to field experiments are: 1) less expensive, 2) physical parameters easily modified, and 3) noise-free environment. The ability to demonstrate ideal results for specific field parameters such as station spacing, signal frequency, etc., over targets of interest can also be of great importance in the design of field surveys. This design does involve both methods to use and how to use those methods.

The work is based on the application of existing software in the Geophysics Department of Colorado School of Mines; no software development work was done. Some minor modifications of programs were made in conjunction with transferring them from the DEC-10 system to the CDC Cyber-720 system. Software used included 2.5-dimensional modeling programs for gravity and magnetics. Two-dimensional models were used in modeling electromagnetics, direct-current electrical method, magnetotellurics and in

seismic software from the exploration industry (AIMS and CGG packages).

The important concept of integrating different methods for optimizing the problem-solving effort and the question of what method or combination of methods to use for specific models were investigated in this work. A few models were selected as representing problems of engineering interest: horizontal and vertical fracture zones, tunnel or void detection, and a basement fault with vertical displacement. By varying such parameters as depth to target, size of target and rock properties like velocity, density, electrical resistivity and magnetic susceptibility, an extensive suite of models were investigated (table 1).

A number of important rock properties are affected by the presence of fractures in a rock-mass. Among these properties are permeability, porosity, deformability and rock-mass strength. In turn, a knowledge of these particular rock parameters is essential to the success of geotechnical activities as diverse as nuclear waste isolation, earthquake prediction, geothermal energy production, rock storage and tunneling.

The detection of tunnels or void spaces is also an important engineering problem in many areas of the world. Old mine workings and forgotten escape tunnels left over

<u>METHOD</u>	<u>MODEL</u>			
	TUNNEL	VERTICAL FRACTURE ZONE	HORIZONTAL FRACTURE ZONE	BASEMENT FAULT
GRAVITY	☆	☆	☆	☆
MAGNETICS	☆	☆	☆	☆
DC ELECTRICAL	☆	☆	☆	☆
ELECTROMAGNETICS		☆	☆	☆
MAGNETOTELLURIC	☆	☆		
SEISMIC	☆			

Table 1. Geophysical methods and geological models used in investigation.

from wars are not unusual in European countries. These constitute a hazard in activities such as construction of large buildings and new mining operations. Appearance of an unexpected tunnel could lead to mine flooding with disastrous consequences. In karst-geology areas the presence of subsurface voids is a problem involving the same dangers.

Many engineering efforts involve soil removal of some sort where the depth to bedrock and the bedrock properties are of great importance. Basement faulting also influences tunneling and excavation at depth where an incompetent rock section could increase cost and risk of operations.

Because of their small target size and therefore difficult detection, as well as their relatively minor economic value, tunnel and void detection are not well covered in earlier works. Several papers (Cook, 1965, Widess, 1973, Stoyer, 1974, Gay, 1963, Ogunade, 1980) show geophysical responses to features which are relatively large in at least two dimensions, but very few discuss the limit of resolution for smaller targets for the techniques employed. The purpose of this thesis is therefore to help fill this gap and summarize the different geophysical methods' applicability to various engineering problems.

Technological advances have produced equipment with a level of accuracy which was previously lacking. A favorable signal-to-noise ratio is still critically important, however, and data summation or stacking procedures provide an effective means of raising the signal-to-noise ratio to a level where meaningful information can be extracted (Lytle, 1979; Spiegel et.al., 1980).

Electrical methods have primarily been used to detect conductors at depth and very few examples of insulator detection can be found in the literature. Electromagnetics have been used extensively to map fracture zones in the past. Lower frequencies approaching direct-current have a somewhat better response for insulators but are lacking in resolution capability (Keller, 1979; Stoyer, in press).

Recent work done at the Lawrence Livermore Laboratories (Lytle, 1979) has shown that high frequency EM can be used for borehole-to-borehole tunnel delineation. The limiting factor is the depth of penetration, since attenuation increases with frequency.

The seismic reflection method has been shown to be able to generate an interpretable response from tunnels at 50 meters depth (Owen et.al., 1976), and a tunnel or void can also be mapped with gravity or magnetics if the target is large compared to the depth of burial (LaFehr, 1979).

## PROBLEMS ADDRESSED

The work has primarily concerned igneous or metamorphic hard-rock environments with densities around 2.65 g/cc, velocities of 5000 m/s, and resistivities in the range of 1,000 to 5,000 ohm-m. This limitation to only one environment was necessary, because several geophysical methods were employed on a number of models, and the volume of data had to be kept at a manageable size.

Tunnel detection is one of the engineering problems investigated in this work. The detection and delineation of tunnels and voids at depth is crucial in many situations, both for military purposes and in civil applications.

In the tunnel-model physical properties for the host rock were chosen to represent a dense, high-velocity and high-resistivity medium. A magnetic susceptibility was included to simulate a homogeneous, slightly-magnetized rock. The modeled medium could represent a granitic rock or a dolomite. A karst geology with air-filled voids could therefore be modeled.

Several geometric parameters were varied to give an estimate of resolution capabilities of different methods for the tunnel detection case. These parameters included depth

to the tunnel and the diameter of the tunnel. Figure 1 shows the basic tunnel model used throughout the work.

Fracture zones are of engineering interest for several reasons; for example, they cause problems in tunneling operations and nuclear waste isolation. On the other hand, these porous and permeable zones are considered as positive features when searching for groundwater and geothermal areas. Vertical or semi-vertical fracture zones outcropping on the surface are more easily discovered and mapped than horizontal features. Although not as obvious at the surface, horizontal zones at depth are very important for example in site selection for nuclear waste disposal. The history of these zones is often linked to the deglaciation period with its sudden reduction in load pressure (Scherman, 1978) .

The fracture-zone models have similar physical rock parameters as the tunnel model with a high-density, high-velocity and high-resistivity host rock. The fracture zone is modeled with a resistivity one to two orders of magnitude lower than that of the host rock. An anomalously low susceptibility, low velocity and low density determine the fracture zone as being porous and hydrothermally altered (low content of magnetite). The depth to the top of the zone and geometry of the zone were varied to determine resolving

# Tunnel Model

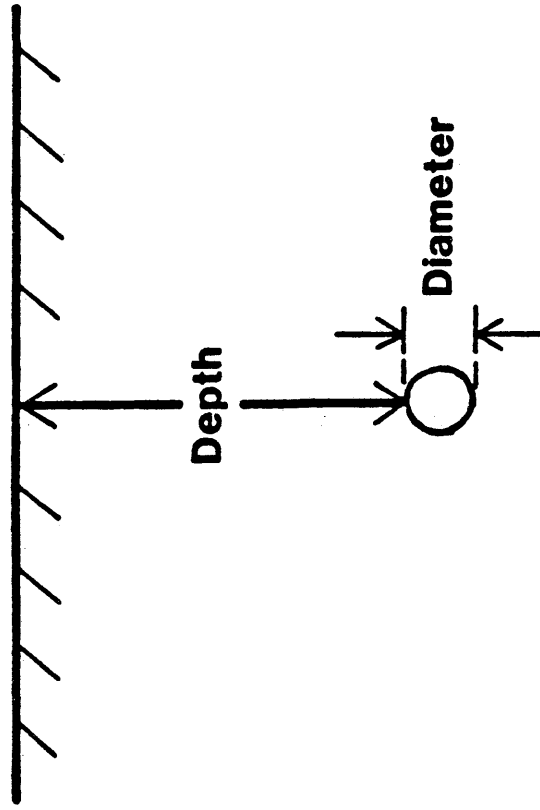


Figure 1. Tunnel model defined in 2-D and with varied depth to top of body.

# Vertical Fracture Zone Model

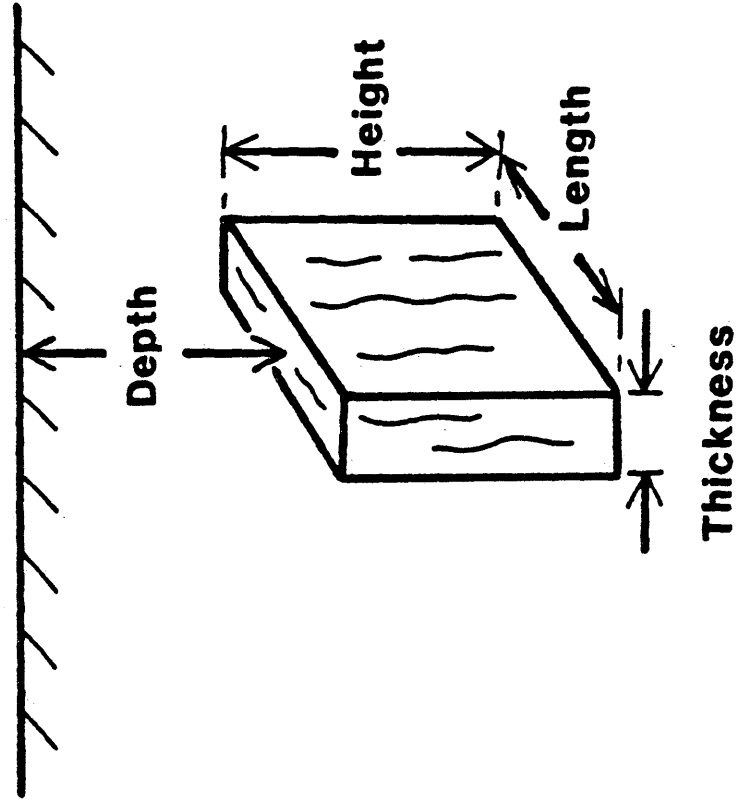


Figure 2. Vertical fracture zone model defined in 3-D and with varied depth to top of zone.

# Horizontal Fracture Zone Model

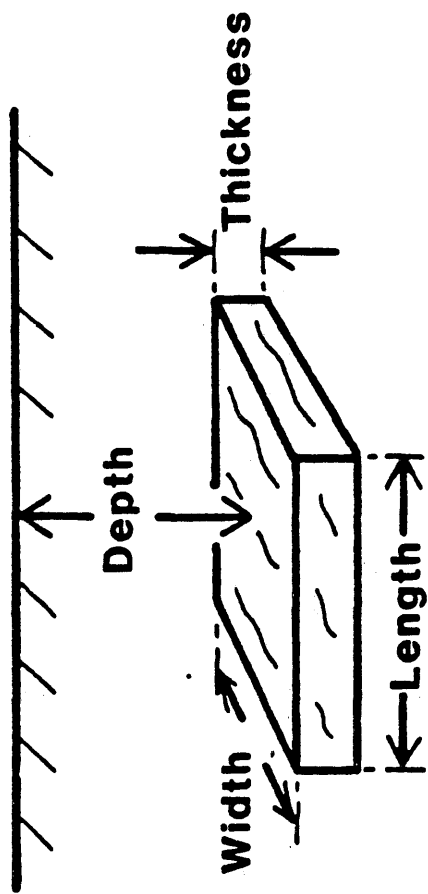


Figure 3. Horizontal fracture zone model defined in 3-D and with varied depth to top of zone.



ability of selected geophysical methods for this target. Figures 2 and 3 show the fracture-zone models used.

In several situations the engineer is interested in depth to bedrock and the condition thereof. A vertical fault with pronounced throw was modeled (Fig. 4) to simulate a condition encountered not only in the case mentioned above, but also of interest in, for example, tunneling operations.

By defining a geophysical model in terms of physical contrasts (eg., gravity contrast, susceptibility contrast) rather than by using specific numbers for physical parameters, the results obtained are usually meaningful in relation to several geologic situations.

## METHODS OF INVESTIGATION

Computer simulation was preferred over analog modeling, since the time required for development of an array of analog models would probably prevent this from being a Master's thesis. Furthermore, the installation of a new

Cyber-720 computer system with several commercial software packages favored the computer modeling approach.

The following geophysical methods were modeled: gravity, magnetics, direct-current electrical method, reflection seismic, electromagnetics and magnetotellurics. These methods can be classified according to a variety of schemes where the distinction between sensing methods mapping, for example, fracture zones in the interior of a rock mass and methods characterizing the fracture pattern at the surface or borehole wall, is one. Another would be the distinction between the passive methods and the active methods. Passive in this context indicates that the source of the anomalous field is not man-made or of controlled origin. Examples of passive methods would be magnetics, gravity and some electromagnetic methods such as the magnetotelluric method. Active methods, on the other hand, include reflection and refraction seismic, electromagnetic methods, radar and sonar. These methods all have controlled sources. I have chosen to divide them using the distinction between wave-propagation techniques and potential-field methods. This classification is often used in dealing with resolution studies to emphasize that wave-propagation techniques are superior in resolution to potential-field methods. The reason is that potential methods measure gross

material properties (density, magnetic intensity, etc.), whereas wave propagation methods can be used for the determination of the geometry of bodies at a distance.

The particular geophysical methods investigated were selected for modeling because they are frequently the techniques employed in the field and because state-of-the-art modeling software was available for these methods.

## POTENTIAL FIELD METHODS

### GRAVITY MODELING

Gravity prospecting involves the measurement of variations in the gravitational field of the earth. Gravity is used extensively in the petroleum exploration industry for mapping large-scale structures such as anticlines, synclines and faults. The use of gravity in engineering geophysics is limited to tunnel and cavity detection and, to some degree, determination of depth to basement. The anomalies are generally smaller in engineering applications than in petroleum exploration, but with microgal surveys the

difference is reduced to a simple matter of scale (LaFehr, 1979).

The gravity field observed at any point represents the summation of the gravitational attraction of all subsurface sources detectable by the instrument employed. Yet the object in interpreting such a field is to obtain information on the individual sources contributing to it. Except in very simple cases, the separation of the observed field into its component parts is quite difficult and sometimes not possible at all. The lack of uniqueness of the gravity field from a subsurface source means that an infinite number of different configurations can result in identical gravity data at the surface. To resolve such ambiguity, other information than that from gravity is needed (Dobrin, 1976; Telford et al, 1976; LaFehr, 1979).

The maximum density variation between different rocks and between rocks and minerals is less than one order of magnitude. This is very small compared to the range of magnetic susceptibility (five orders of magnitude), electrical conductivity (ten orders) and even elastic properties (one order) (Dobrin, 1976).

The ability to resolve anomalies and interpret them in terms of mass distribution depends on 1) the instrument, 2) the field survey procedures, 3) the size and density

contrast of the target, and 4) the environment where the target is located. State-of-the-art techniques must be applied at all stages of the field survey and data reduction to assure microgal accuracy (LaFehr, 1979).

Station gravity is generally repeatable to better than .1 mgal and often down to .05 mgal. New instruments are available with electronic reading systems where sensitivity is as good as two microgal (LaFehr, 1980). Arzi (1975) has shown that an accuracy of better than 20 microgal can be achieved for high precision field surveys. This is a precision of almost one part in  $10^8$  as compared to the earth's gravity field.

The borehole gravimeter should probably be mentioned, although this is a very expensive tool that very few engineering companies now have a chance to utilize in their surveys. Only a few borehole gravimeters are commercially available in the world. The accuracy is somewhat lower (5 to 10 microgal) than for the surface instruments, but the ability to get closer to the anomalous body more than compensates for the lower precision.

## GRAVITY MODELING PROGRAM USED

A program written by John W. Cady of the U.S.G.S. in Denver, was used for the calculation of gravity and magnetic anomalies along profiles. The program also includes inverse solutions for density and magnetization. In Cady's documentation an equation for the vertical gravity field due to a body with polygonal cross-section and finite strike is derived. The equation consists of the two-dimensional equation of Talwani, Worzel, and Landisman (1959), with the addition of end corrections. If the geometry of the body or bodies is specified, the 2.5 dimensional (finite third dimension) equations can be combined with observations of the gravity (and magnetic) anomaly fields to make linear, least-squares solutions for density (and susceptibility or remanent magnetization).

Only the forward mode of the computer program was used for the modeling of gravity and magnetic anomalies in this project. The program is capable of handling 50 field points, 10 bodies with 15 corners per body, topography, densities and susceptibilities. For the magnetic case it will also handle inclination, declination and strength of the magnetic field. Figure 5 shows the gravity model utilized.

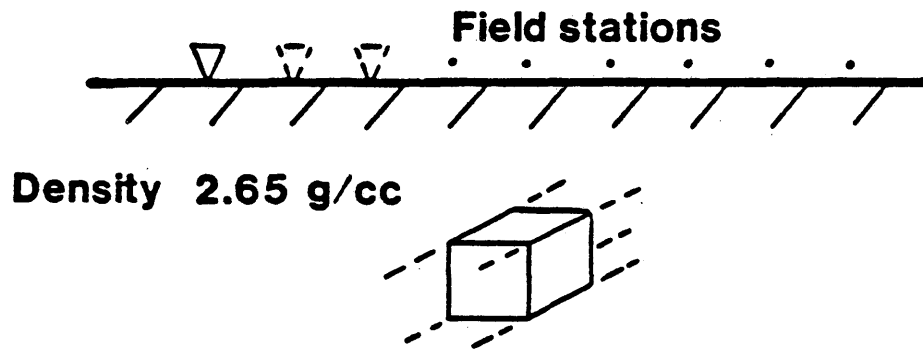


Figure 5. Gravity survey model in 2.5-D. Host rock density 2.65 g/cc.

## RESULTS OF GRAVITY MODELING

A look at the results indicates the small anomalies encountered from the targets examined.

Results for the tunnel model with a density contrast of 2.65 g/cc (Fig. 6) show the maximum detectable depth of a 2 meter diameter tunnel as being approximately 25 meters. This is at the absolute ideal accuracy of the survey (instrument limit). A more realistic accuracy of 20 microgal would require a tunnel with a diameter of 5 meters at the same depth to cause the same anomaly. With a density contrast of 2.0 g/cc (Fig. 7) the anomalies are reduced by some 30 percent, making a tunnel in "soft rock" even harder to detect. Figures 8 and 9 show the actual synthetic anomalies for the tunnel modeled at various depths below the surface.

Modeling results for a fracture zone with a limited height and length (100-by-100 meters), a density contrast to the host rock of .5 g/cc (Fig. 10), and a thickness of 5 meters show a maximum resolvable depth of between 50 and 150 meters depending on limits used. If this zone is extended to semi-infinite length and height (1000-by-1000 meters), this maximum detectable depth increases to range between 500 and 1500 meters (Fig. 11). For a very local fracture zone with dimensions of only 10-by-10 meters (Fig. 12), the

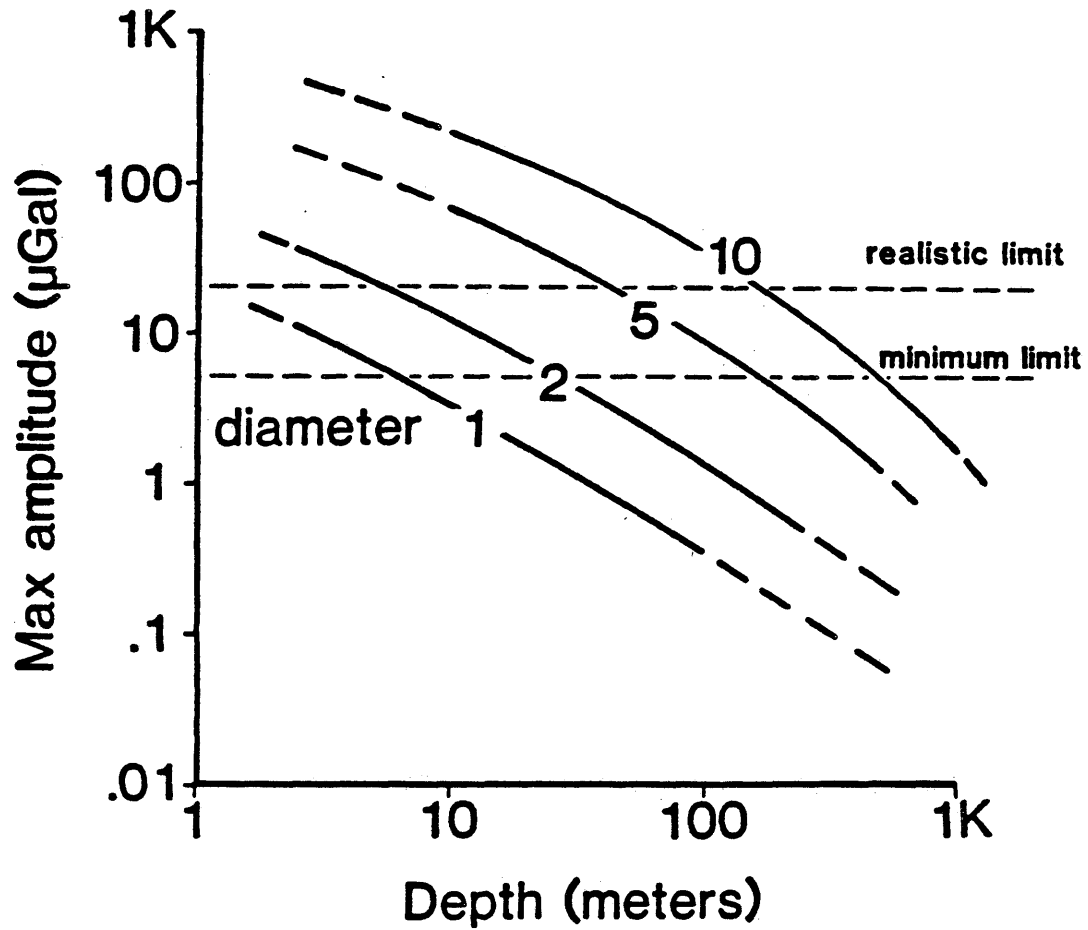


Figure 6. Maximum absolute gravity response over tunnels of various diameters and at various depths. Density contrast -2.65 g/cc.

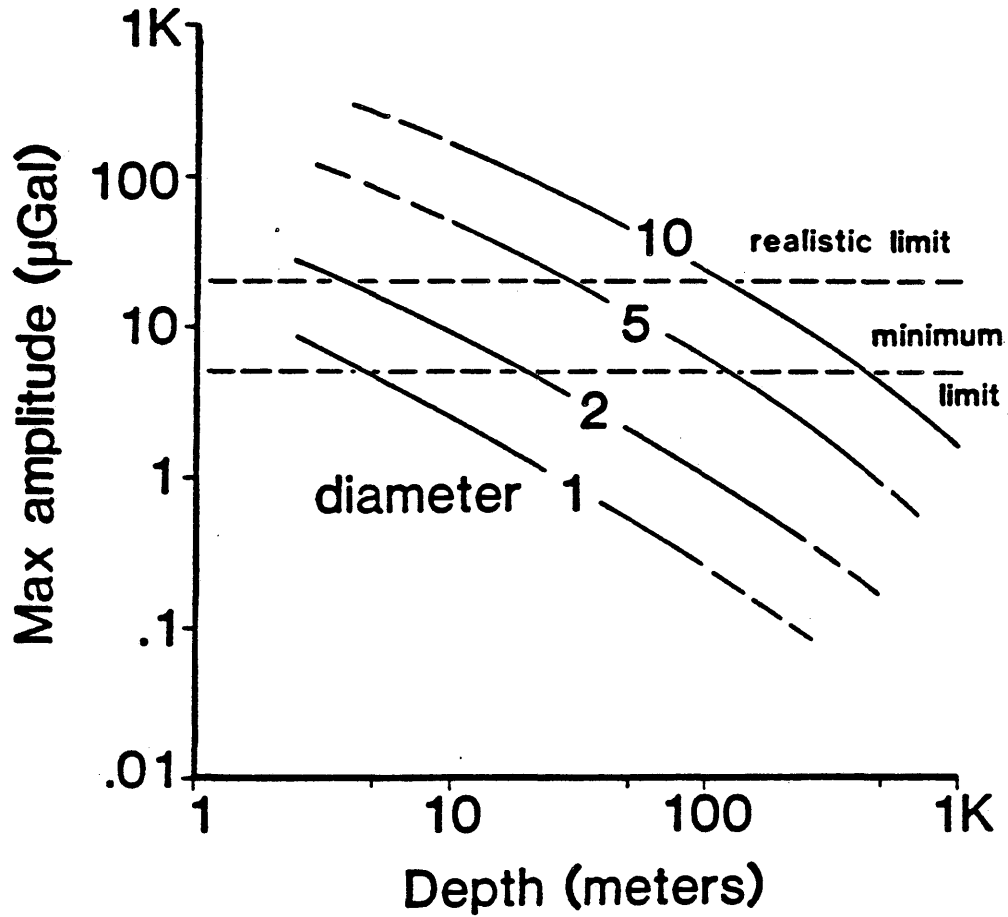


Figure 7. Maximum absolute gravity response over tunnels of various diameters and at various depths. Density contrast -2.00 g/cc.

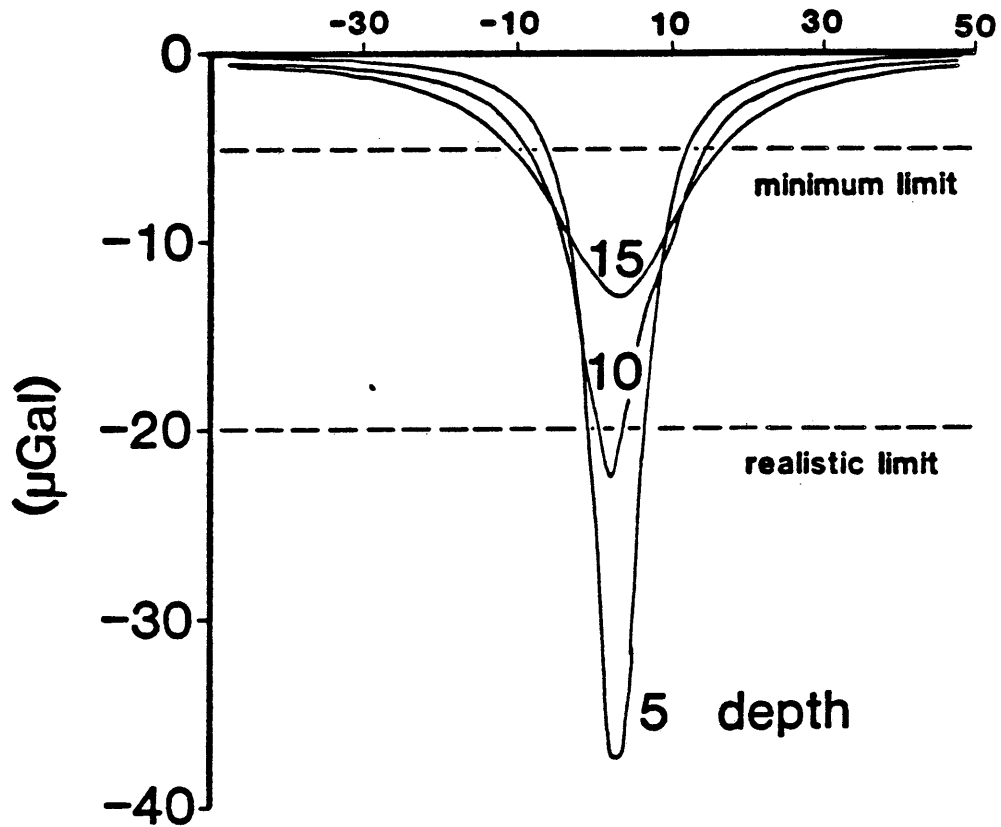


Figure 8. Gravity response curves over 2 by 2 meter tunnel at various depths. Density contrast  $-2.65 \text{ g/cc}$ . Abscissa shows lateral position (in meters) compared to midpoint of body.

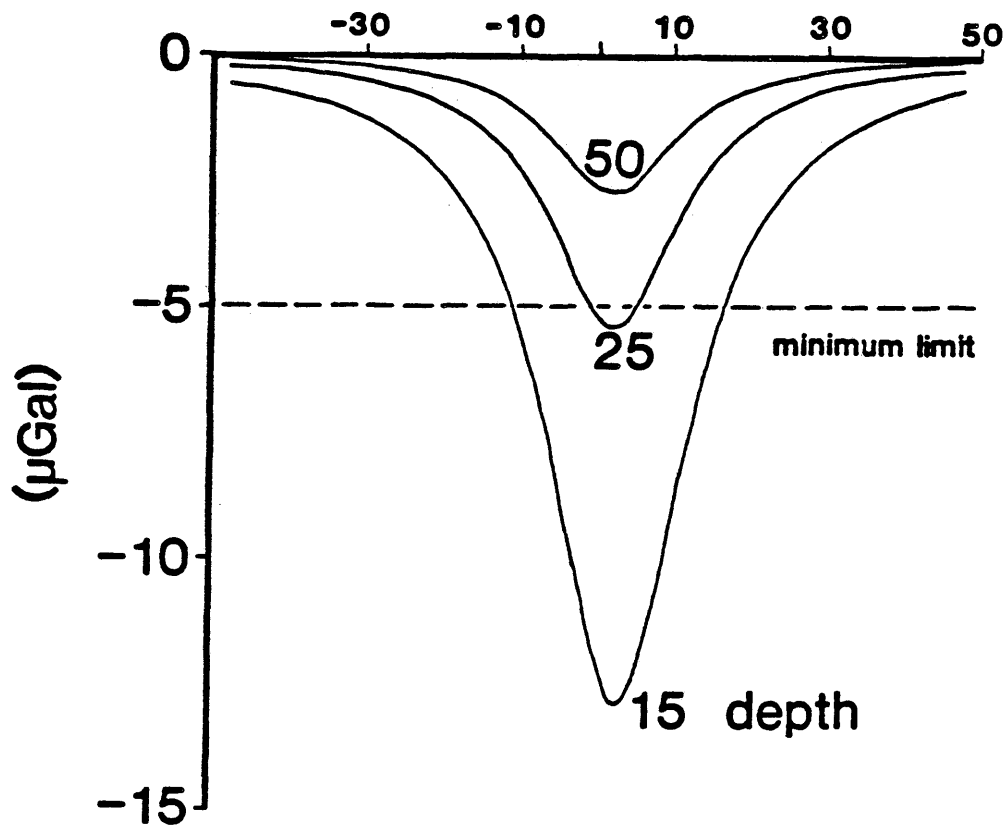


Figure 9. Gravity response curves over 2 by 2 meter tunnel at various depths. Density contrast  $-2.65 \text{ g/cc}$ . Abscissa shows lateral position (in meters) compared to midpoint of body.

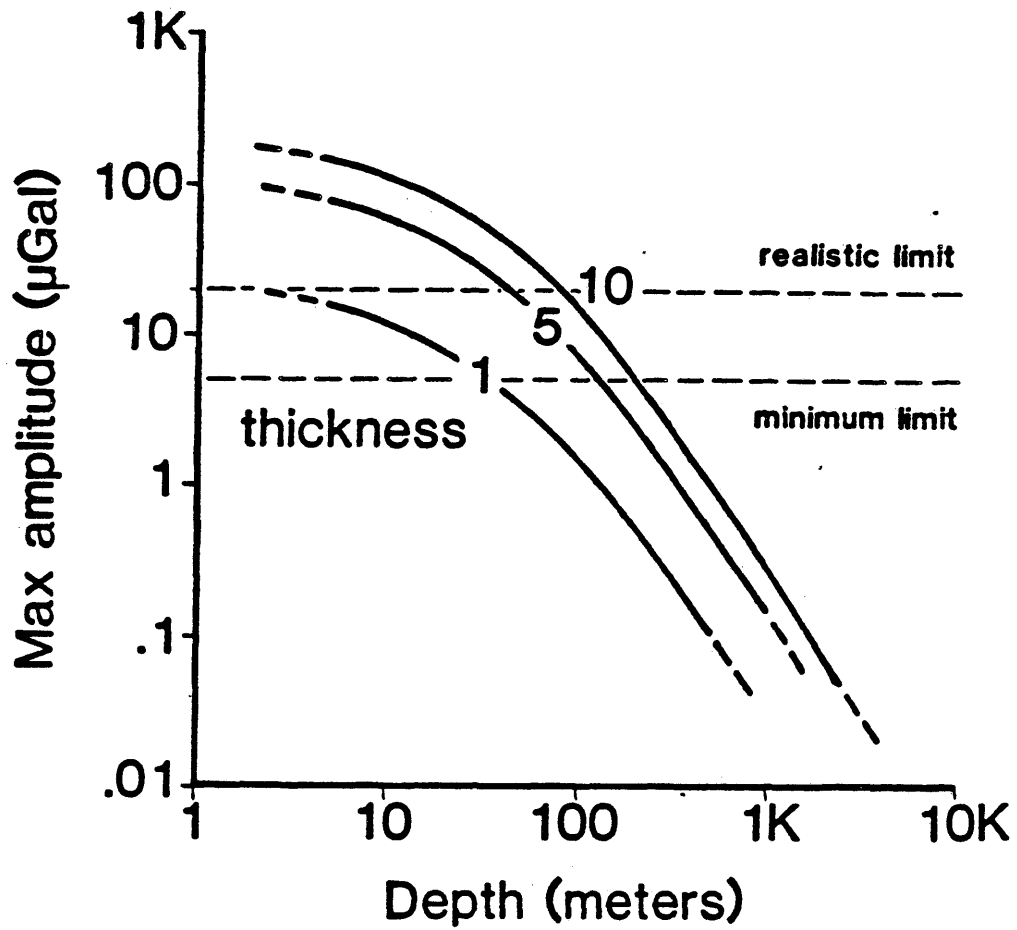


Figure 10. Maximum absolute gravity response over vertical fracture zones of various thicknesses and at various depths. Density contrast  $-0.5 \text{ g/cc}$ . Height and length of zones 100 meters.

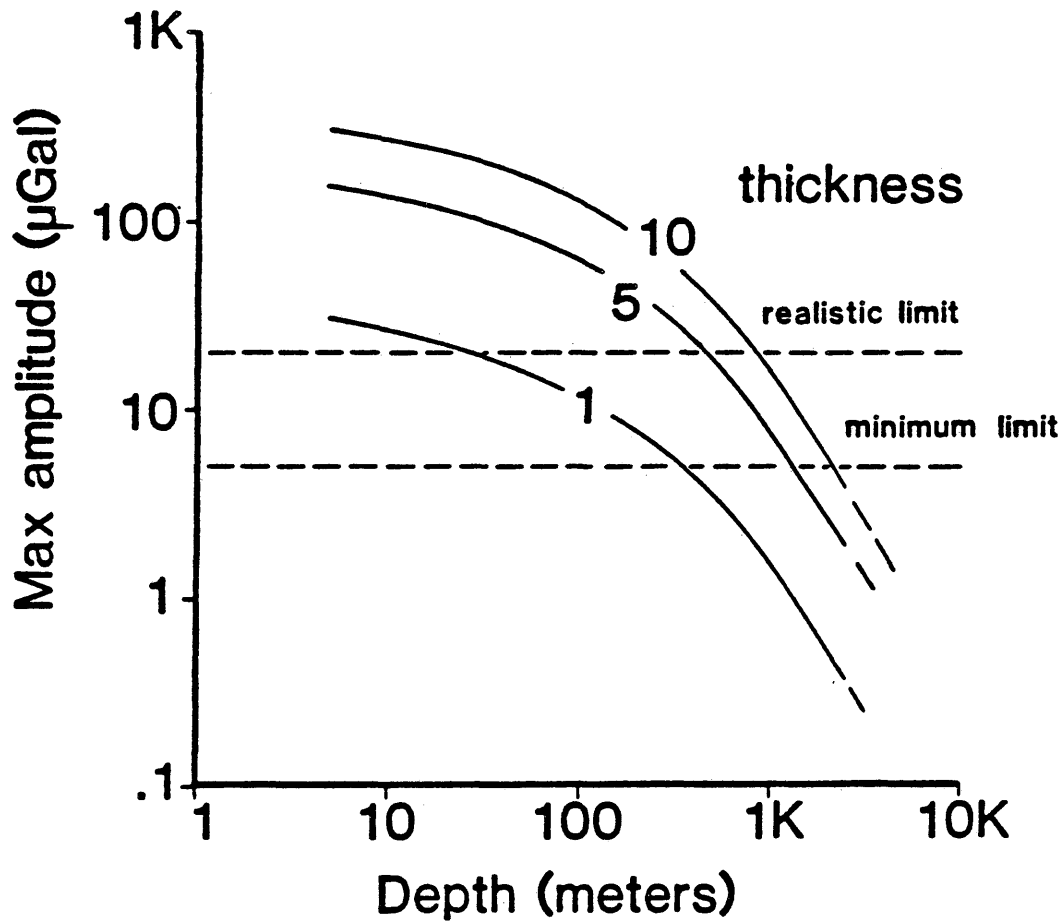


Figure 11. Maximum absolute gravity response over vertical fracture zones of various thicknesses and at various depths. Density contrast  $-.5 \text{ g/cc}$ . Height and length of zones 1,000 meters.

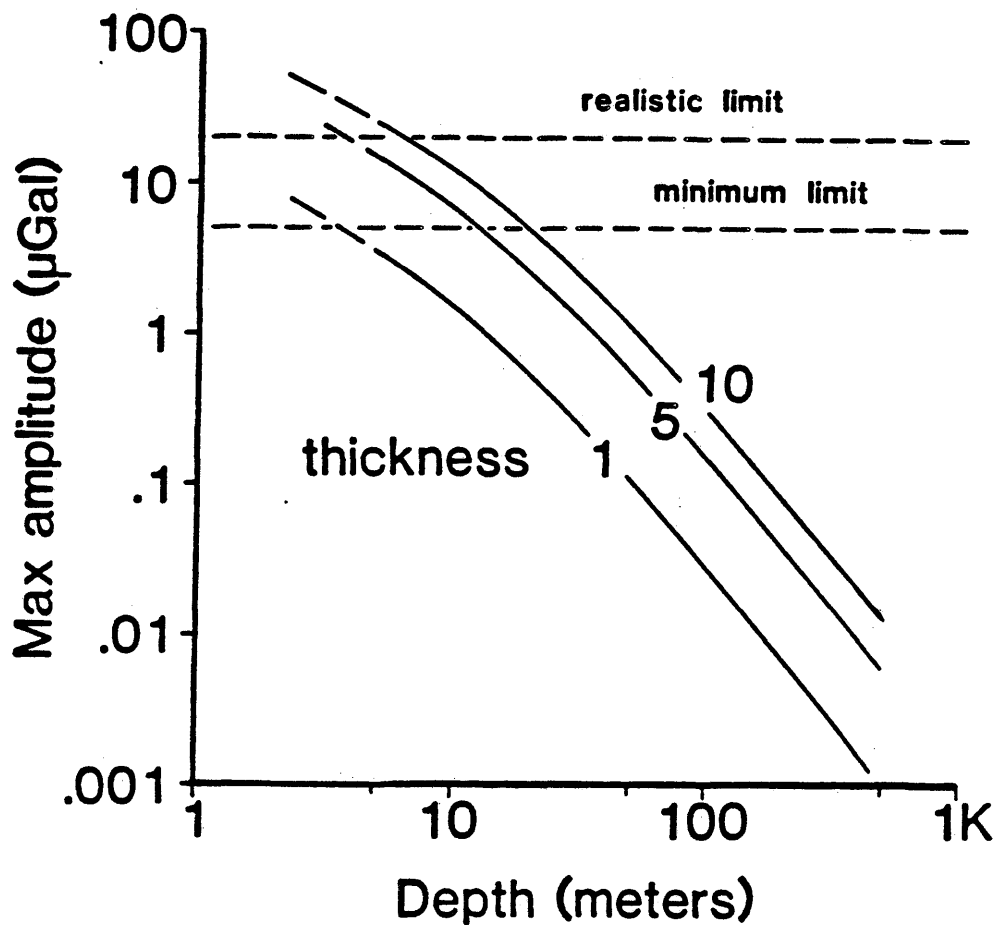


Figure 12. Maximum absolute gravity response over vertical fracture zones of various thicknesses and at various depths. Density contrast  $-0.5 \text{ g/cc}$ . Height and length of zones 10 meters.

depth of a detectable zone is reduced to between 5 and 15 meters. Thus the relationship between extent of zone and detectable depth is linear, and a multiplication of the length by ten also implies a ten-fold increase in the detectable depth.

The gravity anomaly over a horizontal fracture zone with finite length and width was also modeled. The anomalies show the depths of resolvable zones to range from 4 meters for the very local zone (10-by-10 m, Figure 13) to 900 meters for the more regional zone (500-by-500 m, Figure 14), with the in-between zone (100-by-100 m, Figure 15) giving depths of 80 to 180 meters. This is approximately 10 to 20 percent higher than for the vertical feature of the same dimensions. However, the anomalies for a horizontal zone are very broad, and even fairly large anomalies can get hidden in regional variations. This is also true for the next model, the basement fault, and to some extent for all anomalies caused by deep-seated bodies.

The basement fault model (Figs. 16 and 17) causes very large anomalies compared to the others, primarily due to the difference in volume between the entire basement and a finite zone. But the anomalies are, as mentioned above, very wide, and the resolving capability should probably be lowered an order of magnitude or more. This would make the



Figure 13. Maximum absolute gravity response over horizontal fracture zones of various thicknesses and at various depths. Density contrast  $-.5 \text{ g/cc}$ . Length and width of zones 10 meters.

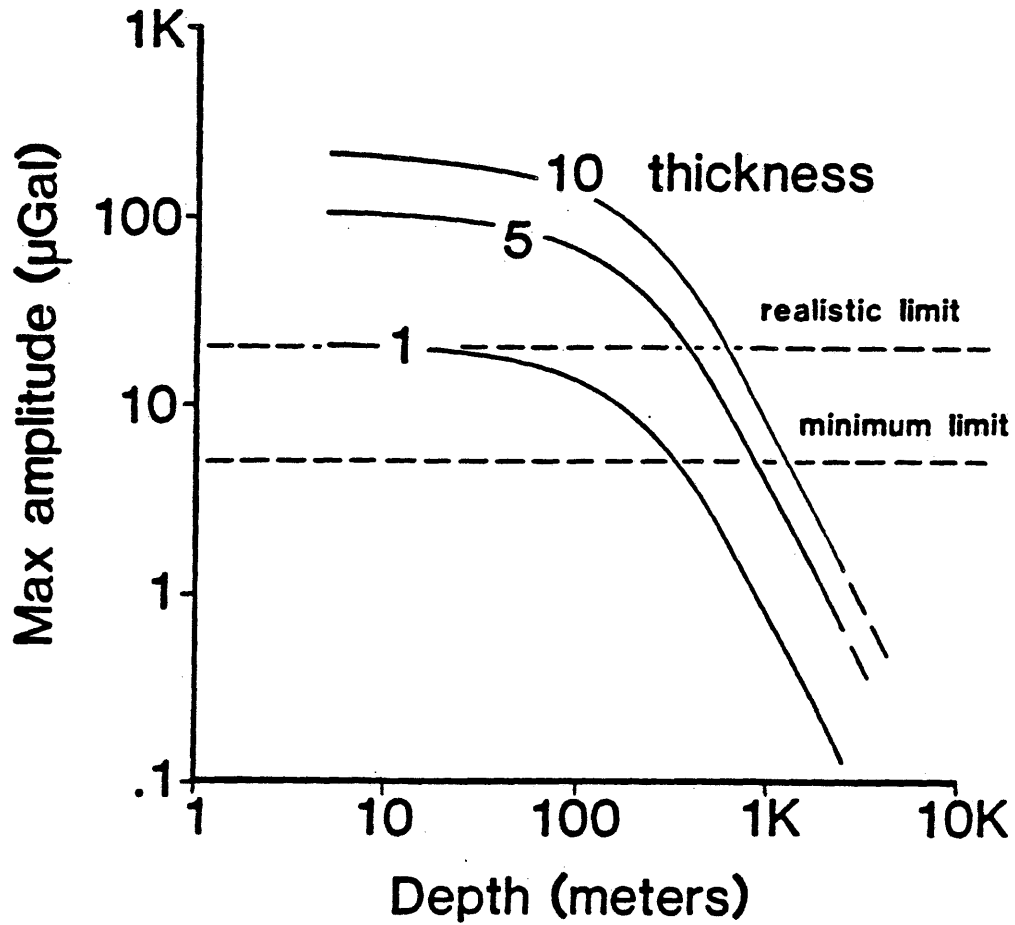


Figure 14. Maximum absolute gravity response over horizontal fracture zones of various thicknesses and at various depths. Density contrast  $-0.5 \text{ g/cc}$ . Length and width of zones 500 meters.

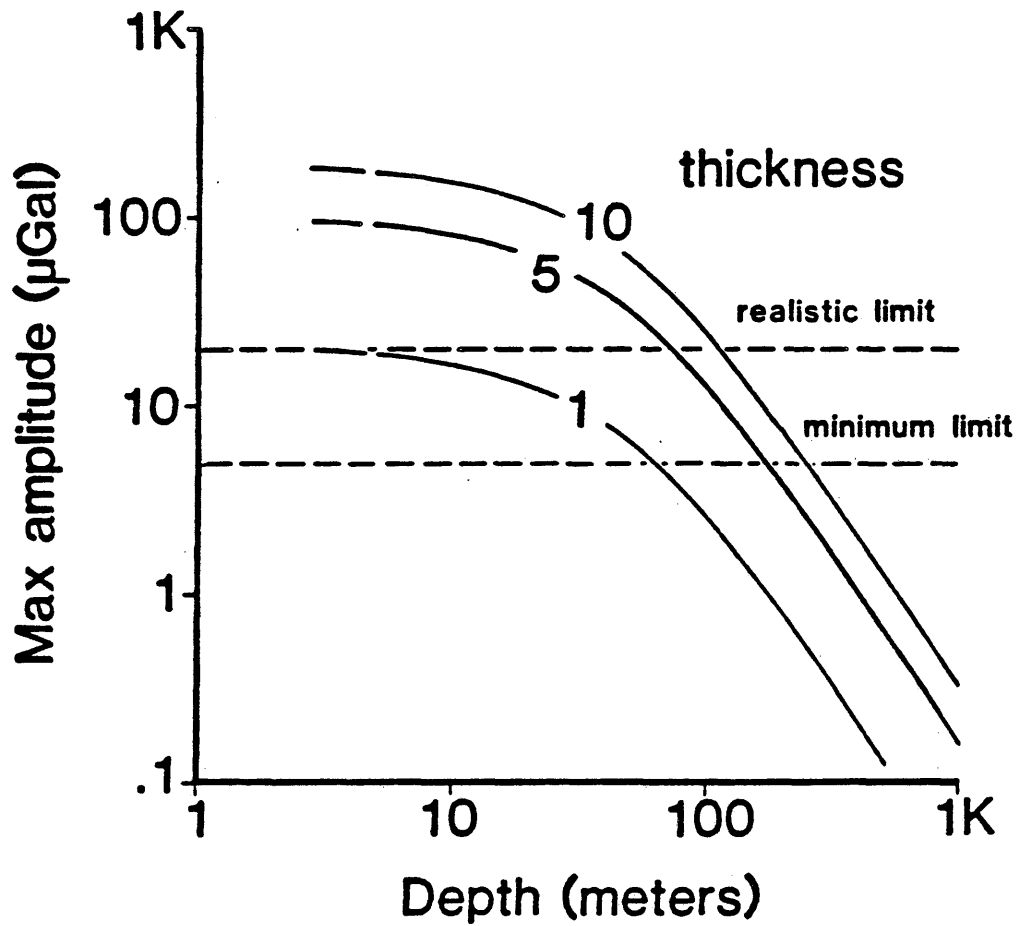


Figure 15. Maximum absolute gravity response over horizontal fracture zones of various thicknesses and at various depths. Density contrast  $-0.5 \text{ g/cc}$ . Length and width of zones 100 meters.

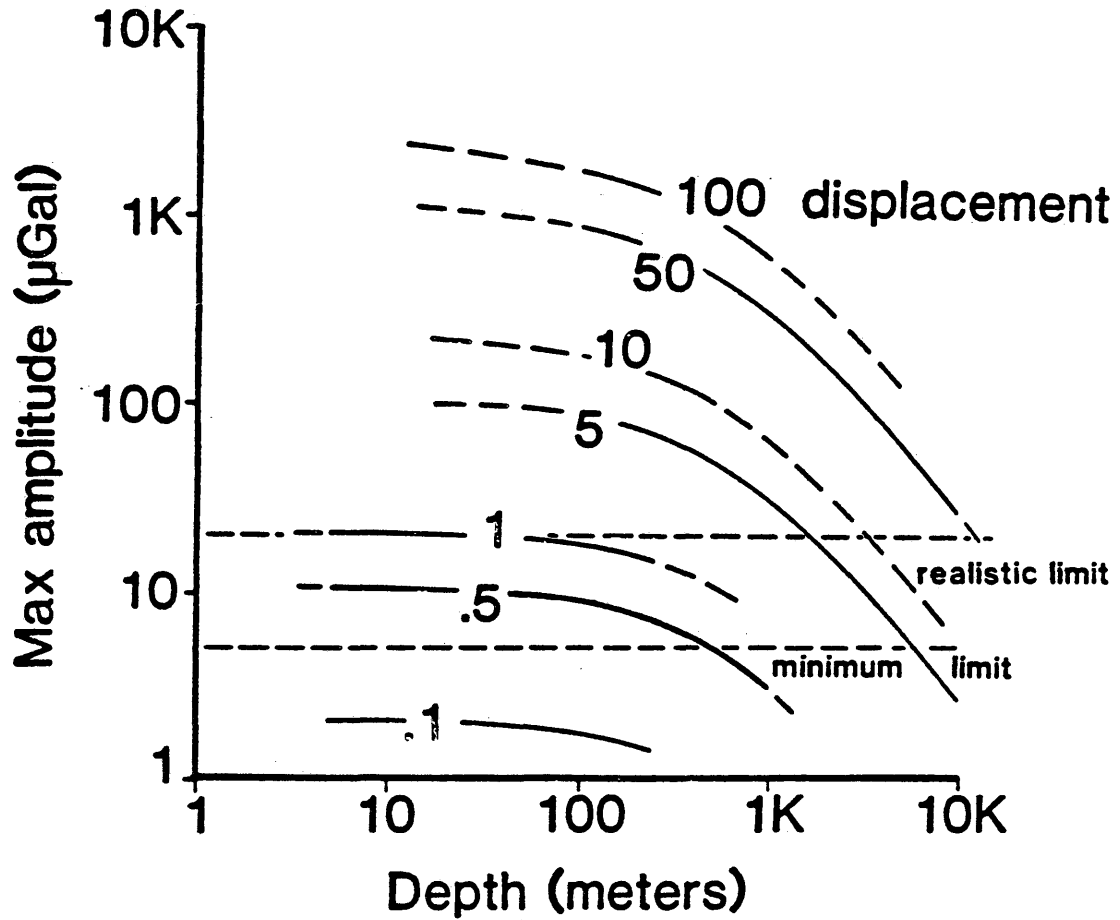


Figure 16. Maximum absolute gravity response over basement fault with various vertical displacements and at various depths. Density contrast .5 g/cc.

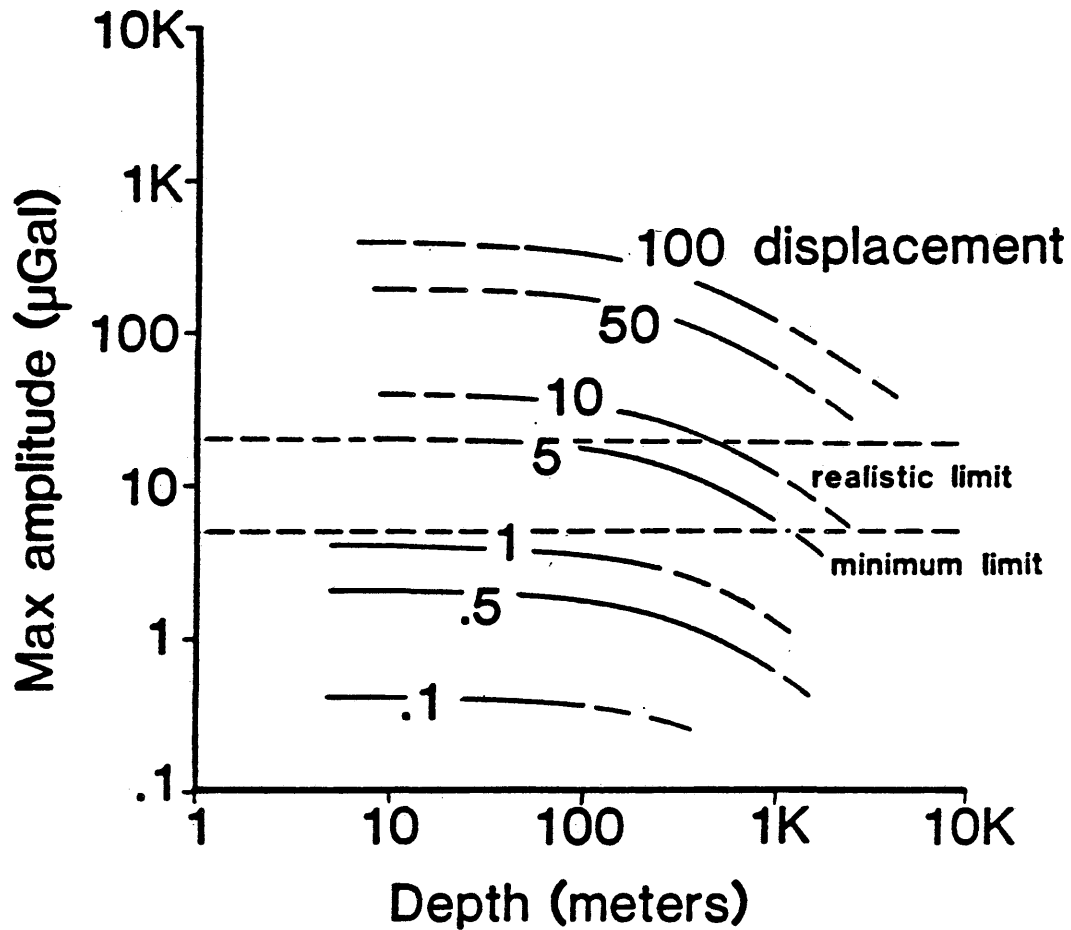


Figure 17. Maximum absolute gravity response over basement fault with various vertical displacements and at various depths. Density contrast .1 g/cc.

minimum detectable throw (of the fault) approximately 10 meters for a density contrast of .5 g/cc and 50 meters for a contrast of .1 g/cc.

### MAGNETIC MODELING

Magnetic methods have been used since the very beginning of geophysical exploration in prospecting for iron-ore deposits. Magnetic and gravity methods have much in common, but where the gravity map shows mainly larger-scale effects, the magnetic map appears to have more detail. This is the result of large variations in the content of magnetic minerals in the near surface rocks. Remanent magnetization of various strengths and directions can further complicate the magnetic picture. Thus the precise interpretation of magnetic data is much more difficult than for gravity data.

The earth's magnetic field strength (H) is approximately 50,000 gammas. A relation between the intensity of magnetization (I) and the rock property determining the induced magnetic field strength, can be written as " $I = kH$ ", where (k) is the magnetic susceptibility. This parameter ranges from .0001 to .1 emu-units for rocks with low magnetite concentration to high

grade iron ore, respectively (Telford et al,1976, Parasnis,1973). Many attempts to establish a quantitative relation between susceptibility and magnetite concentration have been made in the past. Nettleton (1971) defines a linear relationship for low concentrations of magnetite as " $k = 0.003p$ " where (p) is the percentage by volume of the disseminated magnetite.

Noise in the form of short period variations in the external magnetic field caused by solar and lunar diurnal variations, as well as more erratic fluctuations from magnetic storms and lightning, is a problem. In precise work repeat readings should be made with short intervals at previously occupied stations to overcome these noise factors. The best accuracy is obtained if a fixed base station is available with the ability for continuous recording of the magnetic field variations. This data base can later be correlated with the field data to reduce or at best eliminate the noise. The influence of topography can also have a significant effect on data quality. It has been found that terrain anomalies as large as 700 gammas occur at steep (45 degrees) slopes of only 10 meters height in formations containing 2 percent magnetite (Gupta and Fitzpatrick,1971).

The magnetometers used for ground surveys are of three different types, although the accuracy of the fluxgate magnetometer is usually not enough for engineering applications. The nuclear precession magnetometer has a higher accuracy of approximately .1 to 1 gamma. The third category is the optical-pump instrument. These utilize the energy involved in transferring atomic electrons from one energy level to another. Sensitivity is in the impressive range of .01 to .001 gamma. That is an accuracy of one part in 50 million of the earth's magnetic field (Langan, 1966; Reford, 1980). With this extremely high sensitivity, the material close to the surface influences the measurements to a very high degree. The resolution is highly dependent on this fact, but ground surveys over small areas have been repeatable to tenths of a gamma (Langan, 1966).

#### MAGNETIC MODELING PROGRAM USED

The program used for the gravity modeling was also used to simulate magnetic surveys (see gravity section).

The computer program assumes that all total field anomalies are parallel when the summation of the total field from multiple bodies is performed. This approximation, which is the projection of the magnetic field of the anomalous body into the earth's field direction, is accurate only when the perturbing field is small compared to the

earth's field. This is the case for all magnetic modeling in this thesis.

Equations of the magnetic field due to a two dimensional body, with end corrections, were derived by Shuey and Pasquale (1973). They also coined the term "2.5-dimensional" to describe the geometry. The magnetic survey model is illustrated in Figure 18.

#### RESULTS OF MAGNETIC MODELING

Models of vertical and horizontal fracture zones of various extension, a basement fault, and a tunnel were investigated. The shapes of the bodies were defined in two dimensions, that is, in a plane perpendicular to one of the coordinate axes. In the direction of this perpendicular the bodies are of finite extent and uniform cross-section. A magnetic field with an inclination of 60 degrees and 50,000 gammas field strength represented the earth's field. Susceptibility contrasts of .005 emu and .001 emu, which are equivalent to a surrounding medium with concentrations of approximately 3 % and .8 % magnetite, respectively, were used as model parameters.

The magnetic response over a tunnel in a magnetic host medium (Fig. 19) shows that at depths of 5 and 10 meters the anomalies are distinct and measurable. Curve shape does

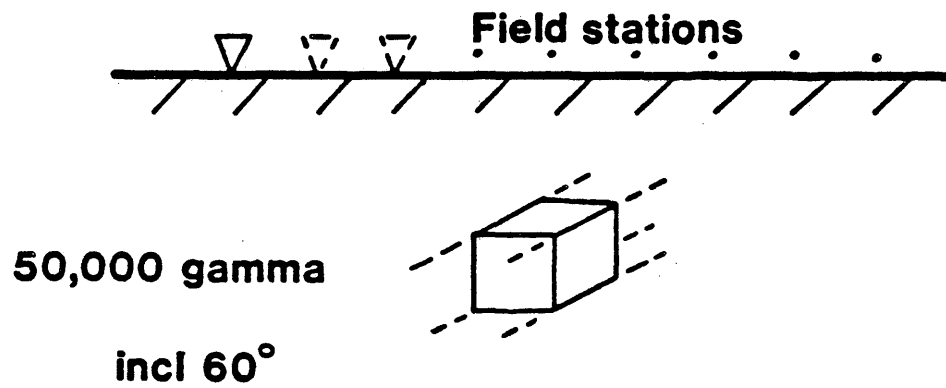


Figure 18. Magnetic survey model in 2.5-D. A field with 50,000 gamma field strength and 60 degrees inclination, represents the earth's magnetic field.

not depend on depth except that curves from deeper features are broader than from shallow. Therefore, horizontal resolution capability decreases with depth. At depths below 15 meters (Fig. 20) the anomaly becomes smaller than the realistic limit of resolution. This limit is set at 5 gammas and indicates what can be achieved in the field in terms of accuracy. Figure 21 illustrates the magnetic response for different tunnel diameters and depths, with instrument resolution capability in the ideal case set as the minimum limit. Since, for interpretation purposes, we would need to see more than just the maximum point of the anomaly, and since there would be near surface noise present, the higher limit is a more realistic estimate of detectability. A tunnel with a diameter of two meters would then be detectable at a depth of 15 meters.

Similar results for a vertical fracture zone with anomalously low magnetite concentration (compared to host medium) and a finite height and length are presented in Figures 22, 23 and 24. For the zone with very limited extent in the vertical plane (10-by-10 meters) and a thickness of 5 meters, the detectable depth is approximately 25 meters. If the thickness is kept constant at 5 meters but the other two dimensions are expanded to 100-by-100 meters, the detectable depth is increased four-fold (110 meters). A 1000-by-1000

meter zone would increase this even further, to a depth of 300 meters as the realistic resolution limit.

Horizontal fracture zones (Figs. 25, 26 and 27) have maximum magnetic responses very similar to that of the vertical feature. An increase of about 10 percent in amplitude is evident from the results. The actual detection depth might be less, though, since the widths of the anomalies have increased. This will decrease the lateral resolution and can also hide the anomalies in regional trends and background noise.

The magnetic response over basement faults with various vertical throws and susceptibility contrasts are shown in Figures 28 and 29. Maximum detectable depth for the 5-meter-vertical-displacement fault range from 100 to 500 meters depending on physical contrast. Results show that for the lower susceptibility contrast the ratio between displacement and detectable depth is approximately 1 to 20. Increasing the susceptibility contrast five times also increases the ratio by the same amount, to 100 over 1.

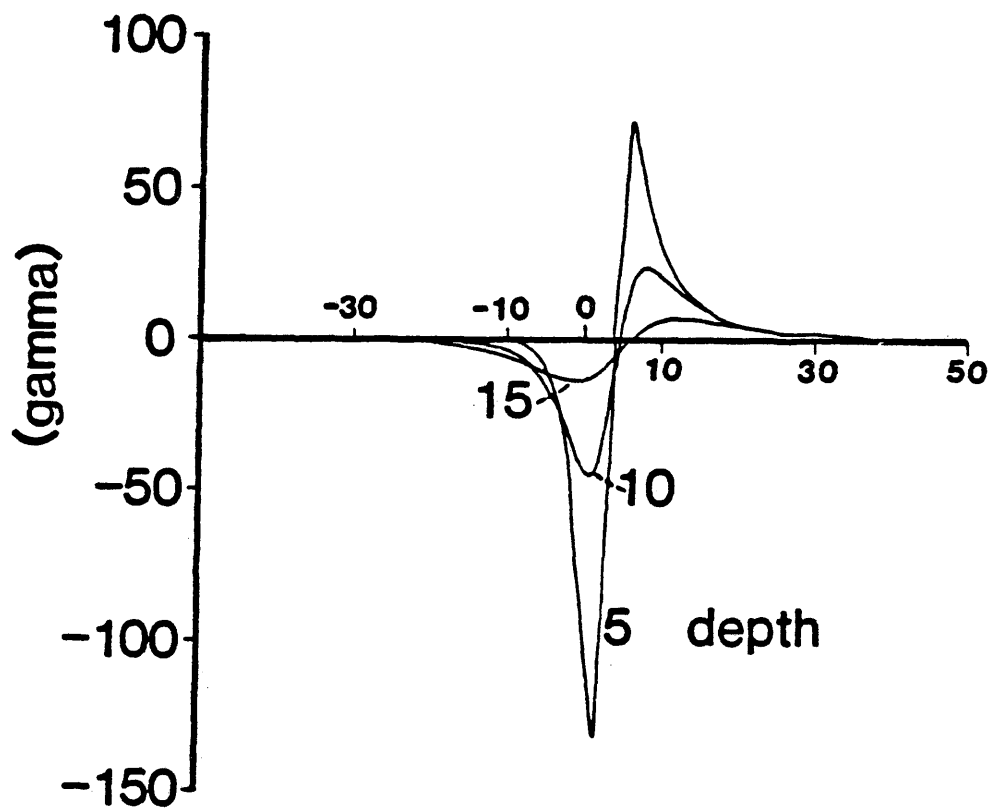


Figure 19. Magnetic response curves over 2-by-2 meter tunnels at various depths. Susceptibility contrast  $-.005$  emu. Abscissa shows lateral position (in meters) compared to midpoint of body.

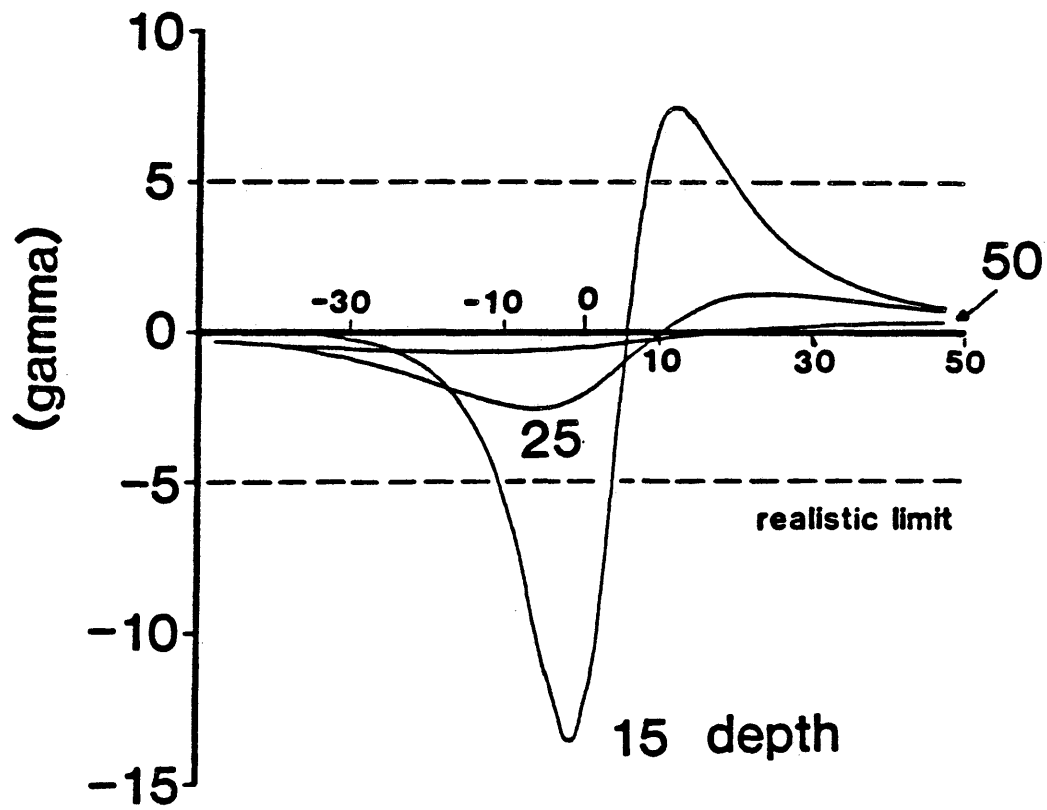


Figure 20. Magnetic response curves over 2-by-2 meter tunnels at various depths. Susceptibility contrast  $-.005$  emu. Abscissa shows lateral position (in meters) compared to midpoint of body.

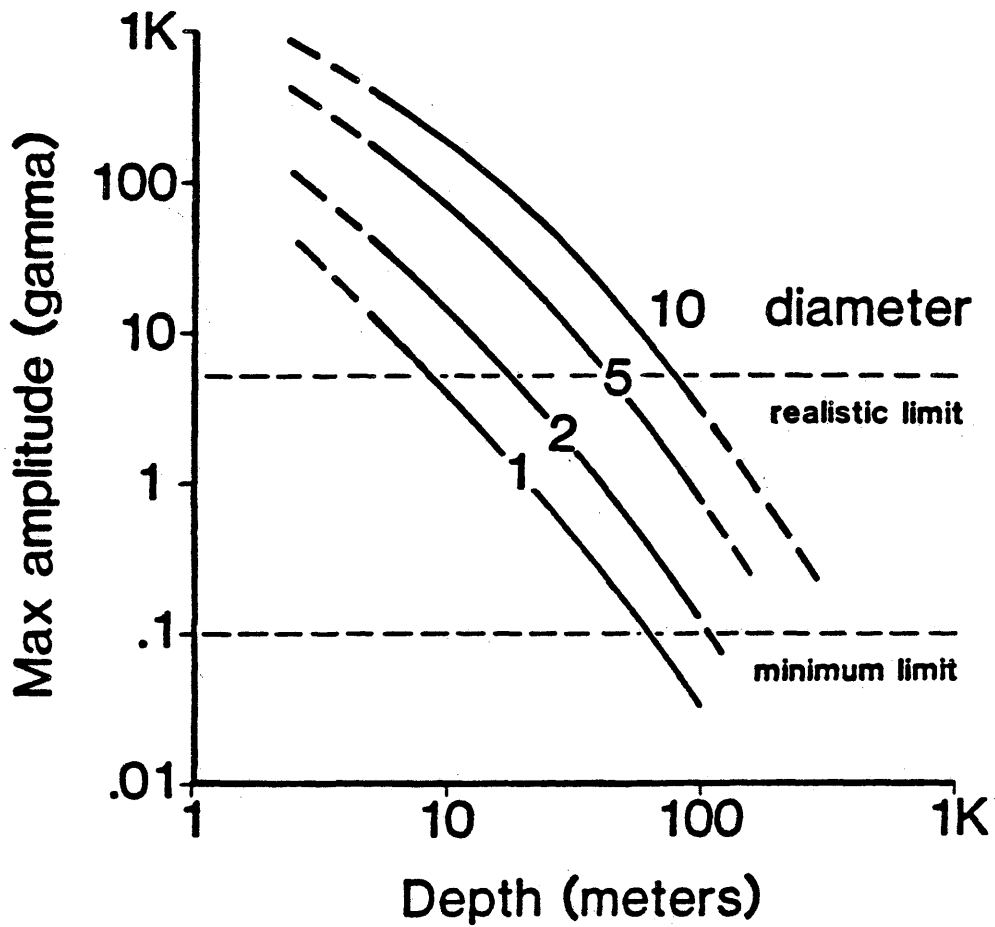


Figure 21. Maximum absolute magnetic response over tunnels of various diameters and at various depths. Susceptibility contrast  $-.005$  emu.

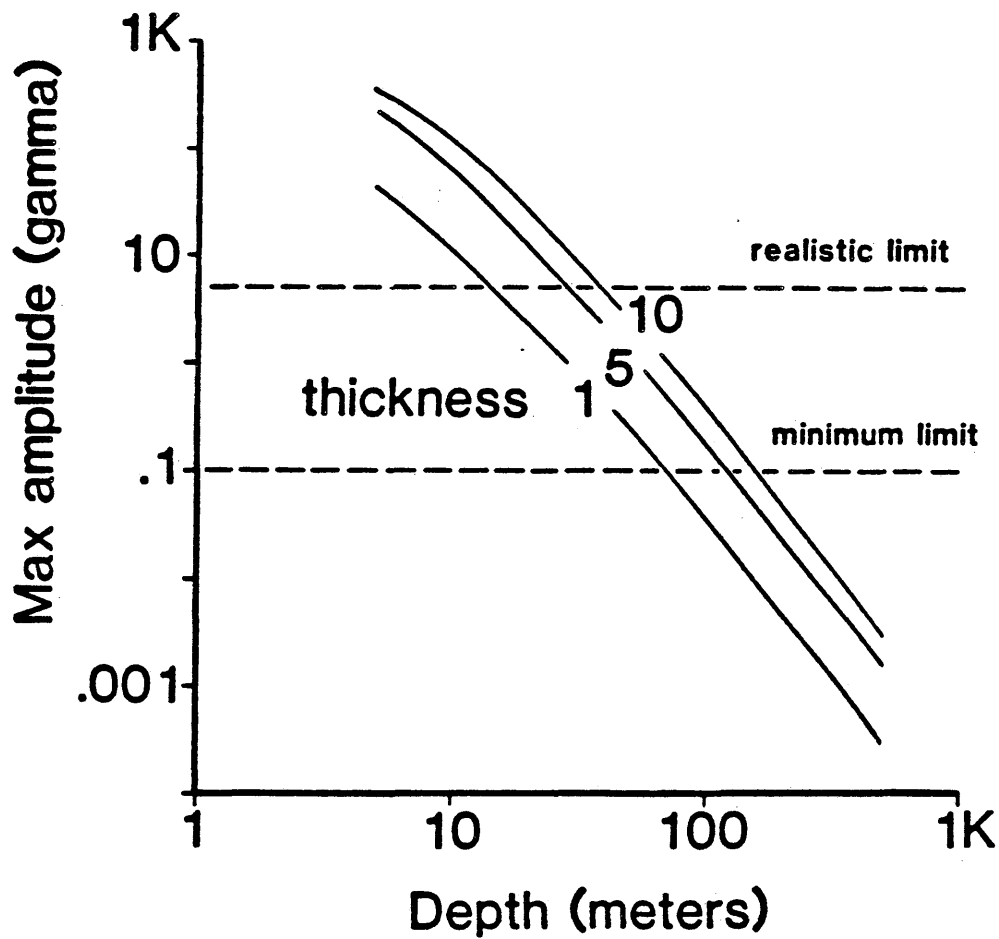


Figure 22. Maximum absolute magnetic response over vertical fracture zones of various thicknesses and at various depths. Susceptibility contrast  $-0.005$  emu. Height and length of zones 10 meters.

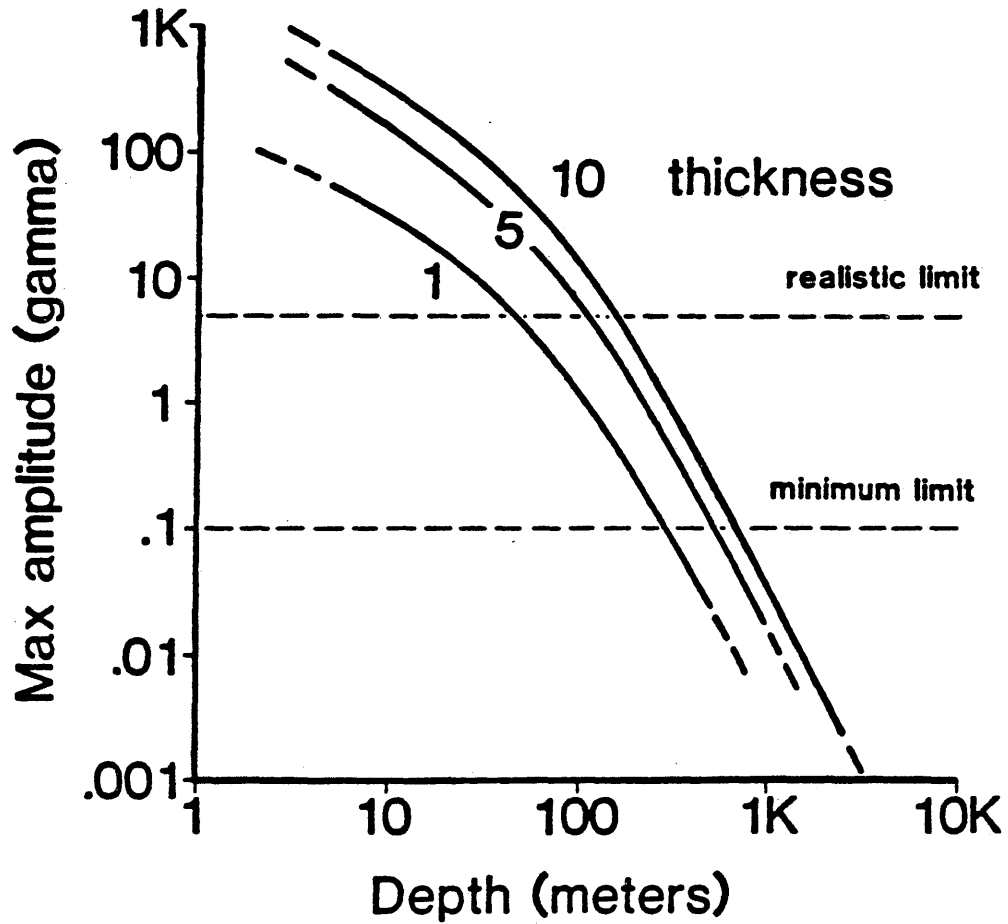


Figure 23. Maximum absolute magnetic response over vertical fracture zones of various thicknesses and at various depths. Susceptibility contrast  $-.005$  emu. Height and length of zones 100 meters.

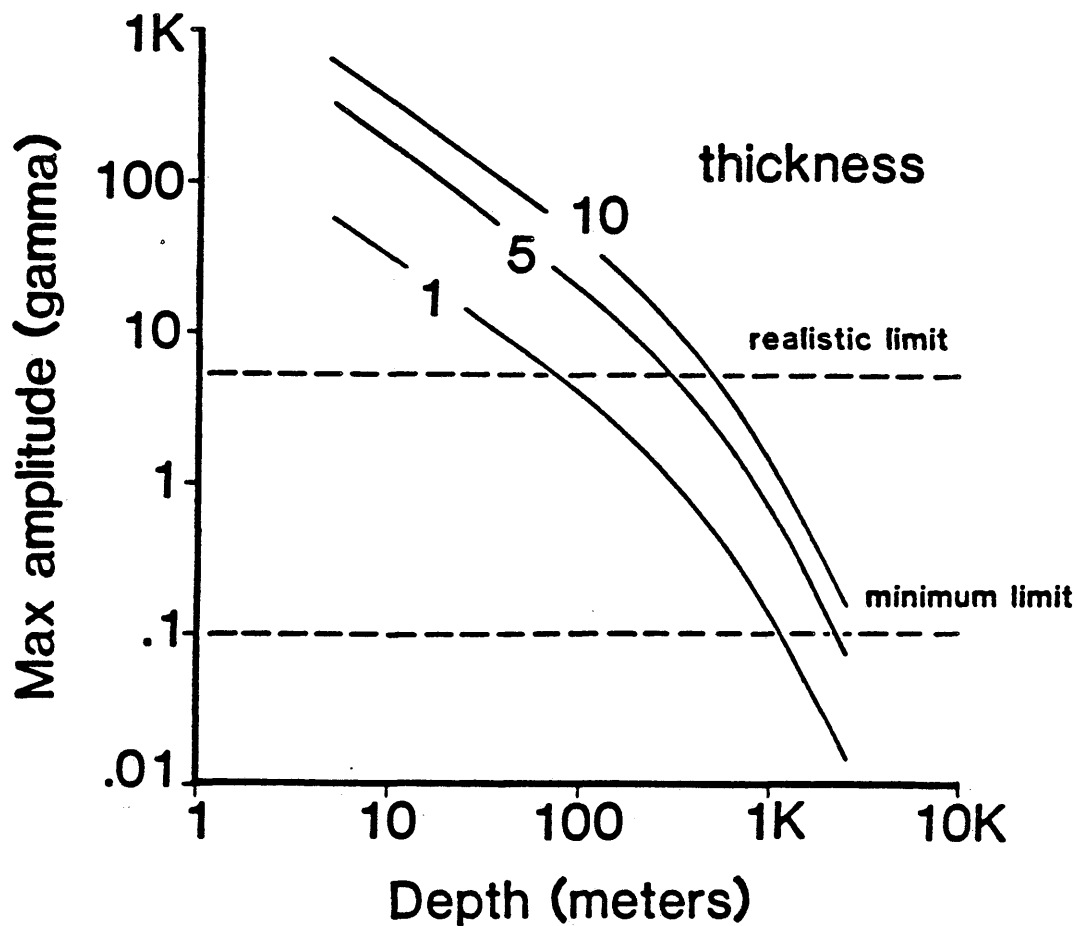


Figure 24. Maximum absolute magnetic response over vertical fracture zones of various thicknesses and at various depths. Susceptibility contrast  $-.005$  emu. Height and length 1,000 meters.

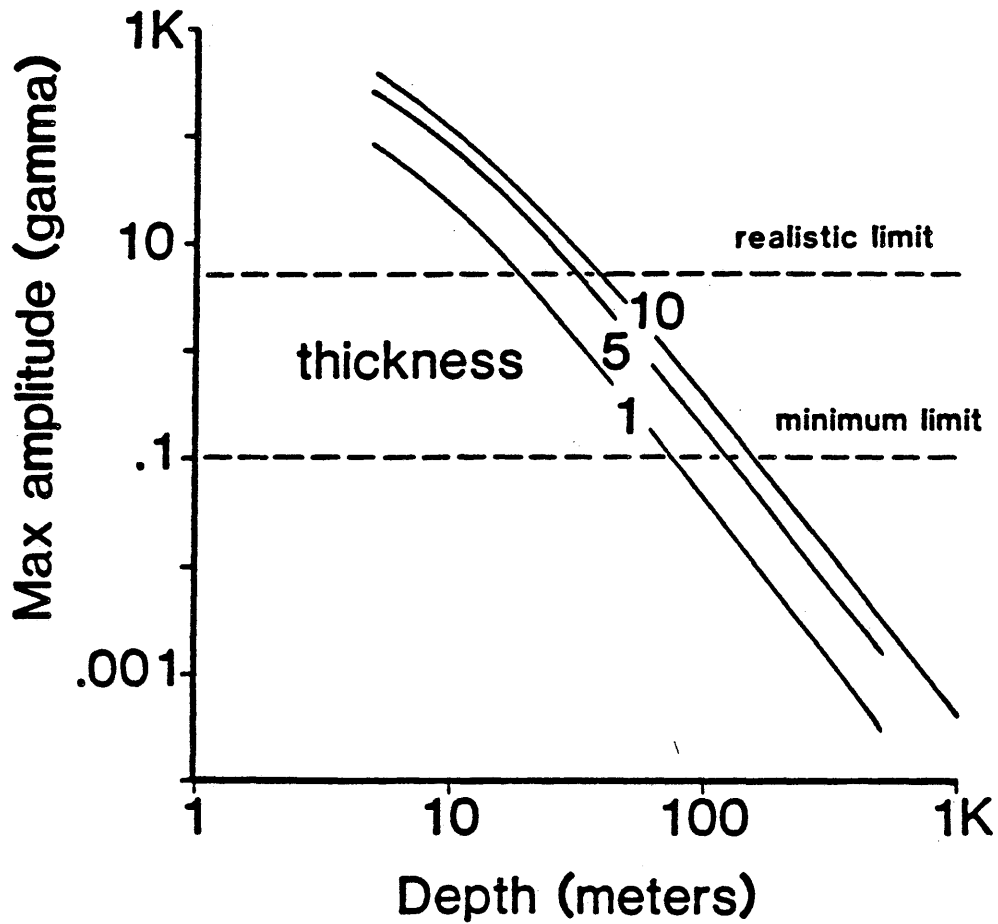


Figure 25. Maximum absolute magnetic response over horizontal fracture zones of various thicknesses and at various depths. Susceptibility contrast  $-.005$  emu. Length and width of zones 10 meters.

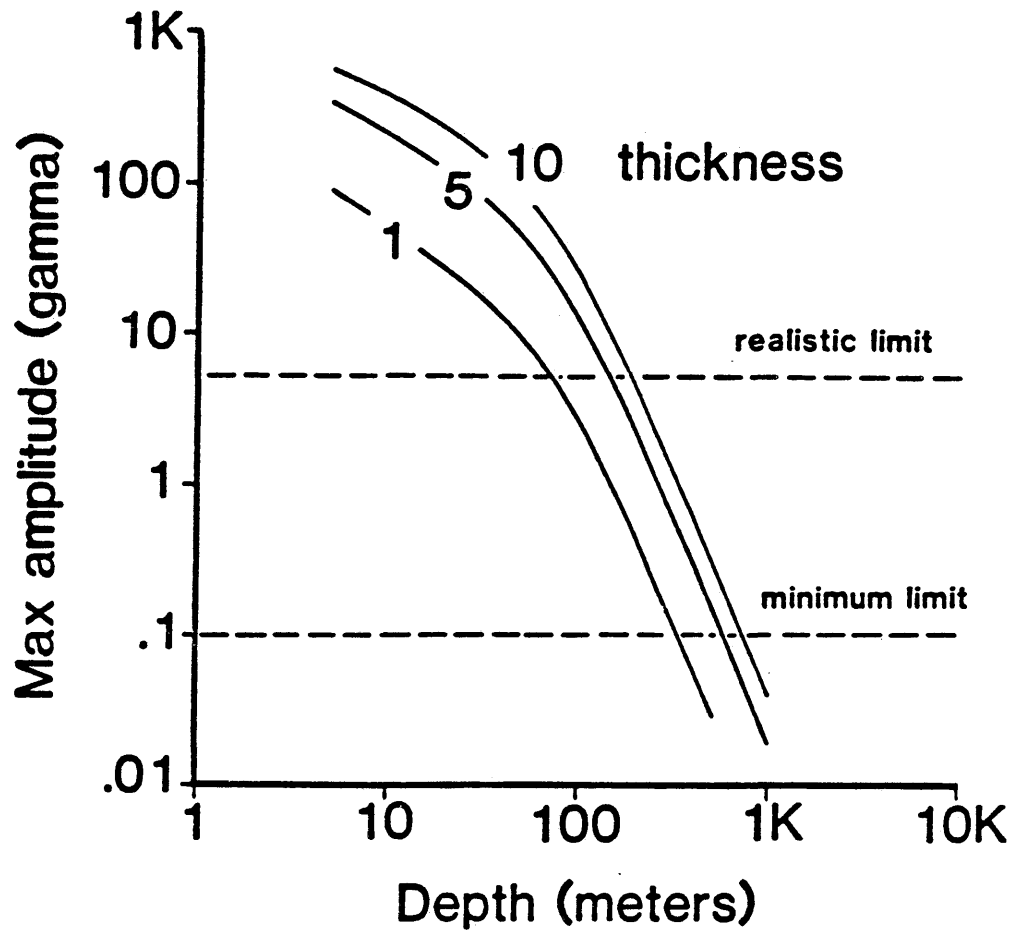


Figure 26. Maximum absolute magnetic response over horizontal fracture zones of various thicknesses and at various depths. Susceptibility contrast  $-0.005$  emu. Length and width of zones 100 meters.

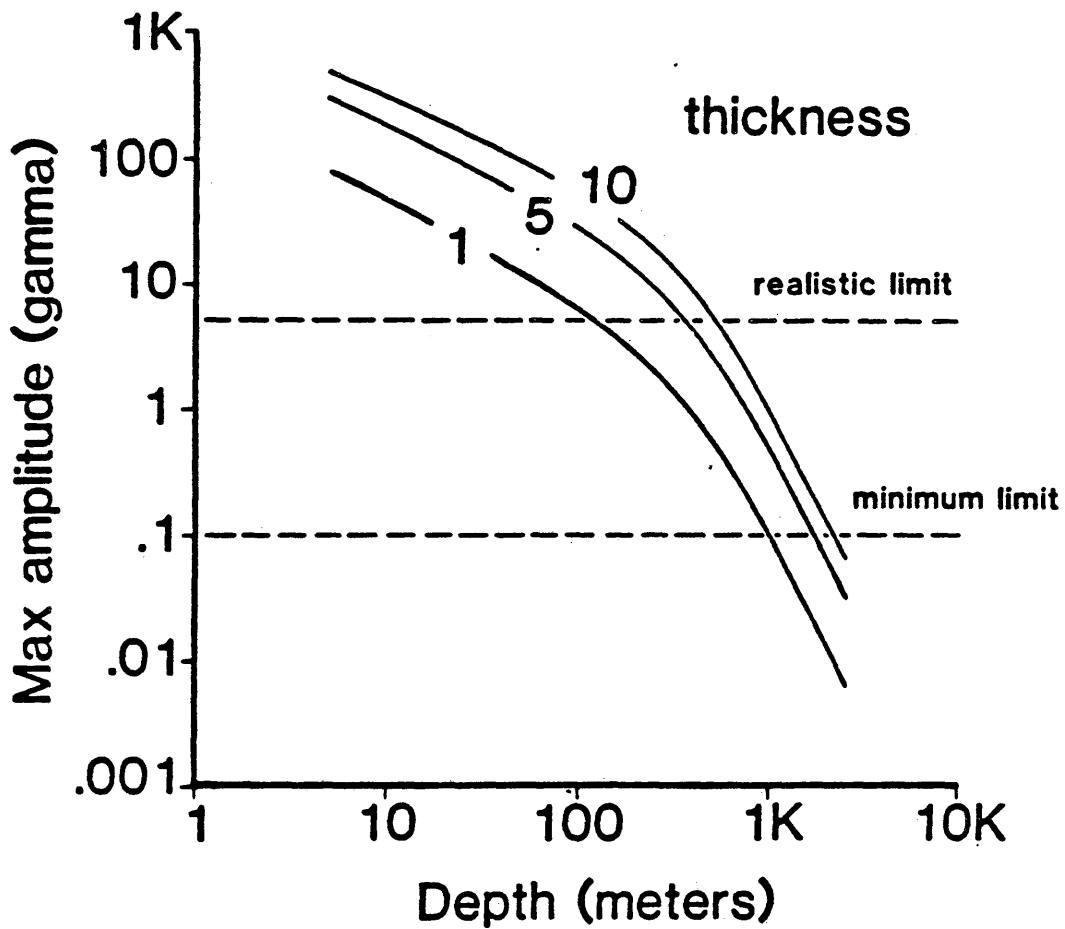


Figure 27. Maximum absolute magnetic response over horizontal fracture zones of various thicknesses and at various depths. Susceptibility contrast  $-.005$  emu. Length and width of zones 500 meters.

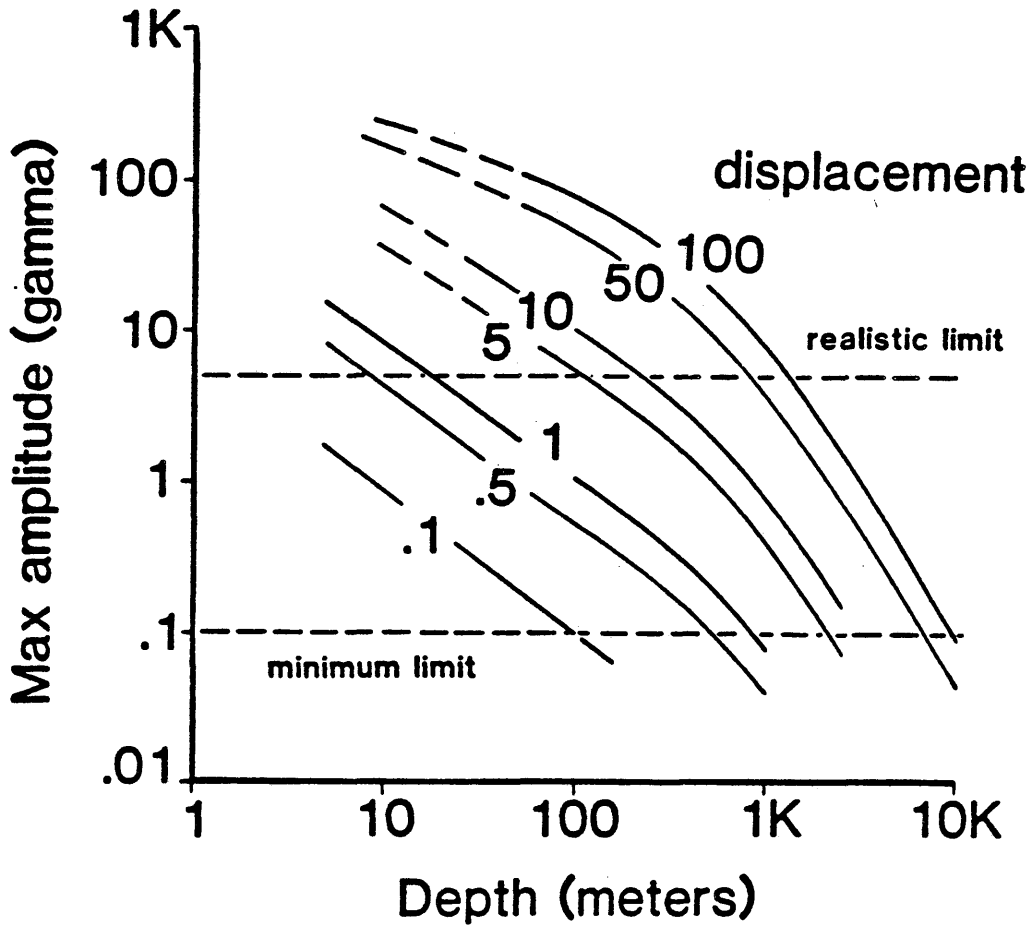


Figure 28. Maximum absolute magnetic response over basement faults with various vertical displacements and at various depths. Susceptibility contrast .001 emu.

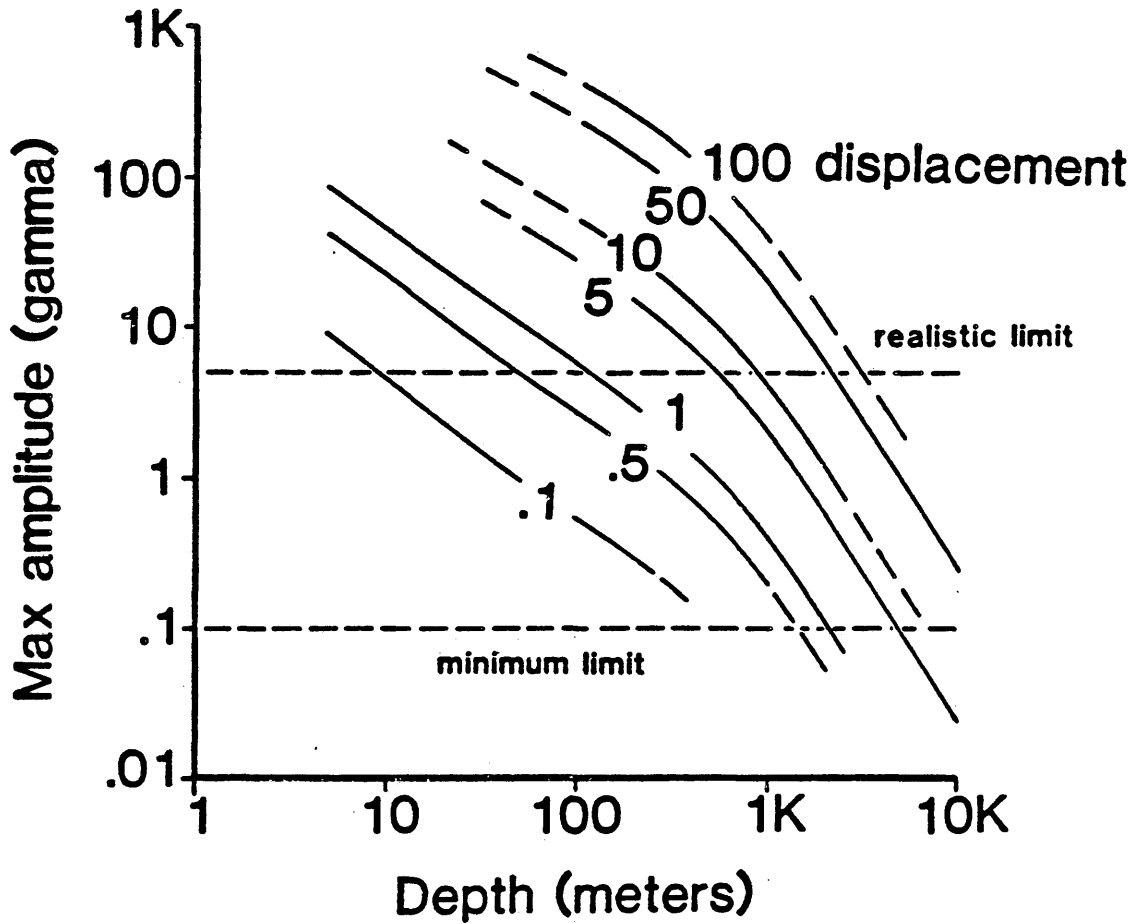


Figure 29. Maximum absolute magnetic response over basement faults with various vertical displacements and at various depths. Susceptibility contrast .005 emu.

## DIRECT-CURRENT ELECTRICAL MODELING

The resistivity method has proven to be more suitable for defining horizontal beds and vertical contacts involving conductivity contrasts, and less useful for delineating bodies of irregular shape (Telford et.al., 1976). Therefore the DC method is used in mapping groundwater level and salinity changes in the groundwater, and in obtaining depth soundings to evaluate resistivity distribution for a layered section of the subsurface. Conductive orebodies have also been a prime target for the employment of the method.

Instrumentation is usually simple and in most cases easily portable. In the horizontal-layered-section case, the inversion of the data and data interpretation are fairly straightforward. With more complex geometries the solution becomes both more difficult to find and also non-unique.

The basis for the method is the ease or difficulty with which electrical current can be driven through the subsurface by an artificially applied voltage. This property is called electrical resistivity and is measured in ohm-meters. Where the solid minerals in the rocks have very poor conductivity, the porewater and presence of metallic minerals increase the overall bulk conductivity of the rock. Porous rocks range in resistivity from 10 to 10,000 ohm-m,

where the value varies approximately as the inverse square of the water content (Keller, 1979). Therefore weathered and fractured zones with increased porosity will be characterized by relatively low resistivities.

The type of display used for resistivity data depends on whether the general problem is that of sounding a layered earth or that of lateral mapping. In the first case the resistivities are plotted versus electrode spacing, creating a curve indicating the number of layers and whether the resistivity is increasing or decreasing with depth. The lateral mapping display, where several spreads are used, can be plotted in a pseudo-section. This will give a rough idea of the spatial resistivity distribution and, to some degree, the resistivity in two dimensions.

To permit the use of direct-current theory, the frequency must be low enough so that electromagnetic coupling does not occur. This frequency limit depends on the depth of investigation and the resistivities present. For shallow measurements and a high resistivity subsurface, frequencies as great as 1,000 Hz can be considered as being direct-current (Keller, 1979). Usually 10 Hz or lower is used.

The direct-current method is not known as being a high-resolution tool. The detectability of a thin resistive horizontal bed at depth depends on the product of the

resistivity and the thickness, called transverse resistance (T), rather than on the resistivity contrast alone. A thin conductive bed's detectability depends on the longitudinal conductance (S), defined as the ratio between thickness and resistivity. The change in apparent resistivity will therefore be dependent on the contrast of these two properties (T and S) to that of the overburden. Also, for detecting thin layers, the contrast in T (or S) value to overburden, should be at least a few percent (Keller, 1979).

Southwest Research Institute (SwRI) has been able to utilize statistical signal enhancement techniques to increase the signal-to-noise ratio in a manner that enables them to see anomalies as small as tenths of a percent (Spiegel et.al., 1980). For a .5 percent anomaly, a T-ratio between the thin layer and overburden should be approximately 2 percent.

## DIRECT-CURRENT ELECTRICAL MODELING PROGRAM USED

The two-dimensional computer program used for the direct-current modeling and the electromagnetic modeling, was written by C.H.Stoyer (1974). The program uses a finite-difference formulation to compute the frequency-domain electromagnetic fields due to a point source in the presence of two-dimensional conductivity structures (Stoyer,1976) (Fig. 30). This is a cost-efficient computer program designed to reduce the full three-dimensional problem to a series of two-dimensional problems.

The solution of Maxwell's equations by finite difference methods constitutes the basis for the program. The technique described by Stoyer uses a Fourier transform over the x-coordinate (strike axis); then for each of several wavenumbers only a two-dimensional problem must be solved numerically. The cross-section of the 2-D electrical earth is represented by a rectangular grid. Grid spacing near the surface should be less than one quarter of the skin depth, defined as  $(2 / (\sigma * 2 * \text{PI} * f * \mu))^{1/2}$  meters) where  $\sigma$  is conductivity in mhos/meter,  $\mu$  is permeability in henries/meter, and  $f$  is frequency in hertz. Other grid spacings should be less than a skin depth. This implies that to be able to model small targets at relatively great

## 2-D DC Electrical Survey Model

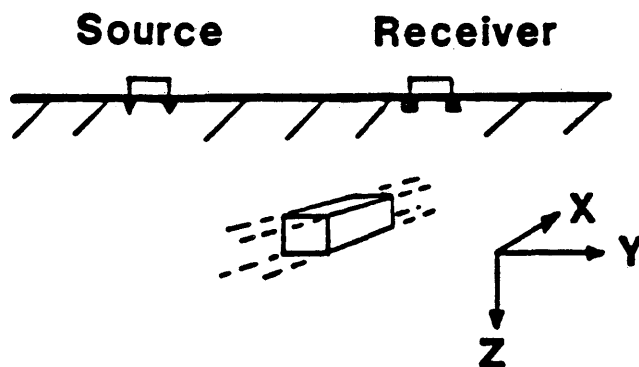


Figure 30. Direct-current electrical survey model in 2-D.

depths, we need a large grid which is computationally costly.

The accuracy of the numerical solution is dependent upon the fineness of the mesh and distance of the grid edges from the areas of interest. In his paper, Stoyer shows that the program results agree to a high degree with scale model experiments and analytic results.

Although the modeling problem has been reduced from three dimensions to two dimensions, the computer time for a 20-by-20 grid using two sources exceeds 1500 system seconds.

#### RESULTS OF DIRECT-CURRENT ELECTRICAL MODELING

The two-dimensional models investigated included vertical and horizontal fracture zones at various depths, a basement fault and a tunnel. Rather than looking at conventional pseudosections the displays in this work are individual response curves. The curves represent response from a fixed source measured at simulated receiver locations along a line perpendicular to strike of body.

The polar-dipole array survey simulated over a 4-by-5 meter tunnel suggests that it is fairly easy to see the target at 5 meters depth, but below 10 meters it is very dubious (Fig. 31). Figure 32 shows results for the same array over a tunnel at deeper locations. The response is

now down to tenths of a percent as maximum anomaly. However, the limit of resolution can be increased by making a large number of measurements.

Responses for an equatorial-dipole array survey over the same body (Figs. 33 and 34) are about half the magnitude of the polar-dipole response. This method is also less used than the polar-dipole.

The response to a vertical fracture zone with a resistivity contrast of 1,000 ohm-m for the host medium to 100 ohm-m and 10 ohm-m, respectively, for the zone, shows that the amplitude of the anomaly is much larger than that for the tunnel case (Figs. 35 and 36). The equatorial-dipole array survey models yield curves with similar amplitudes but different character (Figs. 37 and 38).

Polar-dipole response curves over a basement fault and horizontal fracture zone (Figs. 39 and 40) show high amplitude events for the shallow features. The response decreases rapidly with depth to anomalous body.

Utilizing signal-enhancement techniques a signal amplitude of tenths of a percent might be interpretable, whereas up to tens of percent is usually necessary to interpret anomalies. This implies that the detectable depth

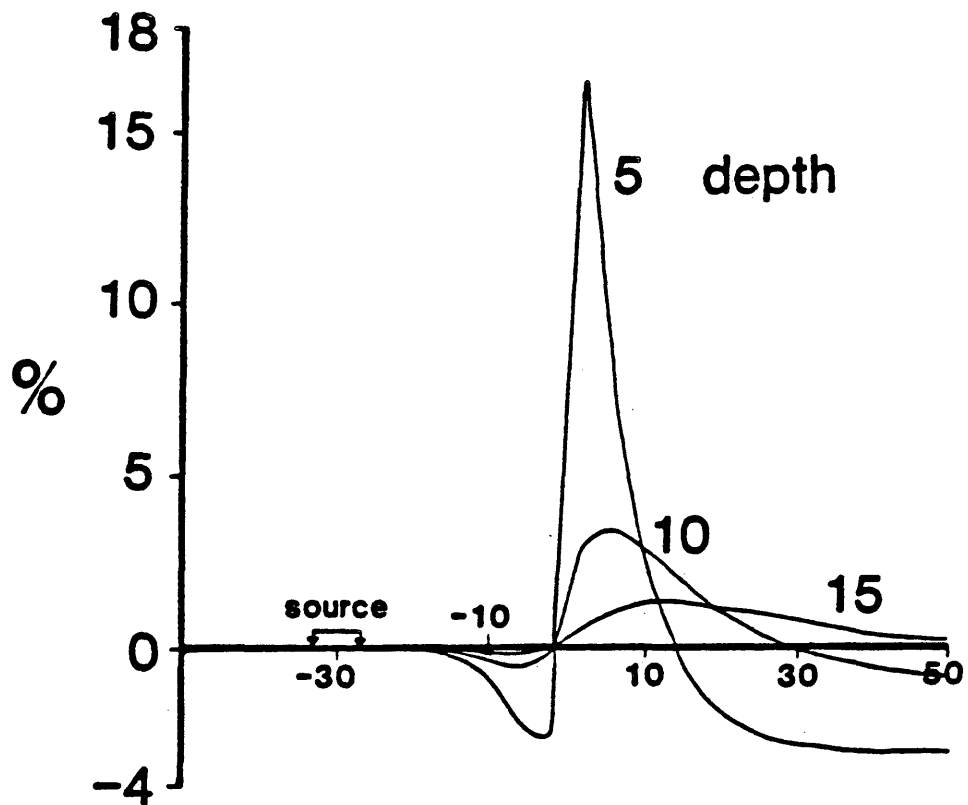


Figure 31. Polar-dipole response curves over 4 by 5 meter tunnel at various depths. Resistivity of host-medium 1,000 ohm-m versus infinite tunnel resistivity. Abscissa shows lateral position (in meters) compared to midpoint of body.

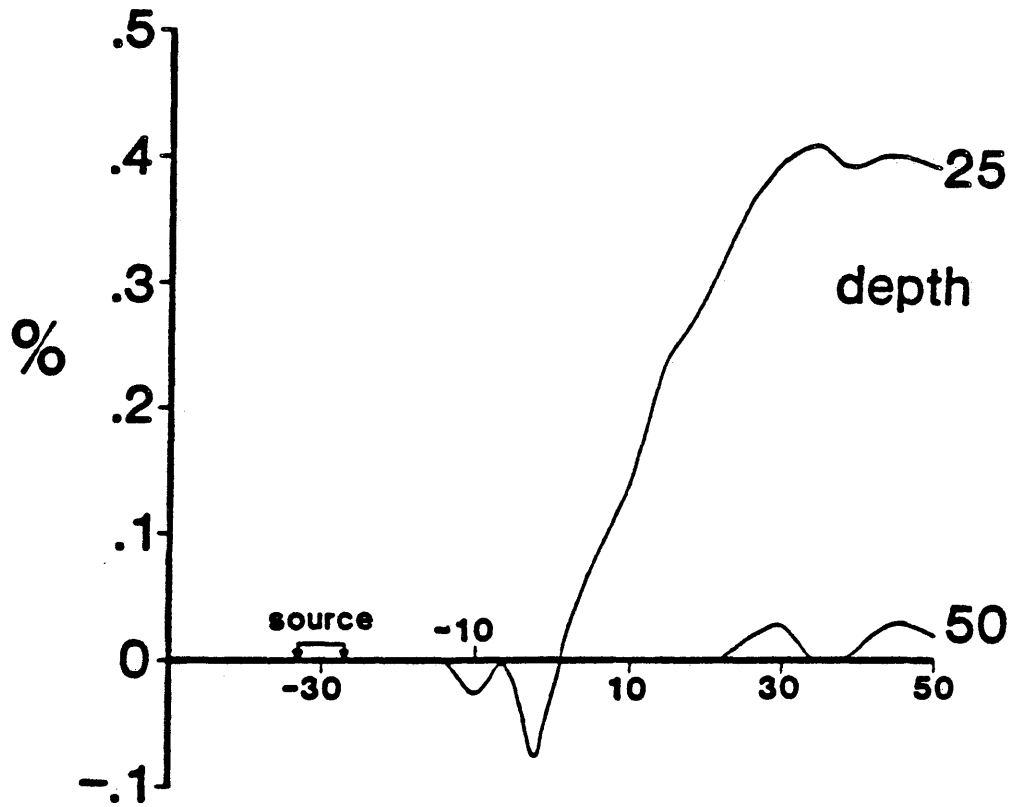


Figure 32. Polar-dipole response curves over 4 by 5 meter tunnel at various depths. Resistivity of host-medium 1,000 ohm-m versus infinite tunnel resistivity. Abscissa shows lateral position (in meters) compared to midpoint of body.

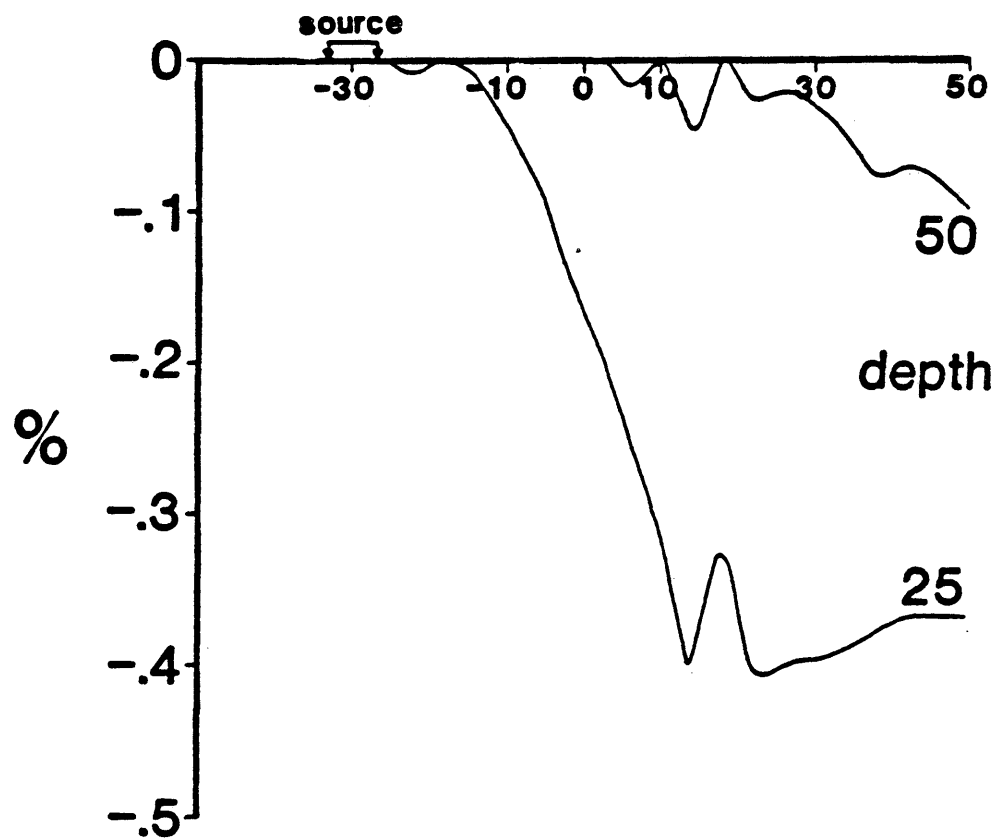


Figure 34. Equatorial-dipole response curves over 4 by 5 meter tunnel at various depths. Resistivity of host-medium 1,000 ohm-m versus infinite tunnel resistivity. Abscissa shows lateral position (in meters) compared to midpoint of body.

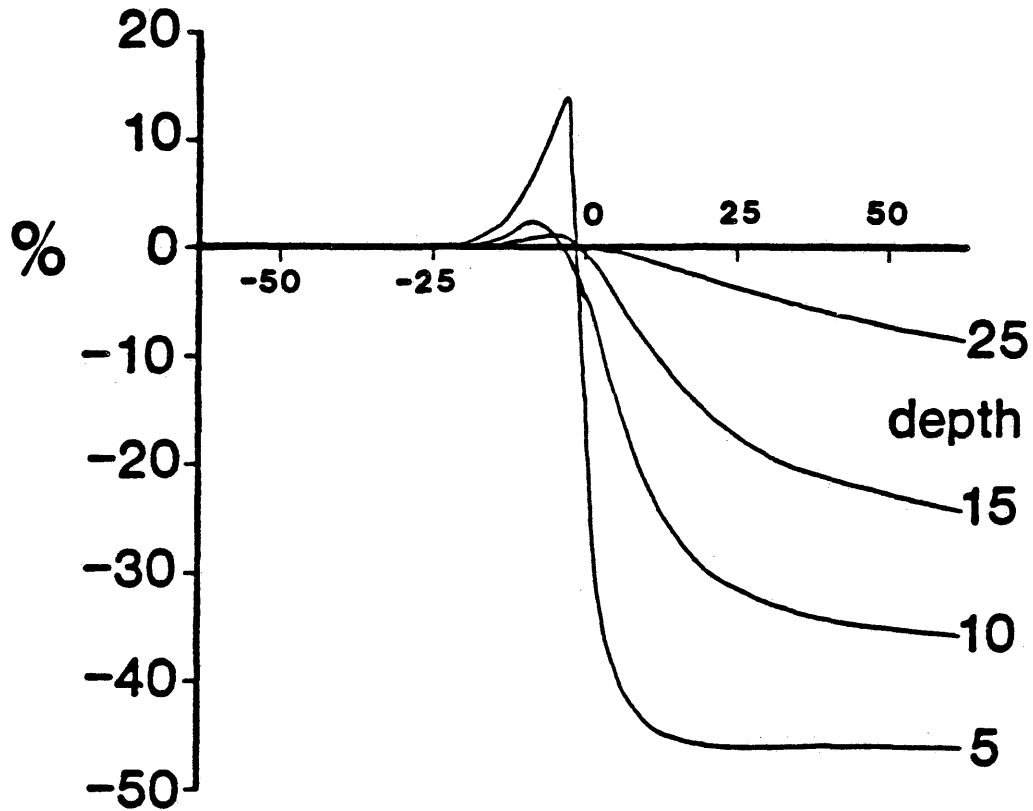


Figure 35. Polar-dipole response curves over 5 meter thick vertical fracture zone at various depths. Resistivity of host-medium 1,000 ohm-m versus 100 ohm-m for fracture zone. Abscissa shows lateral position (in meters) compared to midpoint of body.

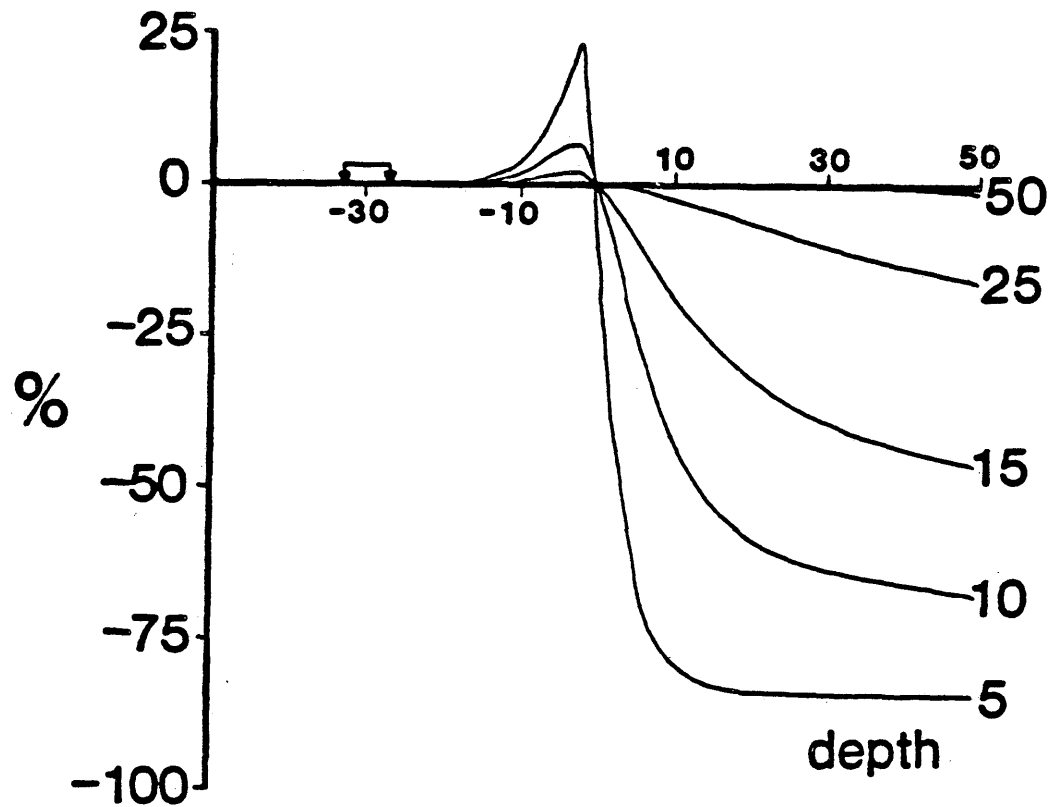


Figure 36. Polar-dipole response curves over 5 meter thick vertical fracture zone at various depths. Resistivity of host-medium 1,000 ohm-m versus 10 ohm-m for fracture zone. Abscissa shows lateral position (in meters) compared to midpoint of body.

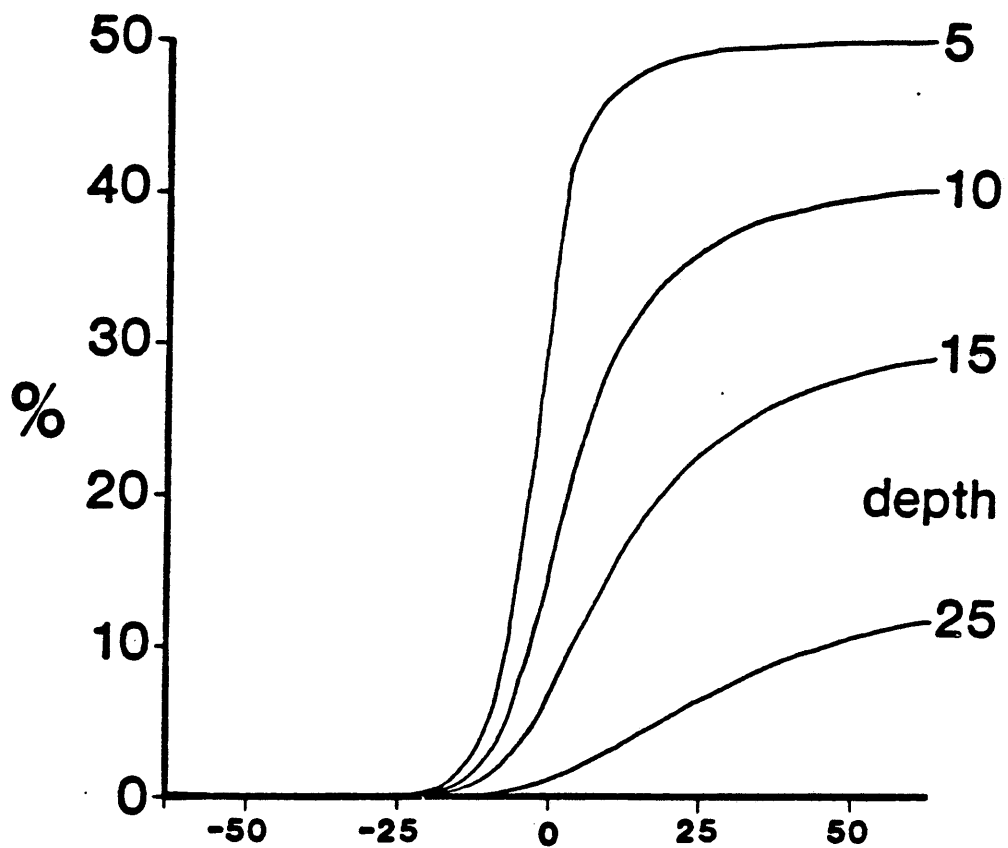


Figure 37. Equatorial-dipole response curves over 5 meter thick vertical fracture zone at various depths. Resistivity of host-medium 1,000 ohm-m versus 100 ohm-m for fracture zone. Abscissa shows lateral position (in meters) compared to midpoint of body.

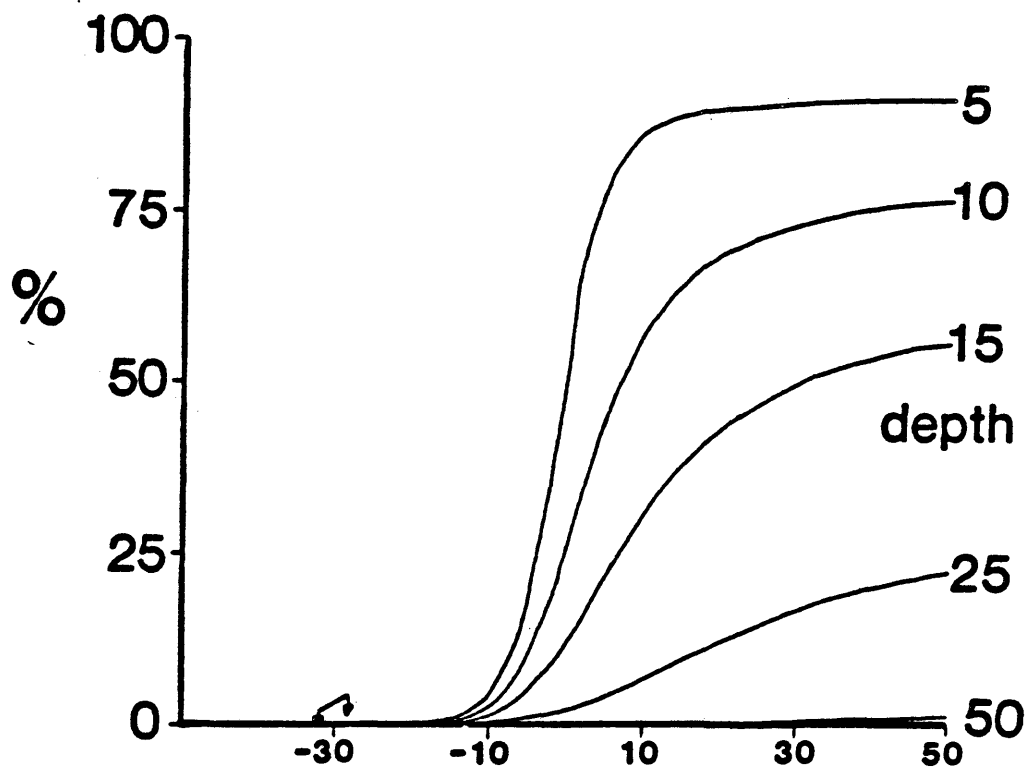


Figure 38. Equatorial-dipole response curves over 5 meter thick vertical fracture zone at various depths. Resistivity of host-medium 1,000 ohm-m versus 10 ohm-m for fracture zone. Abscissa shows lateral position (in meters) compared to midpoint of body.

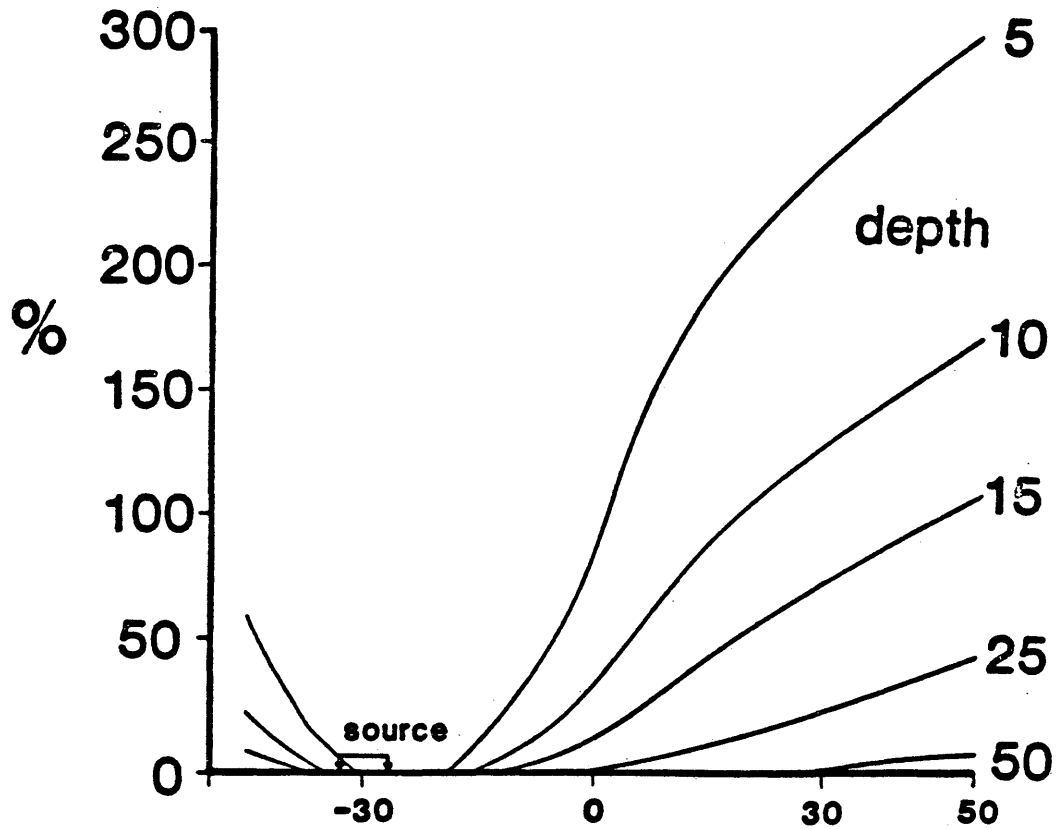


Figure 39. Polar-dipole response curves over basement fault with 5 meter vertical displacement and at various depths. Resistivity of top layer is 100 ohm-m versus 1,000 ohm-m for the basement. Abscissa shows lateral position (in meters) compared to axis of vertical displacement.

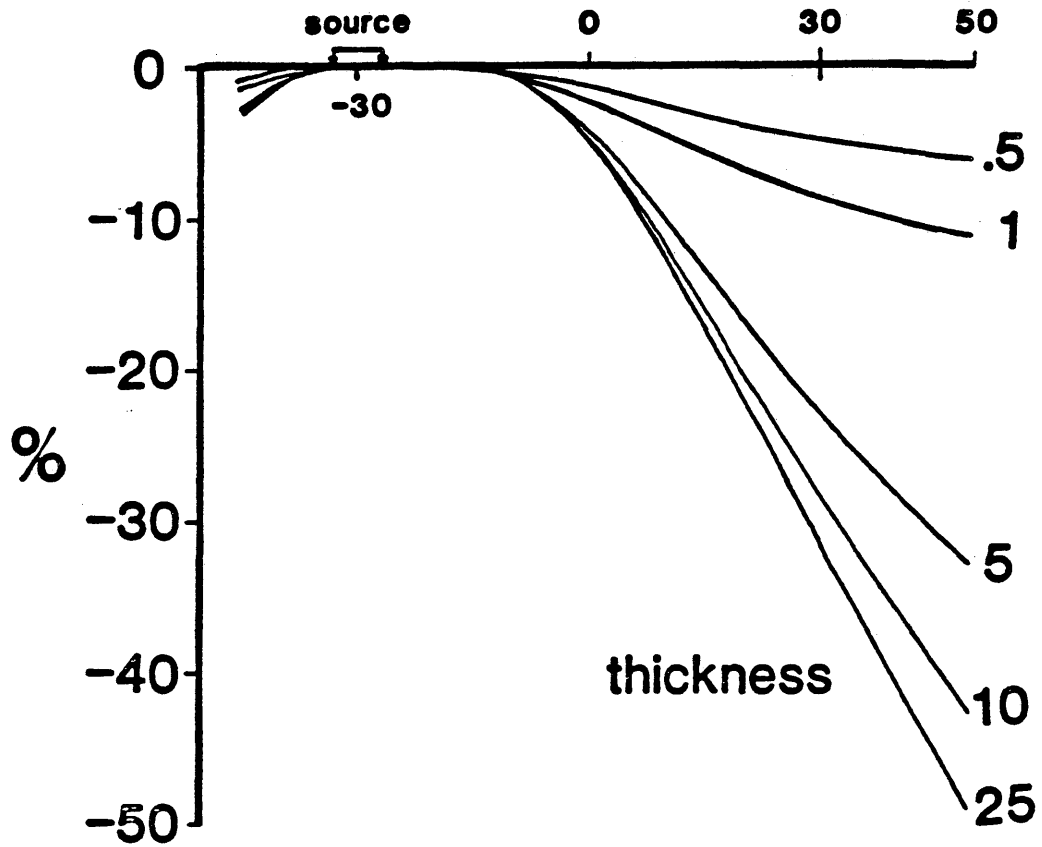


Figure 40. Polar-dipole response curves over horizontal fracture zone of various thicknesses and at 25 meters depth. Resistivity of host-medium 1,000 ohm-m versus 100 ohm-m for fracture zone. Abscissa shows lateral position (in meters) compared to midpoint of body.

can be increased up to ten fold by this procedure, or in the tunnel case, for example, from 5 to 50 meters.

## WAVE PROPAGATION METHODS

### ELECTROMAGNETIC MODELING

Electromagnetics (EM) is one of the most widely used methods for exploration of conductive orebodies and other conductive subsurface features such as high-porosity fracture zones. The response of the technique is best for good conductors at shallow depths and therefore EM is not much used for oil exploration in the United States (Telford et.al., 1976). However, in the Soviet Union wide use is made of the method as an oil exploration tool.

The electromagnetic method is more flexible than the direct-current resistivity method because frequency can be used as a controlling parameter for depth penetration as well as electrode separation. Another advantage is that the source and receiver do not make contact with the earth. This is a great advantage in rough terrain and in the presence of high resistivity surface material (Keller, 1979).

Several source and receiver configuration options are possible by varying the tilt of the loops from vertical to horizontal or by exchanging one loop for a pair of electrodes. When magnetic dipole sources (loops) are used, the most commonly measured quantity is the magnetic field (Stoyer, in press).

The electromagnetic technique is based on the induction phenomenon which occurs when a time-varying magnetic field develops a secondary current. Because electrical conduction is a diffusion process, and because the earth behaves as a conductor, electromagnetic waves lose energy at a rapid rate in it.

EM measurements are sensitive to three physical properties. These are the magnetic permeability (usually set equal to the free space value), dielectric permittivity (generally considered to be zero), and conductivity of the medium. The electrical conductivity is by far the most important physical property for both DC and EM methods (Stoyer, in press). As was described in more detail in the direct-current section, water content is the single most important factor for shallow applications.

Peter and Bardeen (1932) developed an equation for determining the depth of penetration of electromagnetic waves as a function of frequency. They showed that there is

an optimum frequency , "f", that will give the greatest strength of returned signal from a conductor at a depth "h" where the resistivity in the overlying material is "rho". It can be determined from the relation

$$h ( f / \rho )^{1/2} = 10$$

where "h" is depth in meters, "f" is frequency in hertz, and "rho" is resistivity in ohm-cm. For a depth of 50 meters and a resistivity of 5,000 ohm-m, this equation shows that the best frequency is 20 kHz. On the other hand, a 20 kHz signal frequency will have a wavelength of 15 km with a resolution capability of nil for engineering applications. A frequency of 50 MHz with a wavelength of 6 meters is more suited for the resolution needed. But according to the above relationship, this would give an optimum depth penetration of only 1 meter. This example shows the trade-off situation encountered between resolution and depth penetration for electromagnetic waves.

In order to obtain the necessary resolution, one must settle for the very attenuated signal from a megahertz source. This implies that a very large dynamic range is needed to enhance these weak signals relative to the noise. Equipment with a dynamic range of more than 100 dB is currently under development for acoustic crosshole measurements,

indicating a future for weak EM response signals in engineering applications.

Borehole-to-borehole electromagnetic surveys using very high frequencies (10 to 100 MHz) have been used to delineate small, high-contrast subsurface targets (Lytle et.al., 1979). Lytle uses a tomographic approach to determine the lateral and vertical position of the investigated tunnel structures.

#### ELECTROMAGNETIC MODELING PROGRAM USED

The same computer program described for the direct-current electrical modeling was used for the electromagnetic survey simulation.

#### RESULTS OF ELECTROMAGNETIC MODELING

Vertical and horizontal fracture zones, tunnel and basement-fault models were investigated using the electromagnetic method. Signal frequencies of 50 kHz for the simulated surface data and 50 MHz for the crosshole data were employed.

Loop sources in two directions were used for the surface EM survey (Fig. 41). The horizontal magnetic dipole (HMD), with the loop vertical and the field lines parallel to the line of survey, and the vertical magnetic dipole (VMD), with the loop horizontal, were both used.

## 2-D EM Survey Model

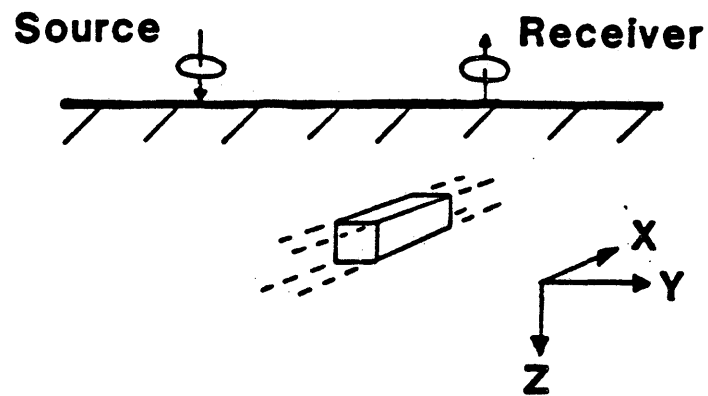


Figure 41. Electromagnetic survey model in 2-D.

Results are presented as a percentage difference between total field and primary field, where a negative number indicates a decrease in field strength with the anomalous body present as compared to a survey without the body. All surface results include both real and imaginary components, giving a complex amplitude response.

Resolution capability of electromagnetics for resistive structures such as tunnels is very weak. For conductive bodies, like the vertical fracture zone, the response is better. Figure 42 shows the response for the VMD-source over a fracture zone with a resistivity of 100 ohm-m compared to the surrounding medium's 1,000 ohm-m. With a resistivity contrast of two orders of magnitude (Fig. 43) the amplitude of the anomaly is higher, but still somewhat less than that for the direct-current method. This is because it is a pure induction phenomenon in the EM case. However, noise from near-surface variations and the cost of the survey would be much less than for the DC survey.

The horizontal magnetic dipole (HMD) response (Fig. 44) is only one third of the VMD's response for the high-contrast resistivity model, and only one fifth in the low-contrast case (Fig. 45). The limitations of the modeling technique are obvious in the irregular response

curves. This noise is introduced by the numerical technique employed.

Figures 46 and 47 show that the responses over a horizontal fracture zone and a basement fault are fairly high in amplitude. In spite of favorable amplitude characteristics, the breadth of the anomalies would very likely cause them to be hidden in background noise, except for shallow features.

A borehole-to-borehole model study was performed with a tunnel in various positions (Fig. 48). A signal frequency of 50 MHz was also employed. In the simulated crosshole surveys, source and receiver were moved together from the bottom of the hole to the top, creating symmetric anomalies. Figure 49 shows the results for the three different tunnel positions. These response curves represent the total complex amplitude, considering both the in-phase (real) and the out-of-phase (imaginary) components. The largest anomaly occurs when the tunnel is in location two, that is, off center but still between the boreholes. An anomaly is still visible when the tunnel is outside the region between the holes (location 3), and this is more pronounced on the in-phase response curve (Fig. 50) which crosses zero several times.

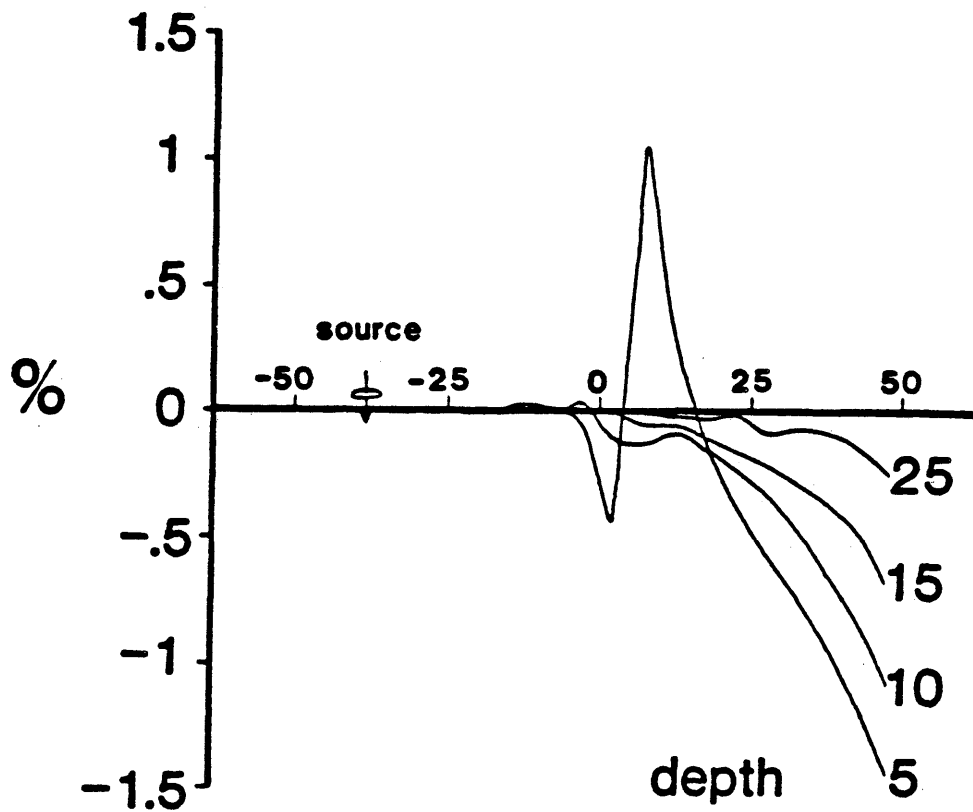


Figure 42. Electromagnetic complex amplitude response over 5-meter-thick vertical fracture zone at various depths. 50 kHz VMD-source. Resistivity of host-medium 1,000 ohm-m versus 100 ohm-m for fracture zone. Abscissa shows lateral position (in meters) compared to midpoint of body.

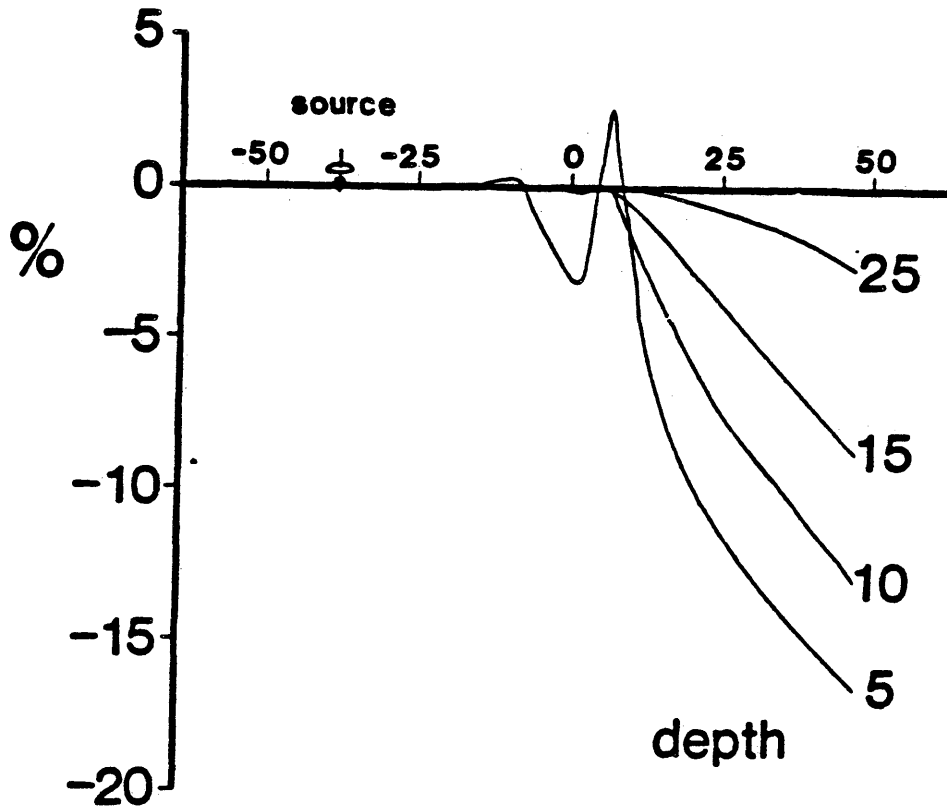


Figure 43. Electromagnetic complex amplitude response over 5-meter-thick vertical fracture zone at various depths. 50 kHz VMD-source. Resistivity of host-medium 1,000 ohm-m versus 10 ohm-m for fracture zone. Abscissa shows lateral position (in meters) compared to midpoint of body.

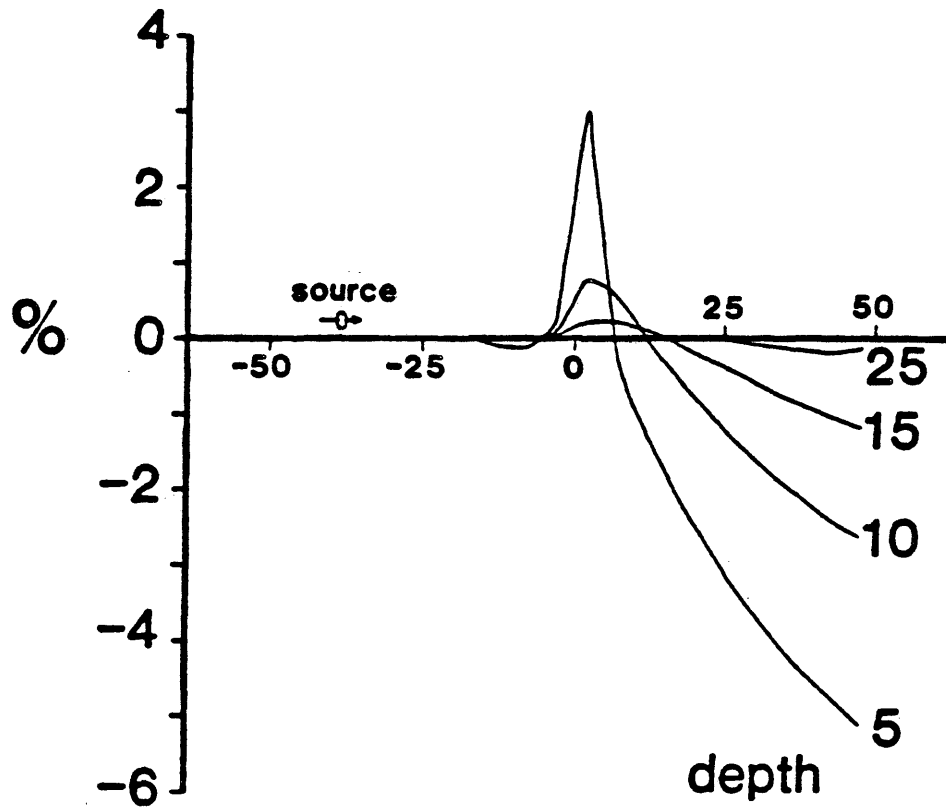


Figure 44. Electromagnetic complex amplitude response over 5-meter-thick vertical fracture zone at various depths. 50 kHz HMD-source. Resistivity of host-medium 1,000 ohm-m versus 10 ohm-m for fracture zone. Abscissa shows lateral position (in meters) compared to midpoint of body.

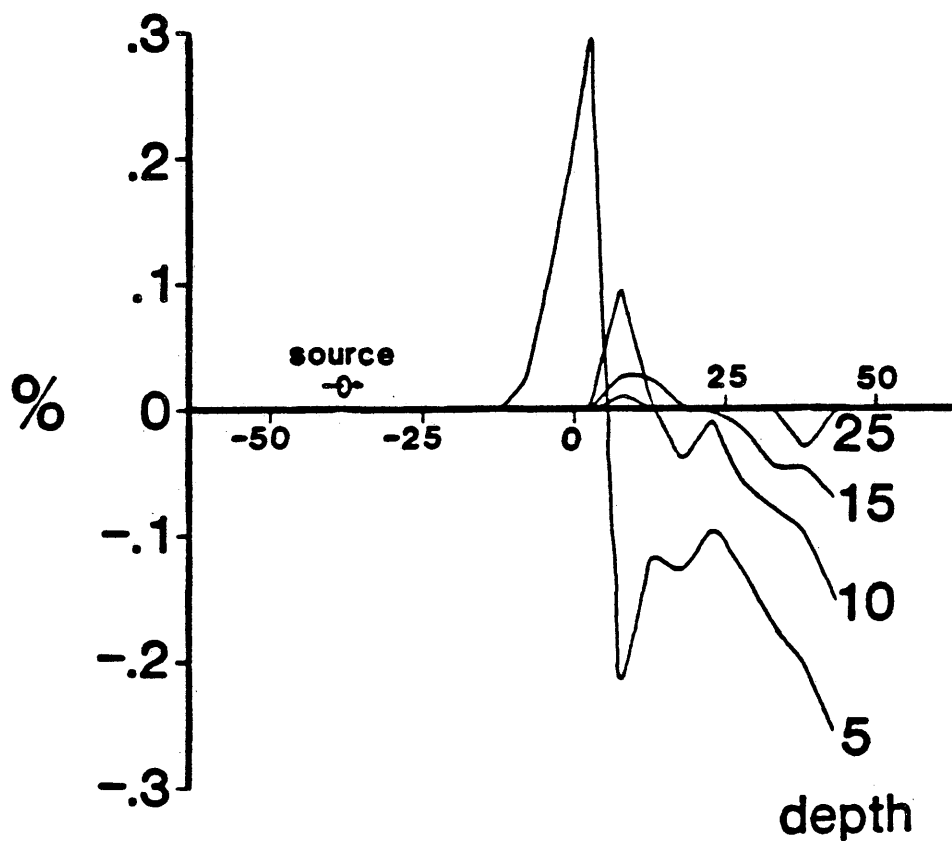


Figure 45. Electromagnetic complex amplitude response over 5-meter-thick vertical fracture zone at various depths. 50 kHz HMD-source. Resistivity of host-medium 1,000 ohm-m versus 100 ohm-m for fracture zone. Abscissa shows lateral position (in meters) compared to midpoint of body.

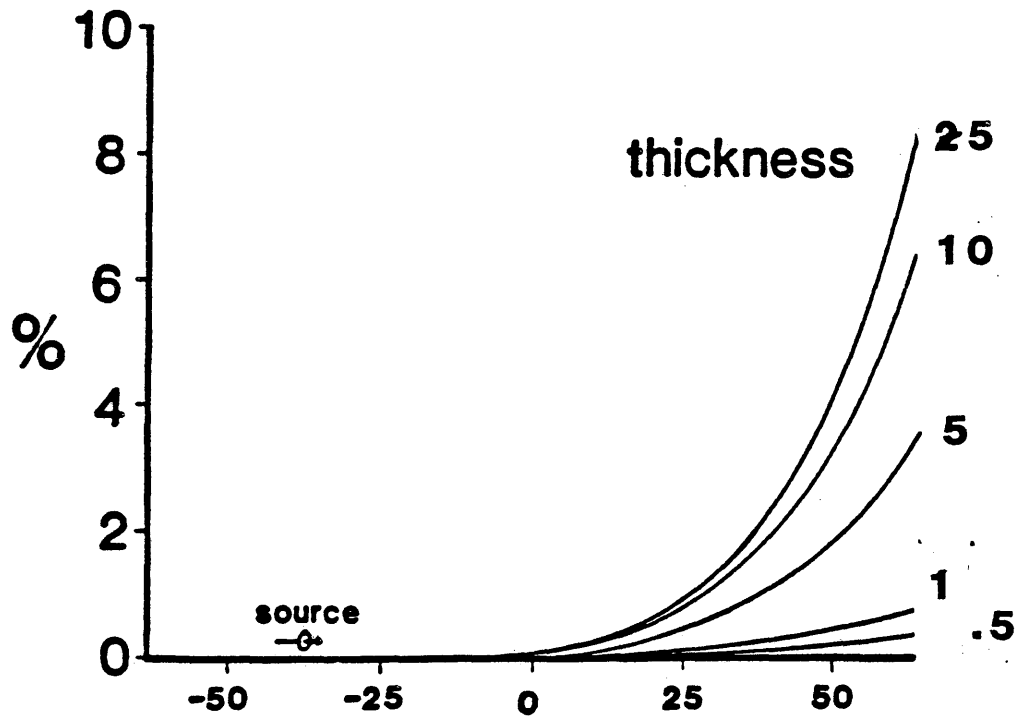


Figure 46. Electromagnetic complex amplitude response curves over horizontal fracture zone of various thicknesses and at 25 meters depth. Resistivity of host-medium 1,000 ohm-m versus 100 ohm-m for fracture zone. Abscissa shows lateral position (in meters) compared to midpoint of body.

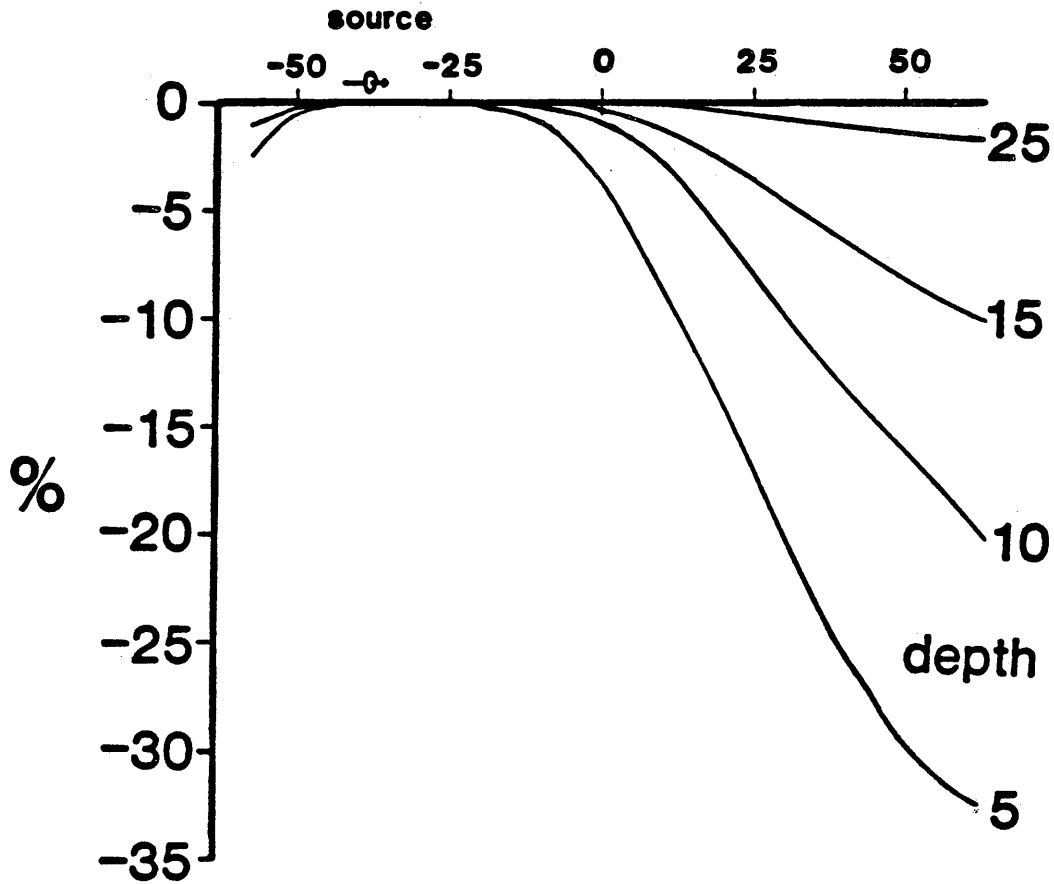


Figure 47. Electromagnetic complex amplitude response curves over basement fault with 5-meter vertical displacement and at various depths. Resistivity of top layer is 100 ohm-m versus 1,000 ohm-m for the basement. Abscissa shows lateral position (in meters) compared to axis of vertical displacement.

## 2-D Borehole-to-Borehole EM Tunnel Model

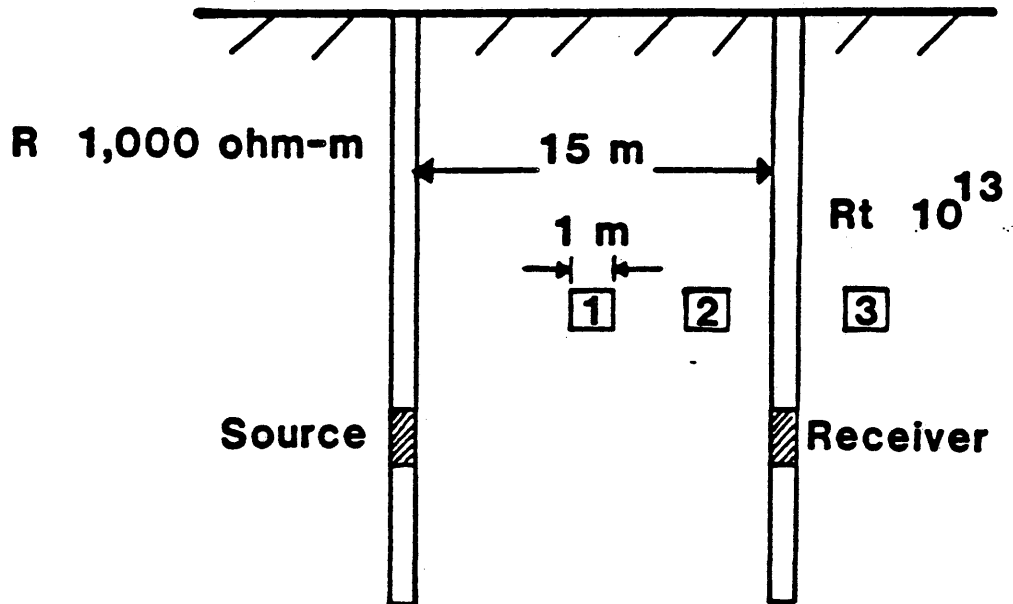


Figure 48. Borehole-to-borehole electromagnetic tunnel model in 2-D. Three tunnel locations modelled. Resistivity of host-medium 1,000 ohm-m versus  $10.E13$  ohm-m for tunnel.

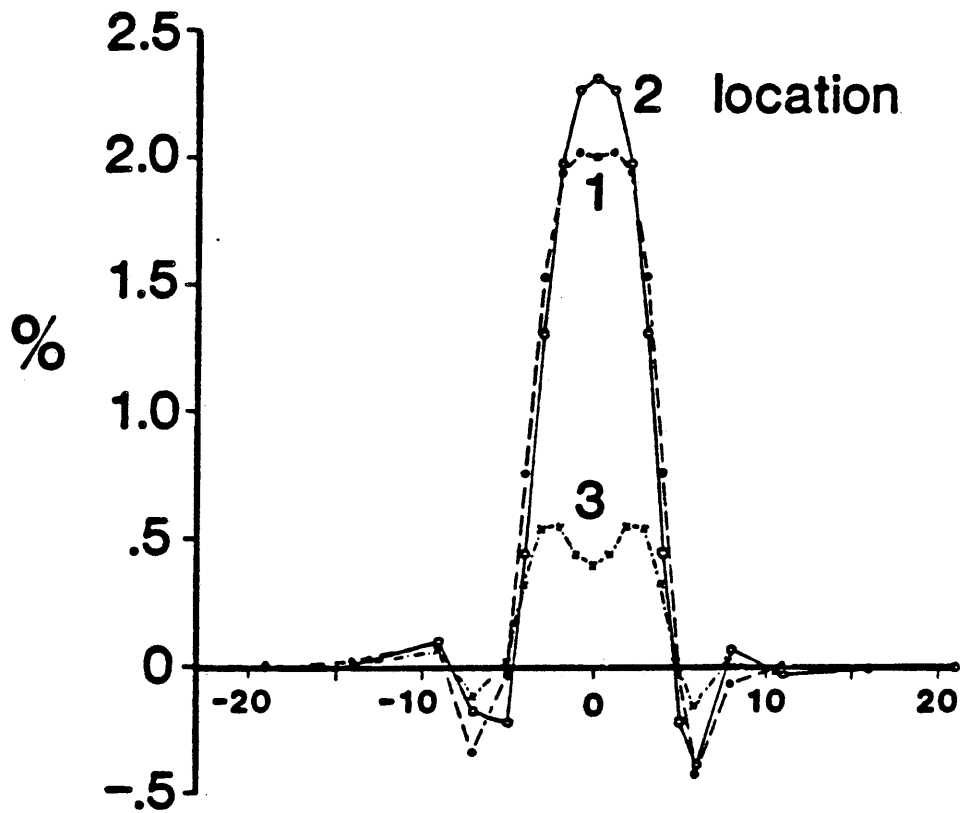


Figure 49. Borehole-to-borehole complex amplitude electromagnetic response curves in presence of tunnel in various locations. 50 MHz source signal. Abscissa shows lateral position (in meters) compared to midpoint of body.

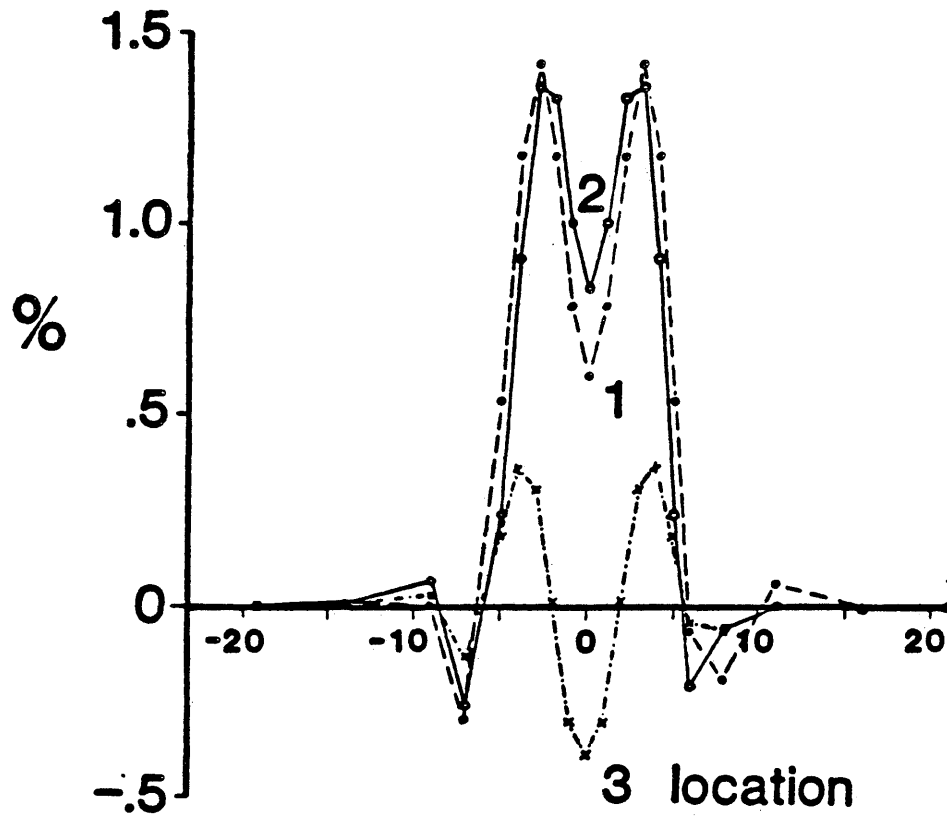


Figure 50. Borehole-to-borehole in-phase (real) electromagnetic response curves in presence of tunnel in various locations. 50 MHz source signal. Abscissa shows lateral position (in meters) compared to midpoint of body.

Although these anomalies are somewhat small, their magnitudes may be increased when many measurements can be made in a relatively quiet environment.

#### MAGNETOTELLURIC MODELING

The magnetotelluric method has been utilized primarily to probe the subsurface at depths on the order of kilometers. Using the very low frequencies (below 1 Hz), a depth penetration to the Mohorovicic discontinuity can be achieved. Engineering applications require higher frequencies, on the order of kilohertz, in order to resolve the small targets involved.

The method can be divided into magnetotellurics (MT) and audio magnetotellurics (AMT), where the latter make use of frequencies in the higher audible part of the spectrum. The MT methods employ as a source the electrical currents that naturally occur in the ionosphere. Artificial sources like radio transmitters can be utilized as plane wave sources. These sources usually transmit in the 10 to 30 kHz range and are therefore ideal for shallow engineering applications.

Field survey measurements include two components of the electrical (E) field and three components of the magnetic (H) field. The magnetotelluric noise can be very significant and therefore the statistical correlation of the E-field with the H-field must be high or the data are not useful (Stoyer, in press). The apparent resistivity can be calculated from simple formulas requiring only a knowledge of the frequency and the strength of two of the field measurements ( $E_x$  and  $H_y$ ) (Keller, 1979). Pseudosections with the period as the depth scale can be made to display the data, although simulated individual response curves are presented in this work.

Resolution depends on the frequency used, and then the trade-off between resolution and penetration, as discussed in the electromagnetic section, has to be considered. Magnetotellurics is not a high resolution tool, as is evident from the results presented in this work.

#### MAGNETOTELLURIC MODELING PROGRAM USED

The computer program used for the magnetotelluric modeling was written by Dr. Stoyer at the Colorado School of Mines after Rodi (1976). This is a finite difference modeling program in two dimensions with conductivities defined for each grid-space. The only other parameter needed as

input is the period of the probing plane wave source. As was the case for the electromagnetic modeling program, the accuracy depends on the fineness of the mesh and how far from the grid-edges the body of interest is located. Nevertheless, the accuracy of the numerical model is supposed to be better than that of an actual field survey.

#### RESULTS OF MAGNETOTELLURIC MODELING

Figure 51 displays the magnetotelluric survey model used. Models of a vertical fracture zone and tunnel were investigated. In the high-resistivity-contrast case, a fracture zone with a thickness of five meters (Fig. 52) gives an amplitude that is similar to that obtained for a simulated artificial source EM survey over the same body. The low-contrast model (Fig. 53) gives similar high amplitudes, also higher response than the EM survey. The anomalies get very broad as the feature appears at deeper locations. However, the noise problems in magnetotelluric field surveys are expected to be much more severe.

The response of MT over a resistive structure is very weak (Fig. 54). The maximum amplitude over a 10-meter-diameter tunnel at a depth of 10 meters is only 6 percent.

### 2-D MT Survey Model

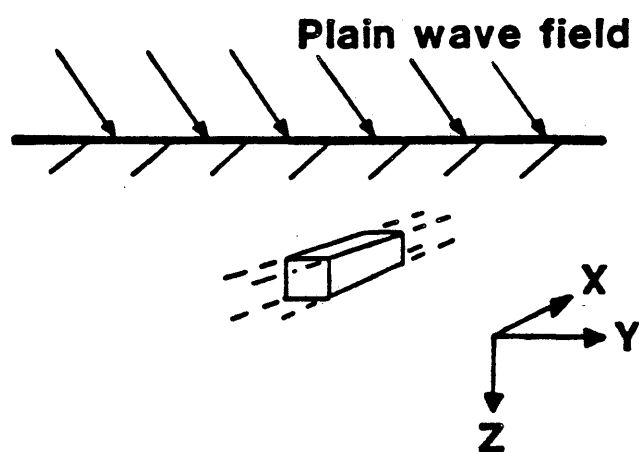


Figure 51. Magnetotelluric survey model in 2-D.

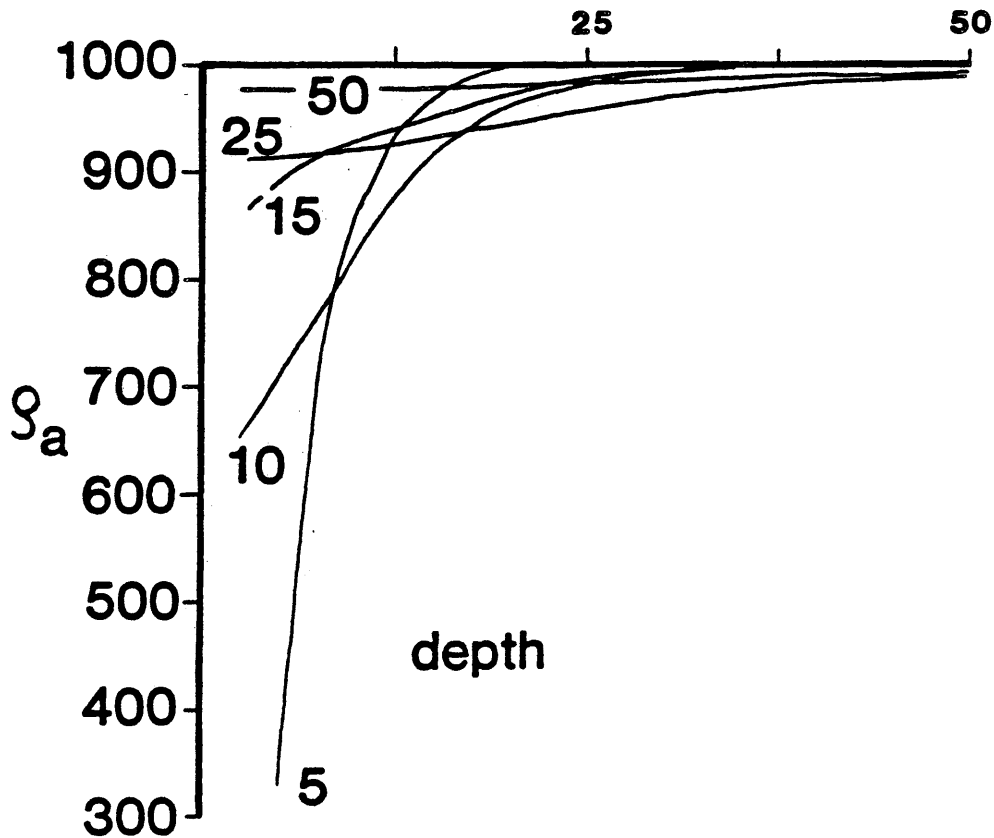


Figure 52. Magnetotelluric response curves (Hx-mode) over 5-meter-thick vertical fracture zone at various depths. Resistivity of host-medium 1,000 ohm-m versus 10 ohm-m for fracture zone. Period of source signal 1.E-4. Abscissa shows lateral position (in meters) compared to midpoint of body.

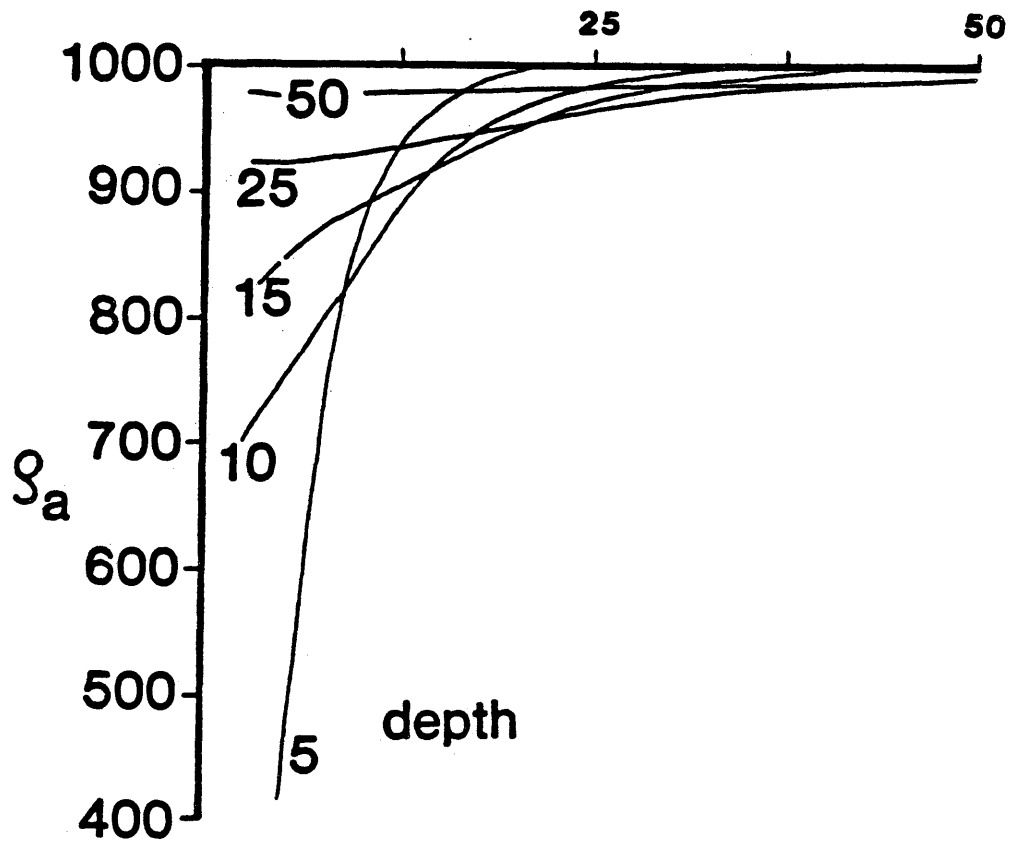


Figure 53. Magnetotelluric response curves (Hx-mode) over 5-meter-thick vertical fracture zone at various depths. Resistivity of host-medium 1,000 ohm-m versus 100 ohm-m for the fracture zone. Period of the source signal 1.E-4. Abscissa shows lateral position (in meters) compared to midpoint of body.

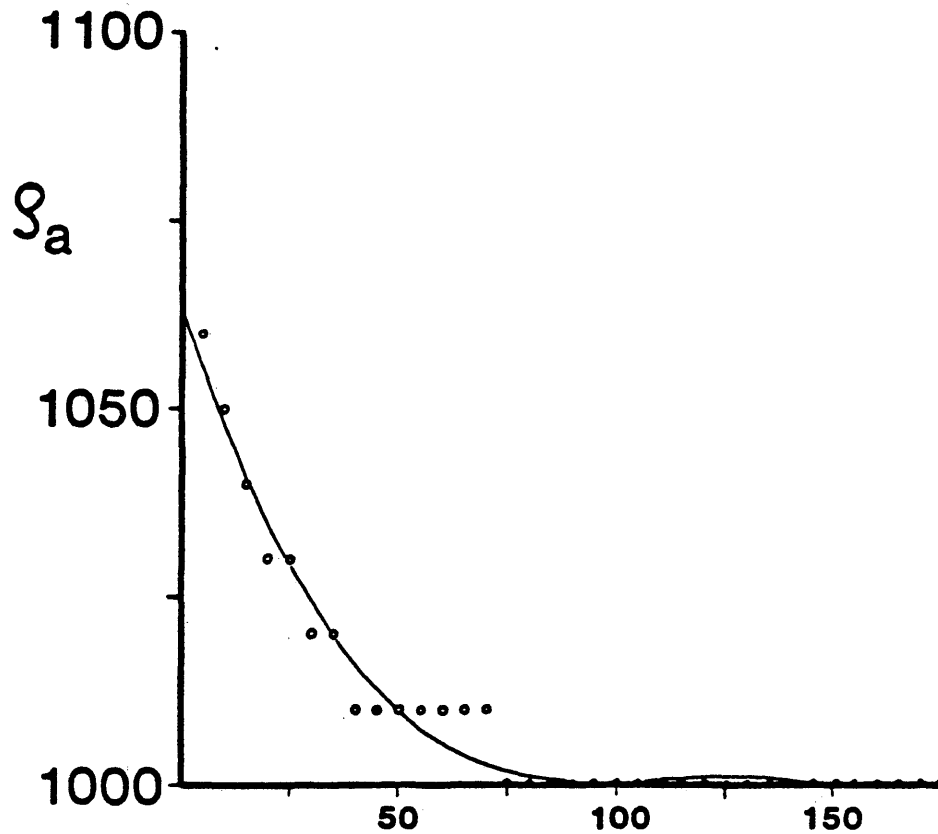


Figure 54. Magnetotelluric response curve over 10-meter-diameter tunnel at 10 meters depth. Resistivity of host-medium 1,000 ohm-m versus infinite tunnel resistivity. Period of source signal 1.E-5. Abscissa shows lateral position (in meters) compared to midpoint of body.

## REFLECTION SEISMIC MODELING

The seismic method is by far the most widely-used geophysical technique. The widespread use of the method is mainly due to its employment in exploration for petroleum, where it is used primarily for finding deep-seated targets. Frequencies used in seismic exploration are often in the 10-to-30-hertz range however high-resolution techniques utilize frequencies up to 125 Hz for 3-D surveys and stratigraphic-trap exploration. Engineering applications require higher frequencies to resolve the relatively small targets at shallow depths. These higher frequencies are more attenuated than the lower frequencies, resulting in the previously discussed trade-off between resolution and penetration. Attenuation of high frequency components of a seismic signal is a result of a combination of factors, such as absorption, scattering, diffraction, varying source and receiver coupling and multipath interference effects (Farr, 1978; Trorey, 1962; McDonal et.al., 1958; Tullos and Reid., 1969; O'Doherty and Anstey, 1971).

A comparison between a typical exploration problem (Fig. 55) and a tunnel detection problem (Fig. 56) was done to exemplify the special difficulties of engineering applications of the reflection seismic method. The

# Scale of Exploration Problem Seismic

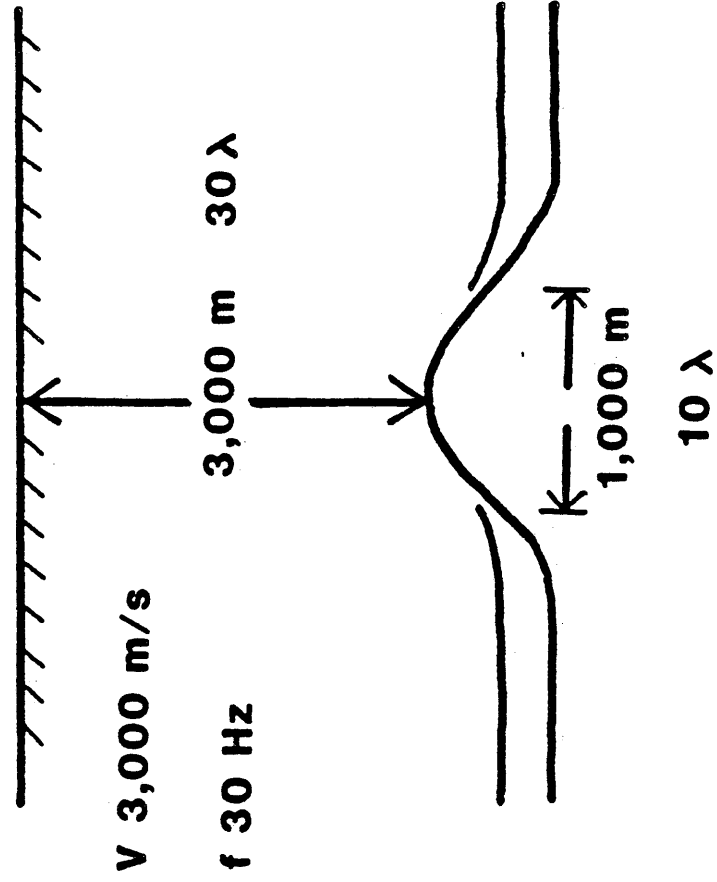


Figure 55. Geological model for petroleum exploration problem. Dimensions in meters and wavelengths derived from assumed velocity and frequency.

# Scale of Engineering Problem

## Seismic

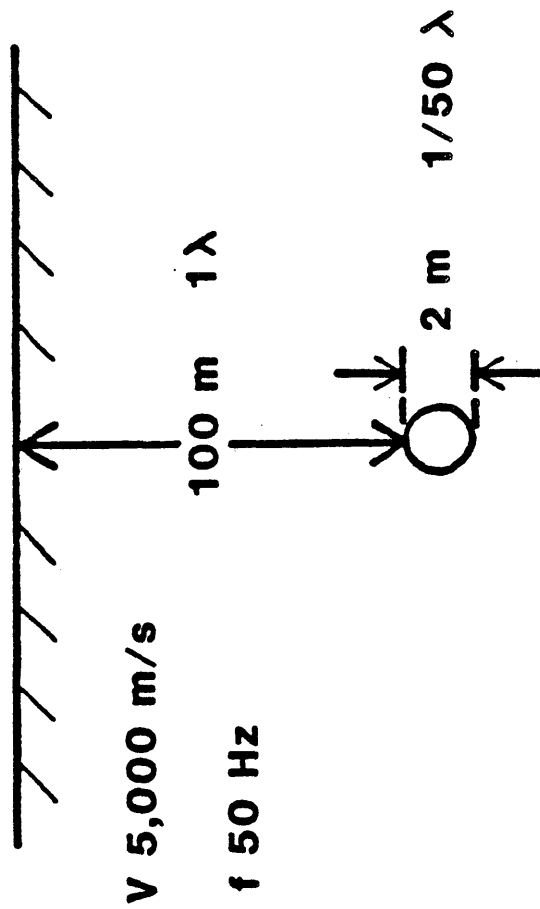


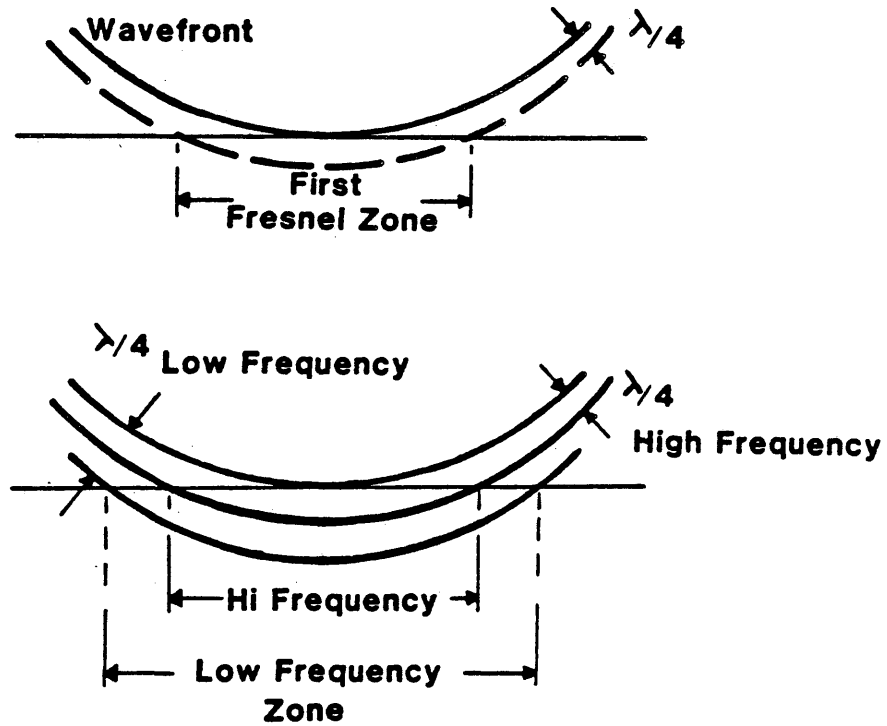
Figure 56. Geological model for engineering problem. Dimensions in meters and wavelengths derived from assumed velocity and frequency.

exploration problem could be modeled as a sedimentary section with an average velocity of 3,000 m/s, a target depth of 3,000 meters, and a target width of 1,000 meters. For a signal frequency of 30 Hz the depth to the body would represent 30 wavelengths and the width of the body 10 wavelengths. For the engineering problem the scale is different. Assuming a hard rock environment with average velocity 5,000 m/s and a higher-frequency seismic signal of 50 Hz, the 100 meters to the target would represent only one wavelength. If the target is a tunnel with a 2 meter diameter, this is, then,  $1/50$  wavelength across. For a very high frequency, like 500 Hz, the diameter still represents only  $1/5$  of a wavelength.

Figure 57 (Sheriff, 1977) shows the frequency dependence of lateral resolution. Modeling using ray theory assumes a reflection comes from a single point on the reflector. This is not true. The spherical wavefront will make contact with the reflector over a finite area. The size of this area depends on the frequency. A low frequency gives a large so-called fresnel zone, whereas a higher frequency leads to a smaller fresnel zone and higher lateral resolution.

Previous authors (Widess, 1973; Farr, 1979) have set the limit of vertical seismic resolution of a thin bed to approximately  $1/12$  of a wavelength. The tunnel and the thin

## Lateral Resolution for Spherical Waves



After: Sheriff, 1977

Figure 57. Frequency dependence of lateral resolution for spherical waves.

bed have comparable spatial dimensions in two directions but differ drastically in the third. This implies that, in contrast to vertical resolution of thin beds, detection of tunnels depends on handling both a vertical and a spatial resolution problem. Relatively higher frequencies are required to provide improved spatial resolution of the tunnel, but they are subject to greater attenuation than the relatively lower frequencies which would resolve a thin bed.

It can be seen in Figure 58 that for a 100-Hz signal the response from the tunnel would be less than 10 % of that from a thin bed, under the assumptions made. This implies that detection of the tunnel requires not  $1/12$  of a wavelength across the target, but rather one wavelength or more. As Figure 56 indicated for the engineering-scale problem, the actual size of the target was  $1/50$  to  $1/5$  wavelength depending on frequency.

The Southwest Research Institute (Owen, et.al., 1976) shows promising results using a conventional seismic reflection technique with field operations adapted to very-high-frequency (more than 500 Hz) detection. By using explosives as sources and hydrophones as receivers, all in water-filled boreholes to get good coupling, high-frequency energy is generated and detected. Since the signals in this situation are of relatively low amplitude, it is very

### Amplitude versus Frequency Tunnel Model

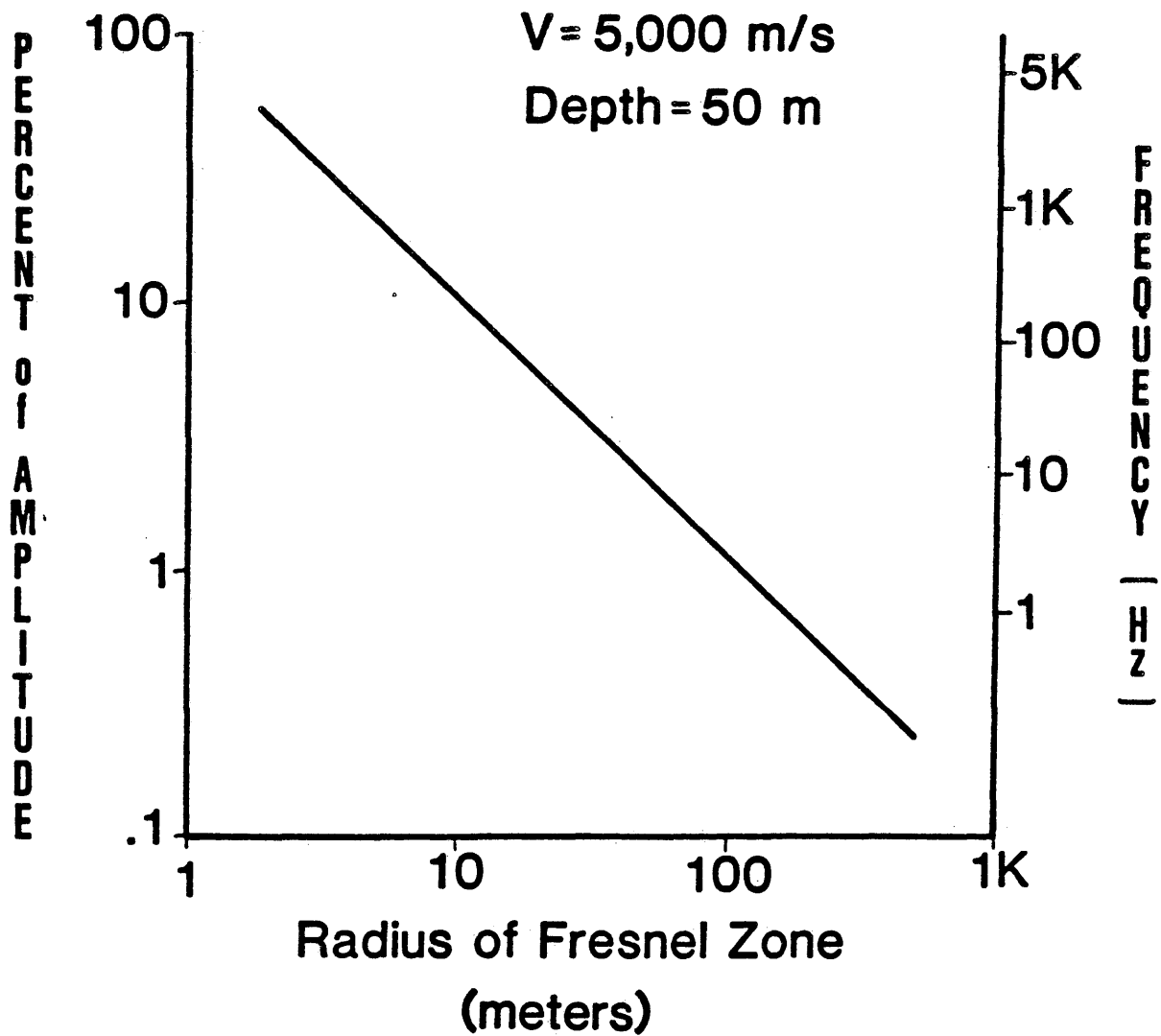


Figure 58. Magnitude of response from tunnel versus response from thin-bed, for various frequencies and fresnel-zone sizes.

important to have receiving equipment with a large dynamic range. Improvement of seismic instrumentation is very rapid, and the upper frequency limit gets higher for every new generation of equipment. Sampling rates of 1/8 msec are now possible in a 12-channel unit that gives high-frequency recording capabilities up to 2,000 hertz.

Several other approaches have been used, such as experimentation with materials for better coupling around sources and receivers (Zietz, 1959), and employment of 2-dimensional field arrays to enhance the signal-to-noise ratio and increase resolution. Acoustic crosshole techniques, using a sparker source in the 50- to 100-kHz frequency range, can effectively resolve small targets if separation between the boreholes is not too great (less than 100 meters) (McCann et.al., 1975).

#### REFLECTION SEISMIC MODELING PROGRAMS USED

Seismic state-of-the-Art exploration modeling software from Compagnie Generale de Geophysique (CGG) and Geoquest's "Advanced Interpretation Modeling System" (AIMS) packages were used in this work. Both a normal-incidence ray-theory program (MODIN) and a vertical-incidence wave-theory modeling program (WEMOD) from the CGG software were tried

and found to be inappropriate for applications involving modeling the sharp curvatures of the tunnel.

The AIMS package also provides a ray-tracing module where the user defines an array of source points from which to trace rays. A common source/receiver configuration was used for both ray-theory and wave-theory modeling. This gives rays emitted on a perpendicular from the deepest reflector and traced upwards. The wave-theory portion of the AIMS software is based on the Kirchhoff theory. Kirchhoff wave-theory modeling assumes that the seismic response of an interface is the integral of the response of all the points on the interface. This program automatically traces diffracting rays from every depth-control-point input by the user. This means that at each surface point, rays will emerge which have been traced for all points defined on each interface. The "spikeogram" (Figs. 60, 61 and 62) is then based on these rays, and to get a realistic synthetic time section these impulses have to be convolved with a user-specified wavelet (Geoquest, 1979).

#### RESULTS FROM REFLECTION SEISMIC MODELING

Only results from the tunnel model (Fig. 59) with various diameters and a depth of 50 meters are presented here. Several authors have already described response for a

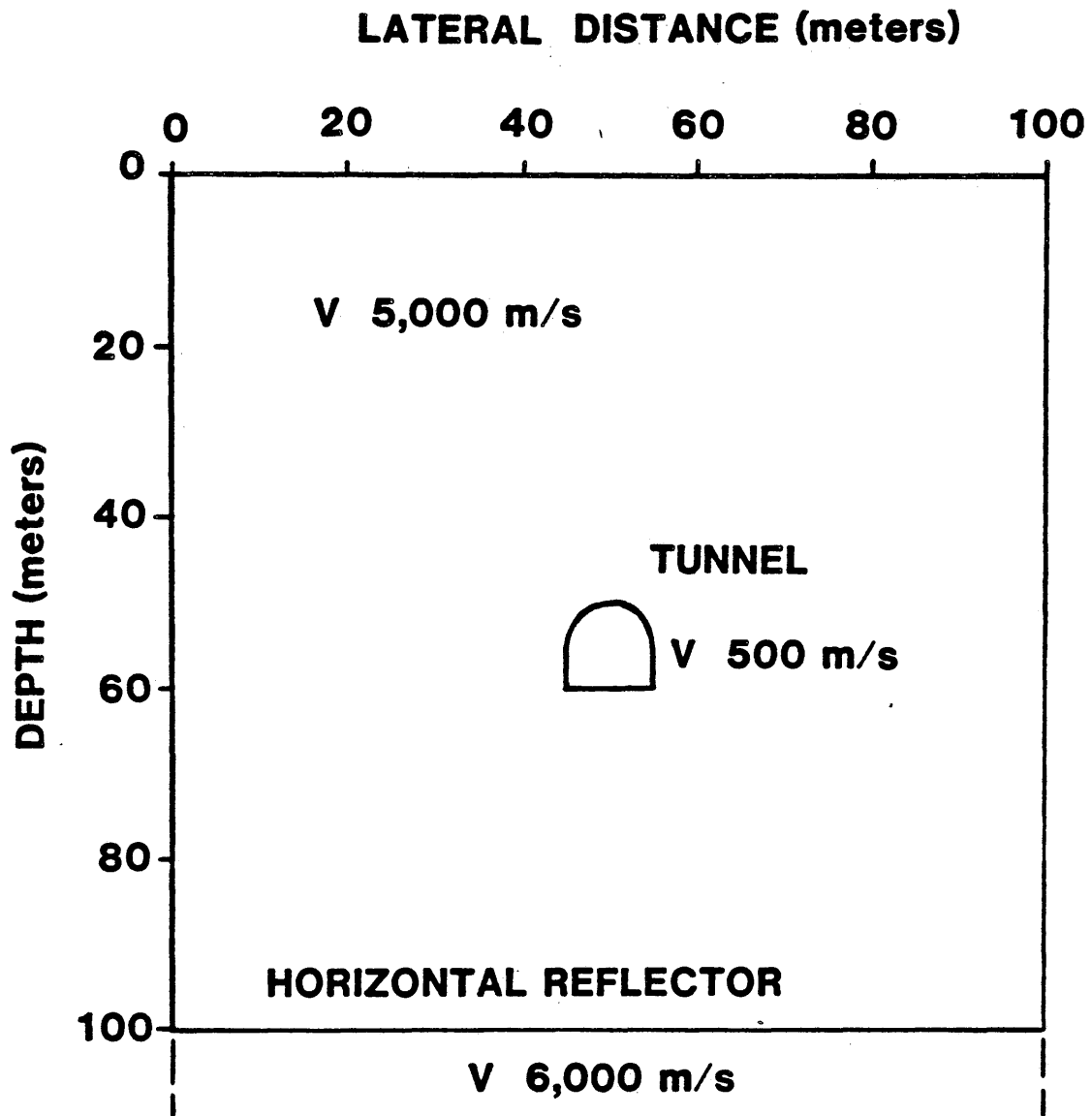


Figure 59. Tunnel model used for reflection seismic modeling.

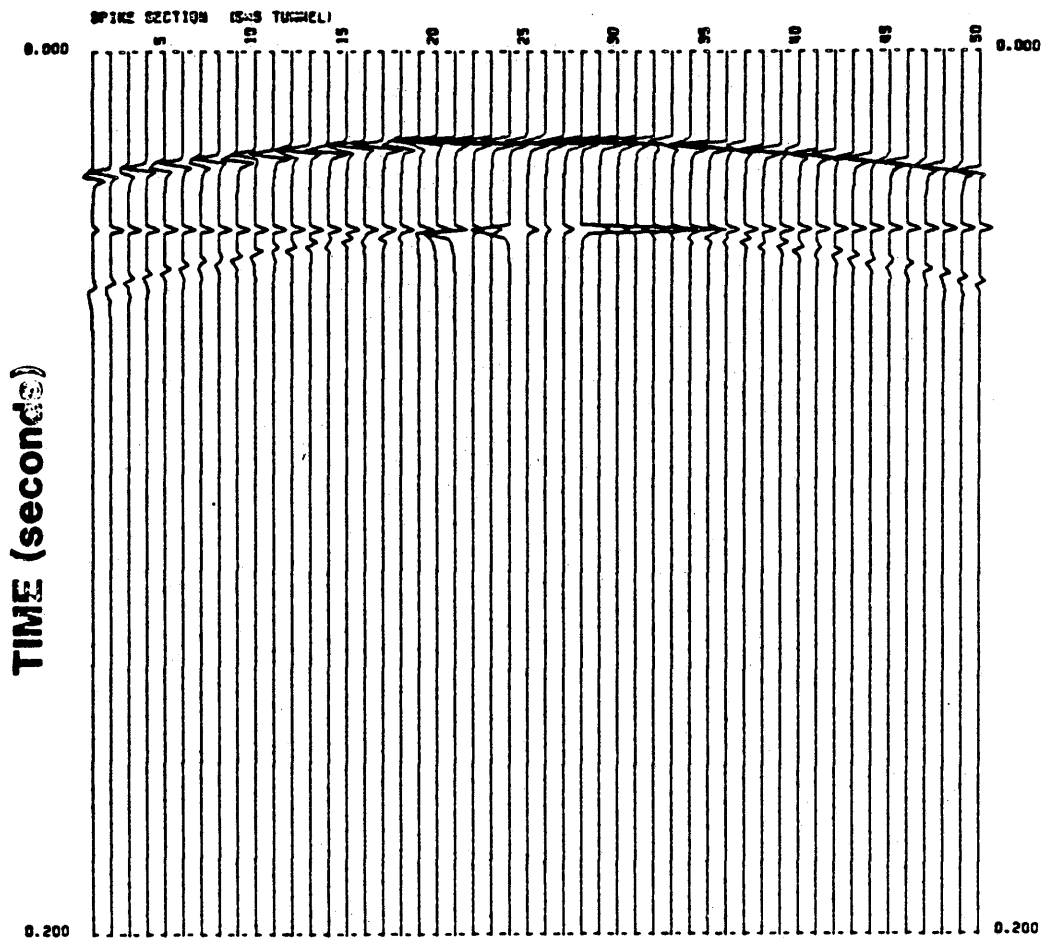


Figure 60. Wave-theory synthetic seismic spike section from tunnel model. Tunnel diameter is 5 meters. Horizontal axis represents trace numbers with 2-meter lateral separation.

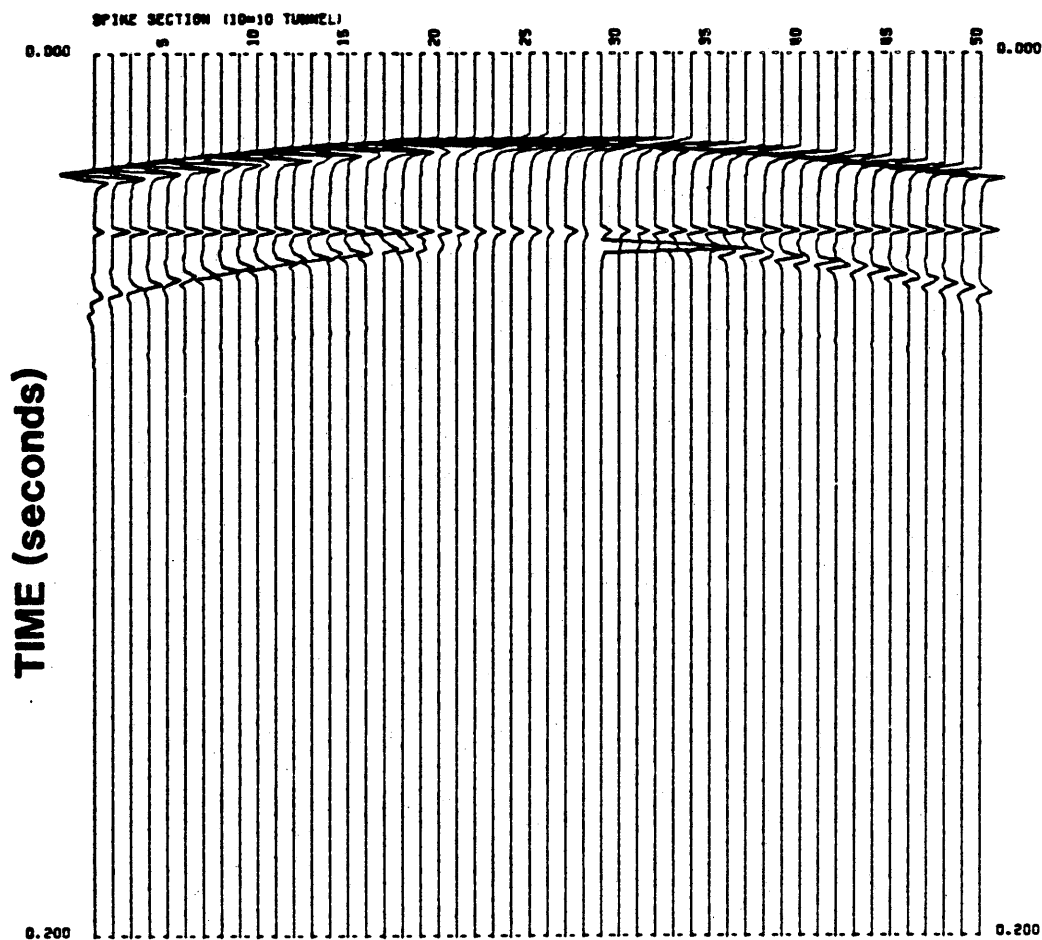


Figure 61. Wave-theory synthetic seismic spike section from tunnel model. Tunnel diameter is 10 meters. Horizontal axis represents trace numbers with 2-meter lateral separation.

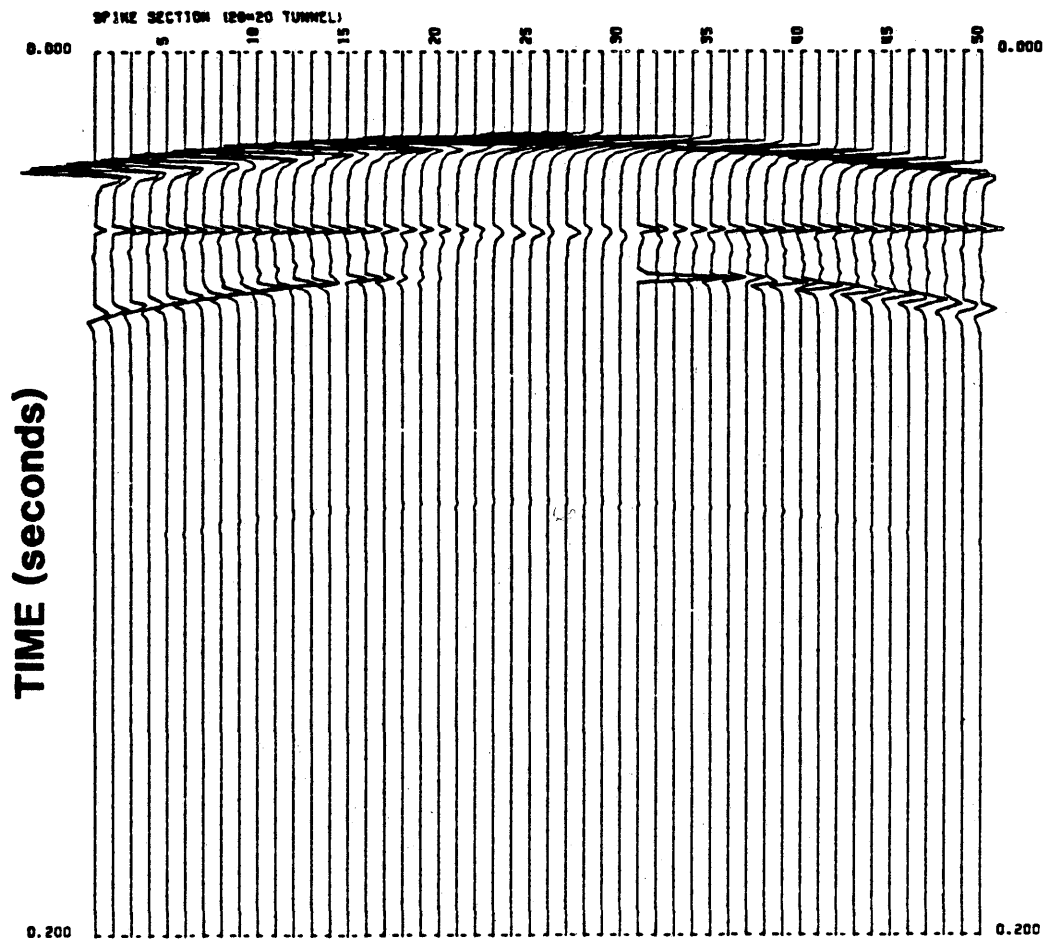


Figure 62. Wave-theory synthetic seismic spike section from tunnel model. Tunnel diameter is 20 meters. Horizontal axis represents trace numbers with 2-meter lateral separation.

horizontal thin bed, and the basement fault and the vertical fracture zone models give similar diffraction patterns as the tunnel, except not as intense.

GeoQuest's AIMS modeling software was used to model the tunnel utilizing both ray-theory and wave-theory techniques with a zero-phase wavelet and signal frequencies of 10-50 Hz. The most obvious difference between the ray-theory and the wave-theory results is seen on the horizontal reflector underneath the tunnel. This event is continuous in the wave theory model with only a decrease in the amplitude under the tunnel (Figs. 60, 61 and 62), whereas the ray-theory model shows a gap in the reflector (Figs. 63, 64 and 65). This difference is due to the upward, normal-incidence ray tracing, where rays from underneath the tunnel will diverge outside the section at the surface. Diffractions from the top of the tunnel give a high-amplitude event for all three tunnel dimensions investigated (Figs. 66, 67 and 68). In the low noise case (noise -36 dB compared to maximum signal) the decrease in the amplitude on the lower horizontal reflector can easily be seen on the 20-by-20 meter tunnel model, but the signal reflected by the 10-by-10 meter and 5-by-5 meter tunnels is too incoherent to make an accurate interpretation regarding the source of the reflection.

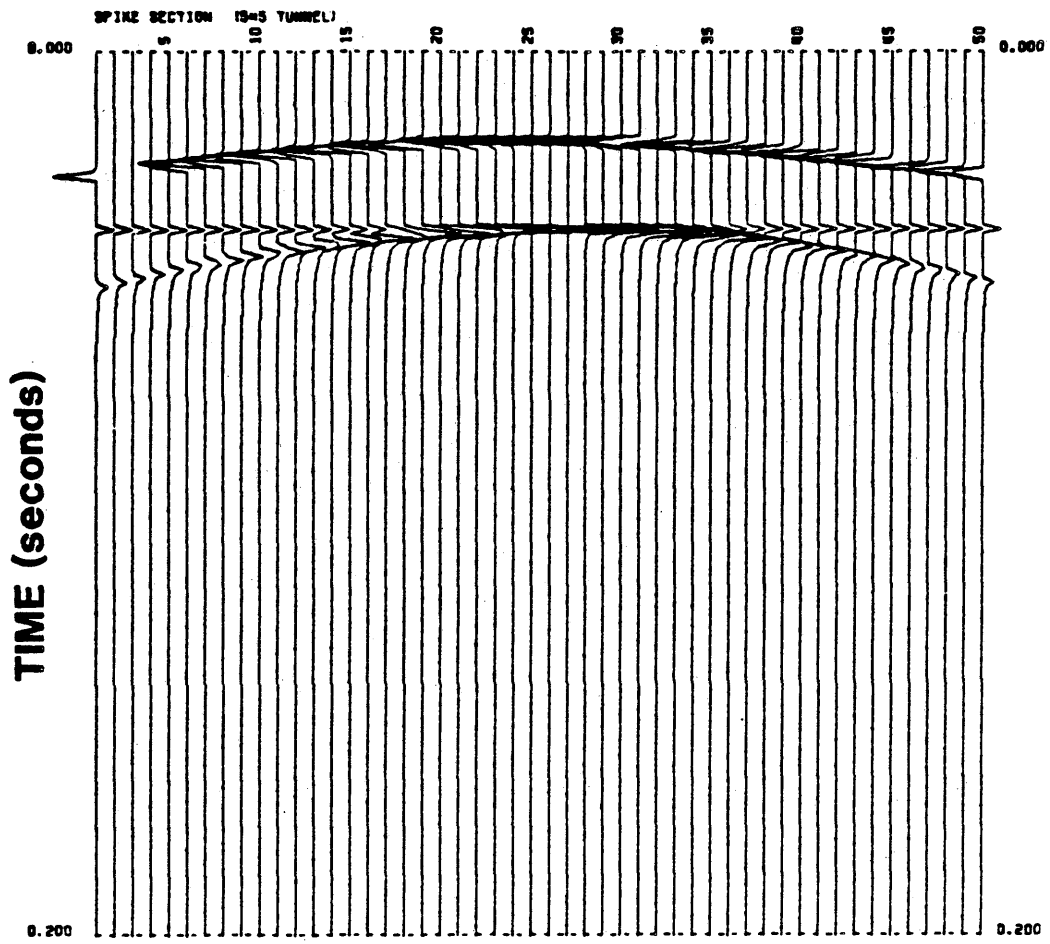


Figure 63. Ray-theory synthetic seismic spike section from tunnel model. Tunnel diameter is 5 meters. Horizontal axis represents trace numbers with 2-meter lateral separation.

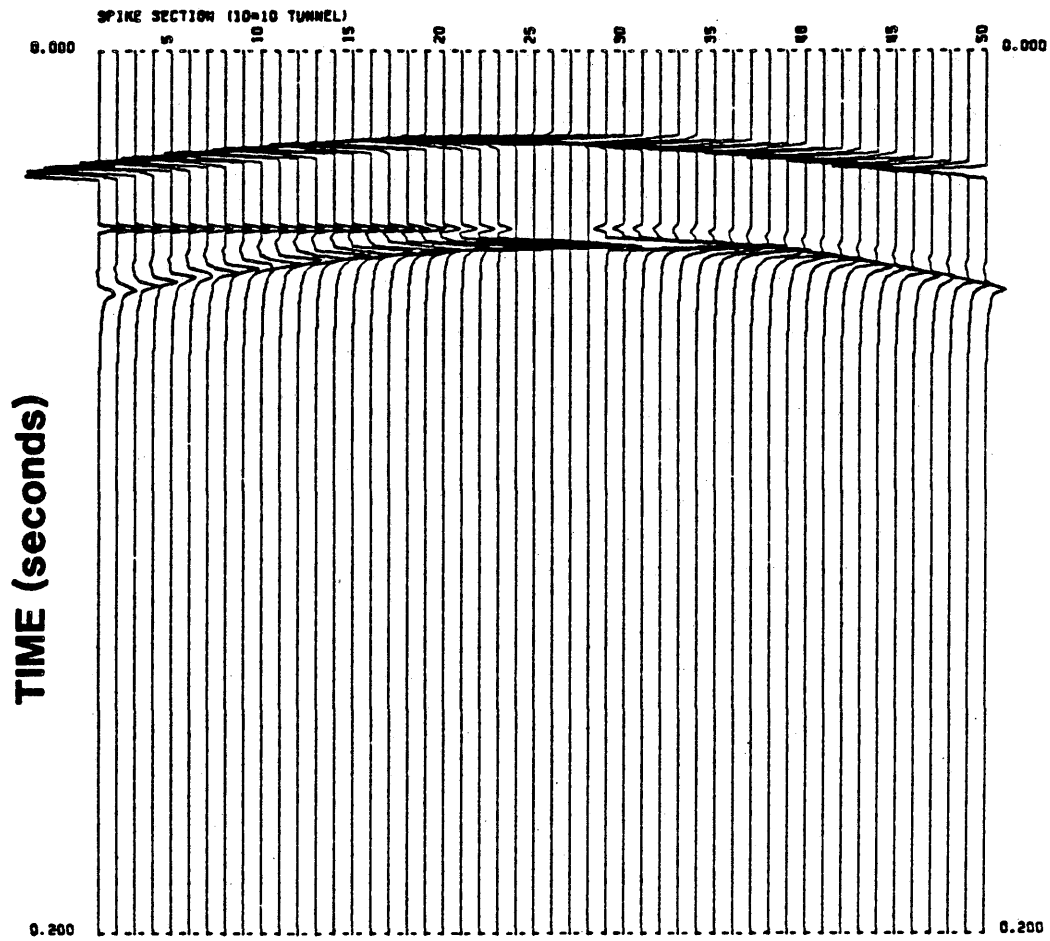


Figure 64. Ray-theory synthetic seismic spike section from tunnel model. Tunnel diameter is 10 meters. Horizontal axis represents trace numbers with 2-meter lateral separation.

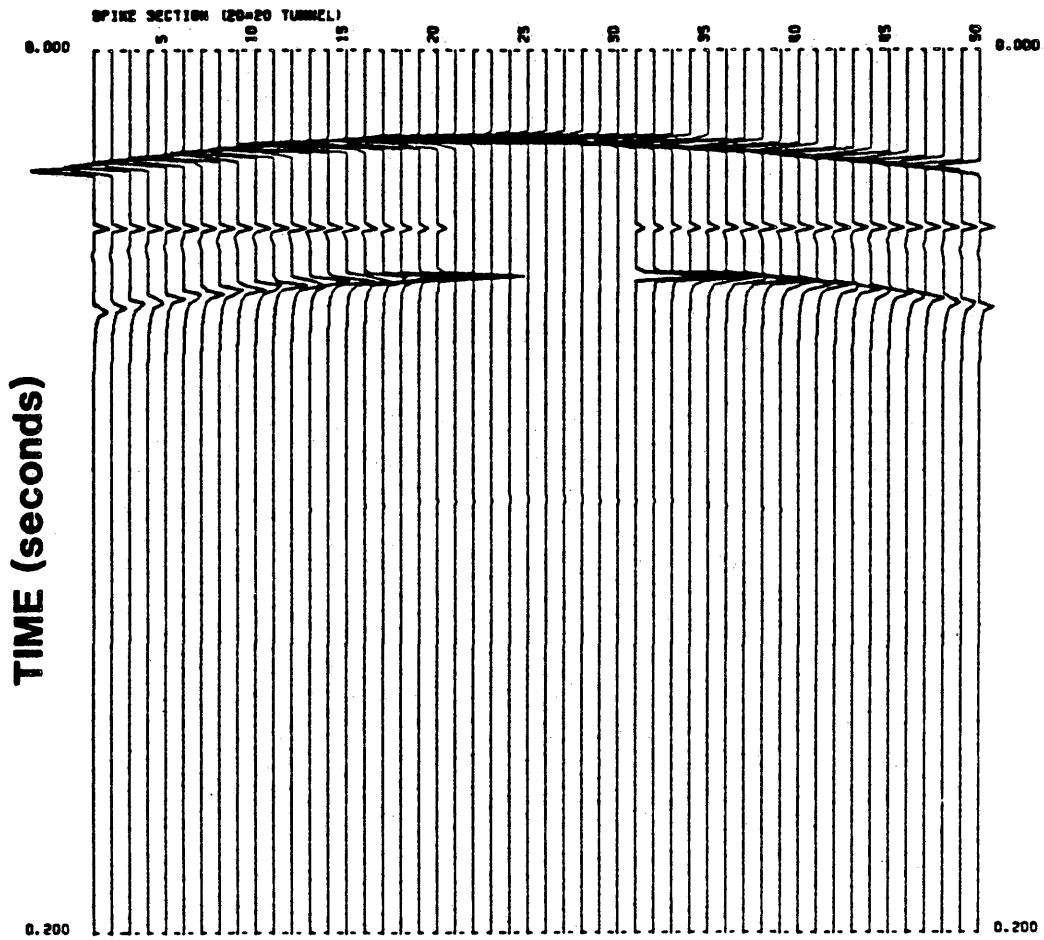


Figure 65. Ray-theory synthetic seismic spike section from tunnel model. Tunnel diameter is 20 meters. Horizontal axis represents trace numbers with 2-meter lateral separation.

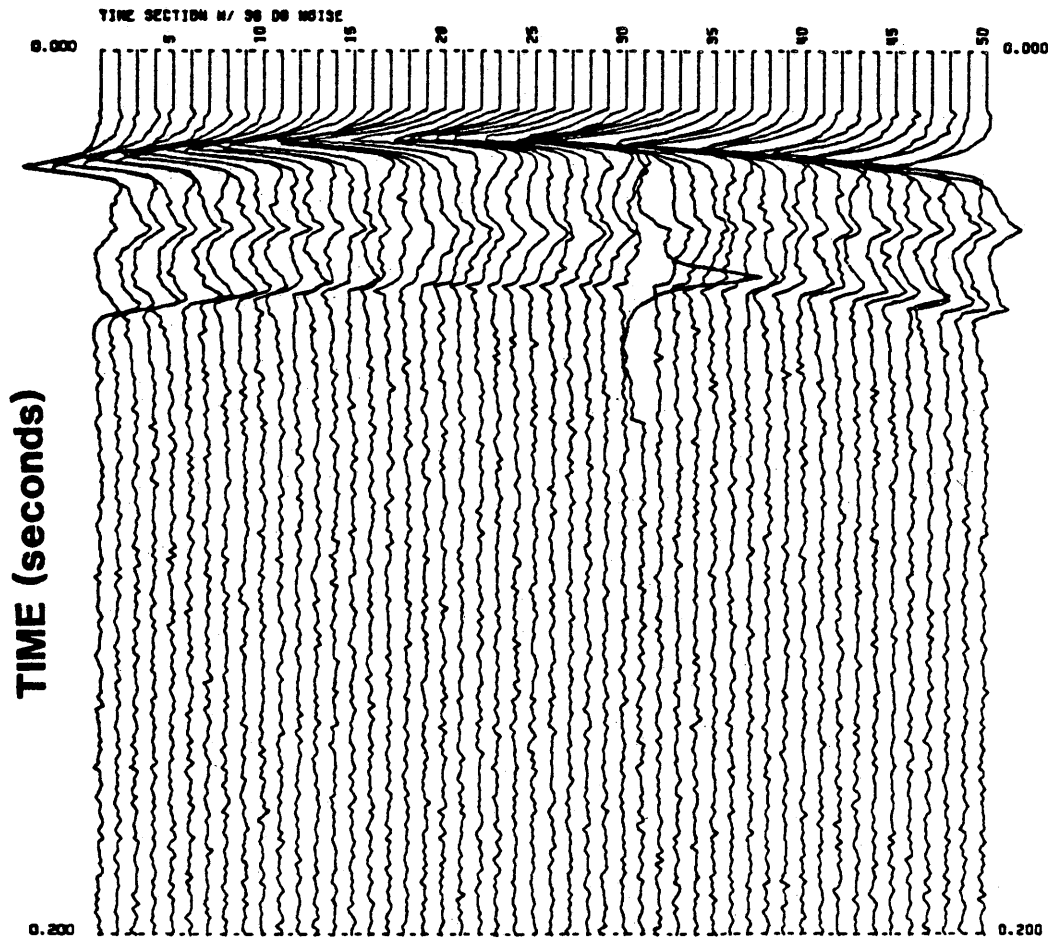


Figure 66. Wave-theory synthetic seismic section from tunnel model. 10 to 50 Hz zero-phase wavelet convolved with spike section. Tunnel diameter is 20 meters. Horizontal axis represents trace numbers with 2-meter lateral separation. Random noise introduced with RMS amplitude 36 dB lower than maximum signal amplitude.

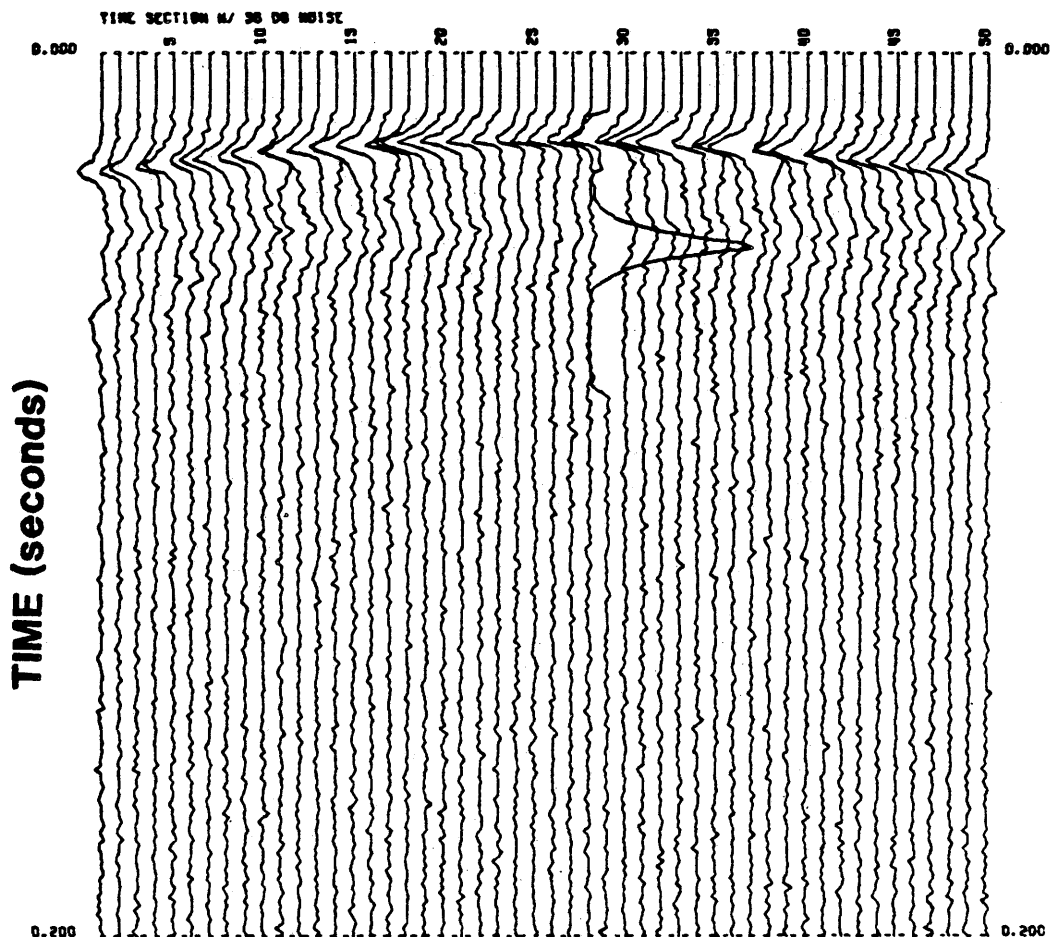


Figure 67. Wave-theory synthetic seismic section from tunnel model. 10 to 50 Hz zero-phase wavelet convolved with spike section. Tunnel diameter is 10 meters. Horizontal axis represents trace numbers with 2-meter lateral separation. Random noise introduced with RMS amplitude 36 dB lower than maximum signal amplitude.

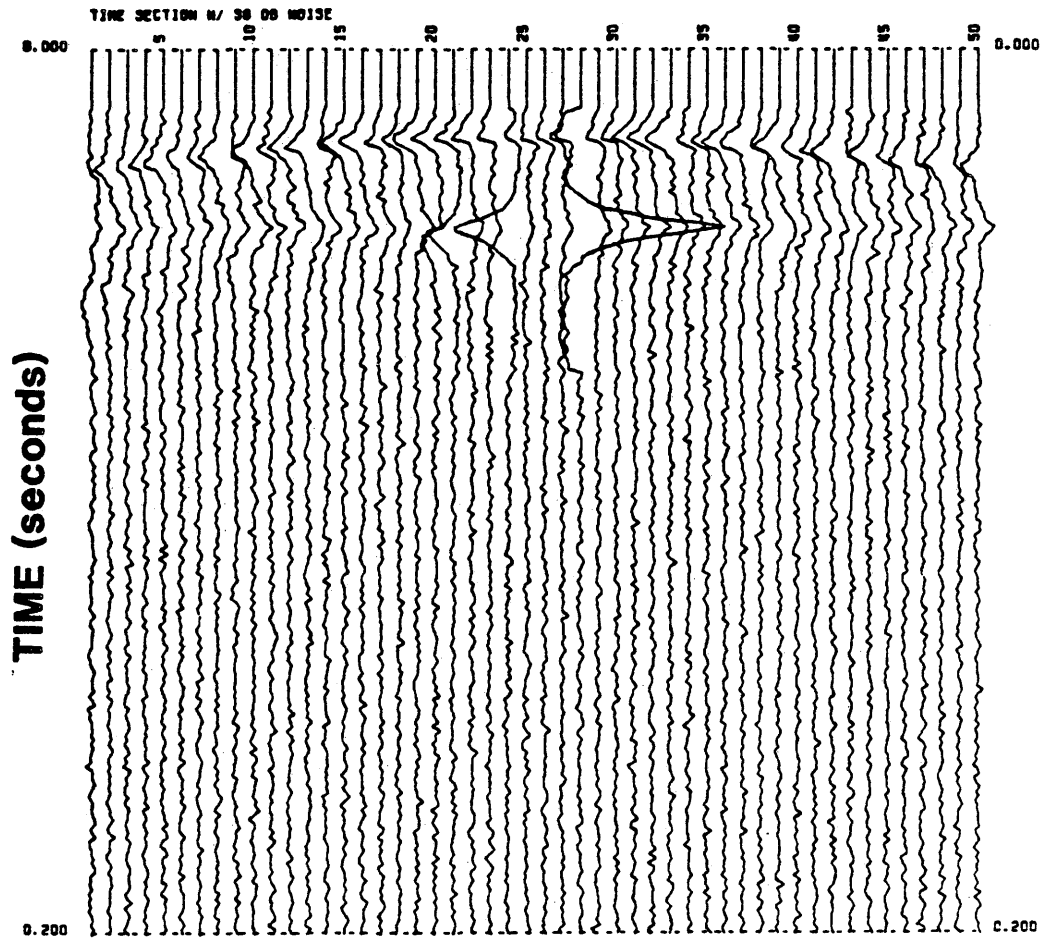


Figure 68. Wave-theory synthetic seismic section from tunnel model. 10 to 50 Hz zero-phase wavelet convolved with spike section. Tunnel diameter is 5 meters. Horizontal axis represents trace numbers with 2-meter lateral separation. Random noise introduced with RMS amplitude 36 dB lower than maximum signal amplitude.

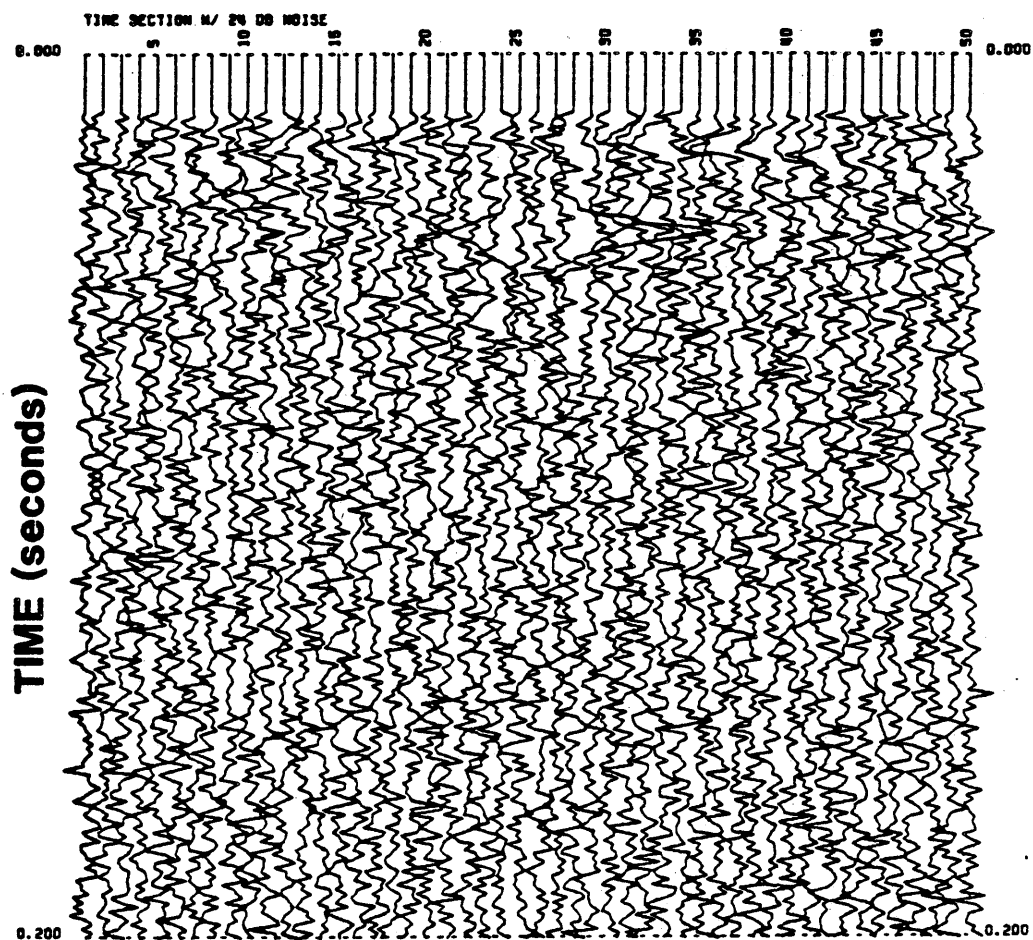


Figure 69. Wave-theory synthetic seismic section from tunnel model. 10 to 50 Hz zero-phase wavelet convolved with spike section. Tunnel diameter is 5 meters. Horizontal axis represents trace numbers with 2-meter lateral separation. Random noise introduced with RMS amplitude 24 dB lower than maximum signal amplitude.

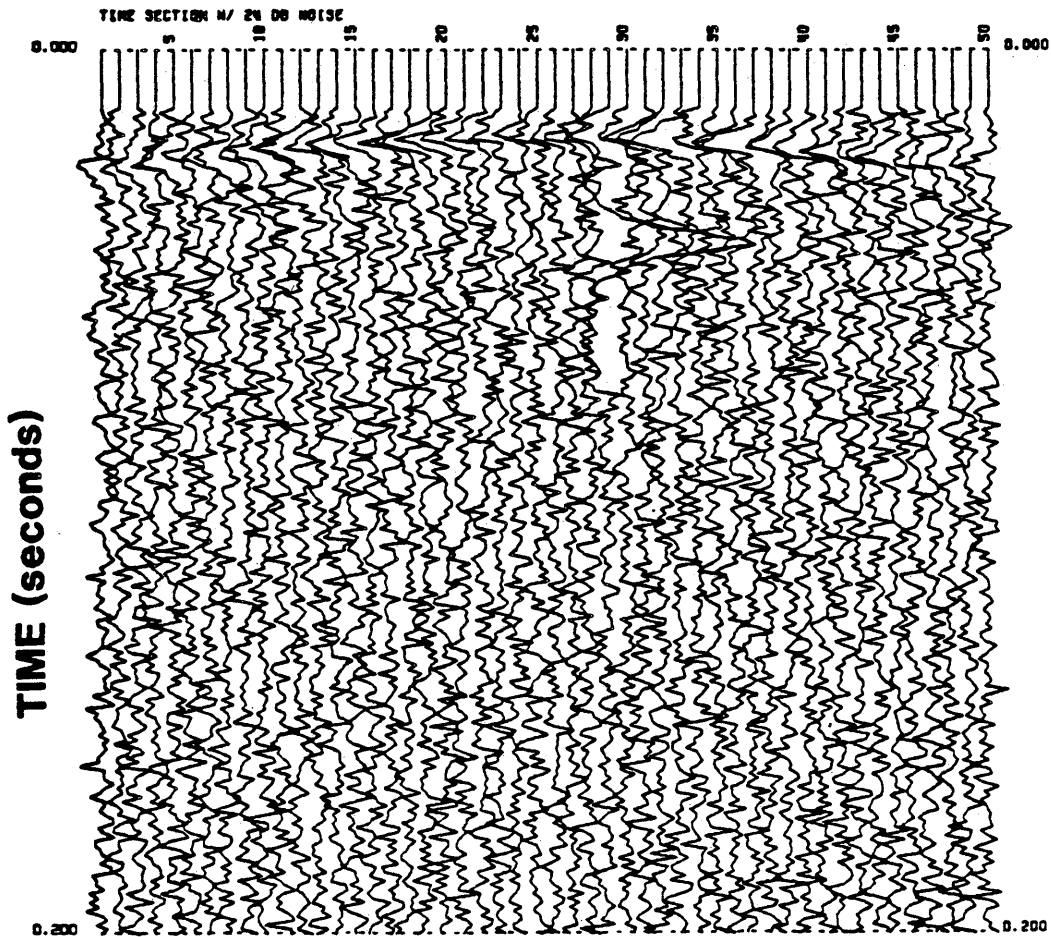


Figure 70. Wave-theory synthetic seismic section from tunnel model. 10 to 50 Hz zero-phase wavelet convolved with spike section. Tunnel diameter is 10 meters. Horizontal axis represents trace numbers with 2-meter lateral separation. Random noise introduced with RMS amplitude 24 dB lower than maximum signal amplitude.

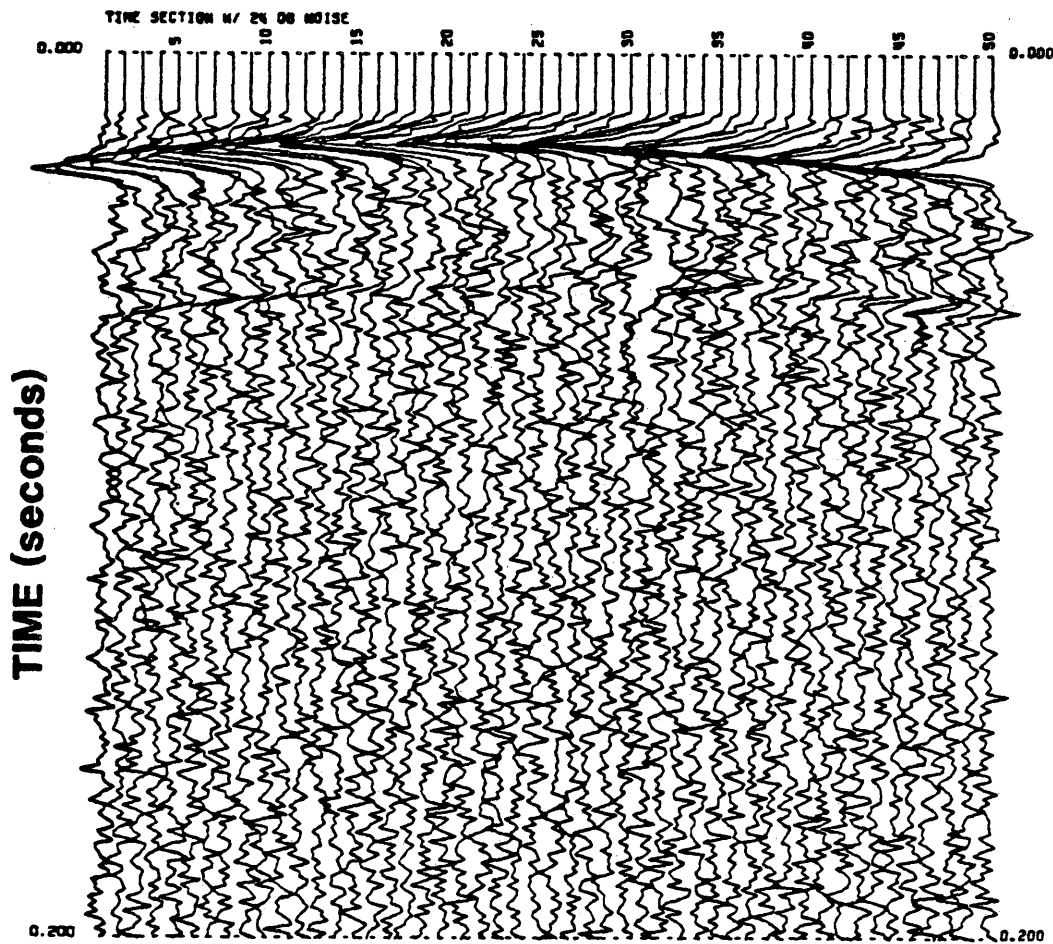


Figure 71. Wave-theory synthetic seismic section from tunnel model. 10 to 50 Hz zero-phase wavelet convolved with spike section. Tunnel diameter is 20 meters. Horizontal axis represents trace numbers with 2-meter lateral separation. Random noise introduced with RMS amplitude 24 dB lower than maximum signal amplitude.

If the random noise level is increased (-30 dB and -24 dB below signal level), the incoherent noise will distort the time section and decrease the resolution. A 5-by-5 meter tunnel will not be detectable with a noise -24 dB lower than the maximum signal amplitude (Fig. 69), whereas the 10-by-10 meter tunnel is still interpretable with this S/N ratio (Fig. 70). Therefore we may resolve a 5-by-5 meter tunnel in an ideal low-noise environment, even utilizing lower frequencies than Owen et.al. successfully used in field surveys (Owen et.al., 1976). A 20-by-20 meter tunnel gives a high-amplitude, coherent diffraction event that is easily distinguished even at this noise level (Fig. 71).

Note that the high amplitude artificial spikes at 40 ms are not a model response, rather software generated noise.

## CONCLUSIONS

Computer simulation of geophysical methods can be a very valuable tool in the effort to determine the resolution capabilities of different techniques. There are limitations, of course, since some of the phenomena which occur naturally can be difficult or impossible to model mathematically and computationally. In addition, although often far less expensive than field experiments, computer costs can be fairly high. Each EM-plot shown here, for example, represents some 10,000 system seconds and an approximate cost of 700 dollars.

For the tunnel-detection problem the borehole-to-borehole electromagnetic and the seismic reflection methods appear to be most effective for detecting deeper-lying structures, while gravity and magnetics give adequate resolution only for shallow features. All surface electrical methods, including electromagnetics, direct-current resistivity and magnetotellurics, show very weak response over a resistive body. Viewed on a continuum, the methods perform as follows:

## HIGHEST RESOLUTION

Crosshole EM

Reflection Seismic

DC Electrical

Surface Electromagnetics

Magnetics

Gravity

Magnetotellurics

LOWEST RESOLUTION

Of course, high-resolution techniques such as borehole-to-borehole electromagnetics exhibit relatively shallow penetration. Perhaps the best combination of tunnel-detection methods among the techniques modeled would be the seismic reflection method, the direct-current electrical method, and crosshole techniques (electromagnetics or acoustics). The combined use of these methods enhances target resolution because the anomalous body has simultaneous contrasts in two physical parameters (resistivity and velocity). Each single method employed shows a very weak anomaly but a combination of the individual responses would give a more reliable interpretation. Both magnetics and gravity shows response indicating better depth resolution than the electrical methods but, on the other hand, they

both lack in lateral resolution. A 5 meter diameter tunnel would be detectable at 50 meters depth for gravity, magnetics and reflection seismic. The direct-current electrical method and the electromagnetic method give a maximum detectable depth of only 5 to 10 meters without the use of signal enhancement techniques.

The vertical fracture zone detection problem might best be solved with electrical or magnetic methods, under the conditions stated in this work. The potential field methods have poor lateral resolution of deep seated features. Because of the extent of the target and the conductivity of the body compared to the host rock, the response of the electrical methods to the feature is much higher than for the tunnel. Ranging from highest resolution to lowest resolution for the vertical fracture zone model, the methods can be ordered as follows: EM--DC--MT--Magnetics--Gravity

The electromagnetic method has better resolution than the direct-current method for conductive features, although not immediately obvious from response curves due to shortcomings in programs and lack of trying all possible source placements.

The magnetic method shows a detectable depth of approximately 100 meters, but this does not take the limiting factor of lateral resolution into consideration.

The amplitudes of the responses for the horizontal fracture zone are high for all methods compared to those for the vertical feature. Only for zones of very limited lateral extent and at shallow depth can the amplitude response be interpreted as significant for resolution studies. Larger bodies at deeper locations show very broad response curves, and these could very easily be hidden in the regional trend or in low-spatial-frequency noise. The direct-current resistivity method shows the most favorable results when omitting the reflection seismic method (resolution of thin beds in seismic applications has been thoroughly treated by other authors). A one meter thick zone at 25 meters depth is detectable using the DC method, under the assumptions made.

A basement fault displays a similar broad anomaly as for the horizontal fracture zone. Because of the greater anomalous volume, the amplitudes of the response have increased. Also, in this case the direct-current method shows better results than electromagnetics, whereas gravity and magnetics are hampered by the lack of lateral resolution to higher degree. For a basement fault with 5 meters vertical displacement, the DC measurements indicate a detectable depth of approximately 50 meters without the use of signal enhancement techniques.

The geophysical method considered must have a measurable response which depends on target size, physical contrasts between target and surrounding material, and background noise. To summarize the resolving capabilities of the geophysical methods as indicated by computer modeling, the following can be stated:

The magnetic method, under good conditions, has adequate resolution for shallow targets. For deeper-lying features, magnetic anomalies become too broad to give good lateral resolution. This is the case for the gravity method as well.

DC resistivity and EM techniques both give fairly low amplitude response to the resistive bodies modeled.

Crosshole EM has the best resolution, as expected, but the attenuation of the very-high-frequency signal makes it usable only for targets close to the boreholes, and the cost of drilling boreholes must be considered. Crosshole acoustic measurements would also provide relatively high resolution.

The seismic method's resolution capability could not be clearly defined by the exploration software utilized. There is a need for special purpose modeling programs and field techniques for engineering applications. Perhaps the seismic reflection method represents the best compromise

between resolution and penetration, but a non-standard approach might be more effective than simply scaling-down the oil-exploration techniques. Future seismic modeling of small engineering targets should possibly focus on the information that is contained in the scattered and diffracted components of a broadband seismic signal. This would thereby allow lower frequencies with better penetration (and easier field procedure) to be utilized.

Synthetic magnetotelluric data show very low resolution potential.

It should be emphasized that almost all conditions and surveys are site-specific, and therefore these results should be seen as: 1) indications of general trends, and 2) demonstrations of the capabilities of modeling. It is also important to remember that a homogeneous and isotropic host medium was used, and that anisotropy would reduce resolution.

Finally, the modeling study illustrates the enhancement of interpretative insight which can result from the analysis of several different geophysical data sets for a single problem.

## REFERENCES

- Arzi, A.A., 1975, Microgravimetry for engineering applications: Geophysical Prospecting, vol. 23, no. 3, pp. 408-425.
- Cady, J.W., 1977, Calculation of gravity and magnetic anomalies along profiles with end corrections and inverse solutions for density and magnetization: USGS Open File Report 77-463, p. 101.
- Cook, J.G., 1965, Seismic mapping of underground cavities using reflection amplitude: Geophysics, vol. 30, no. 4, pp. 527-538.
- Dobrin, M.B., 1976, Introduction to geophysical prospecting ; New York, McGraw-Hill, p. 630.
- Farr, J.B., 1979, Seismic wave attenuation and rock properties: in C.H. Dowding editor, (Proceedings) Site Characterization and Exploration Workshop, American Society of Civil Engineers, pp. 302-320, New York, New York.
- Gay, S.P., 1963, Standard curves for interpretation of magnetic anomalies over long tabular bodies: Geophysics, vol. 28, no. 2, pp. 161-200.
- GeoQuest, 1979, Advanced Interpretation Modeling System (AIMS) users reference manual: GeoQuest International Inc., Houston, Texas.
- Gupta, V.K. and Fitzpatrick M.M., 1971, Evaluation of terrain effects in magnetic surveys: Geophysics, vol. 36, no. 3, pp. 582-589.
- Keller, G.V., 1979, Resistivity surveys and engineering problems: in Geophysical Methods in Geotechnical Engineering, American Society of Civil Engineers, Preprint 3794, pp. 1-50, New York, New York.
- LaFehr, T.R., 1980, History of geophysical exploration--Gravity method: Geophysics, vol. 45, no. 11, pp. 1634-1639.

- LaFehr, T.R., 1979, Gravity and magnetic methods: Paper held at American Society of Civil Engineers Convention, Atlanta, October 23-25, 1979, p.22.
- Langan, L., 1966, A survey of high resolution geomagnetics: Geophysical Prospecting, vol. 14, no. 4, pp. 487-503.
- Lytle, R.J., 1979, Geophysical characterization using advanced data processing: in C.H. Dowding, (Proceedings) Site Characterization and Exploration Workshop, American Society of Civil Engineers, pp. 291-300, New York, New York.
- Lytle, R.J., Laine E.F., Lager D.L., and Davis D.T., 1979, Cross-borehole electromagnetic probing to locate high-contrast anomalies: Geophysics, vol. 44, no. 10, pp. 1667-1676.
- McCann, D.M., Grainger P. and McCann C., 1975, Inter-borehole acoustic measurements and their use in engineering geology: Geophysical Prospecting, vol. 23, no. 1, pp. 50-69.
- McDonal, F.J., Angona F.A., Mills R.L., Sengbush R.L., Van Nostrand R.G. and White J.E., 1958, Attenuation of shear and compressional waves in Pierre Shale: Geophysics, vol. 23, no. 3, pp. 421-439.
- Nettleton, L.L., 1971, Elementary gravity and magnetics for geologists and seismologists: SEG Monograph series, no. 1, Tulsa, Oklahoma.
- O'Doherty, R.F. and Anstey N.A., 1971, Reflections on amplitudes: Geophysical Prospecting, vol. 19, no. 3, pp. 430-458.
- Ogunade, S.O. and Dosso H.W., 1980, The inductive response of a horizontal conducting cylinder buried in a uniform earth for a uniform inducing field: Geophysical Prospecting, vol. 28, no. 4, pp. 601-609.
- Owen, T.E. and Darilek G.T., 1976, High-resolution seismic reflection measurements for tunnel detection: Southwest Research Institute, Interim Technical Report, SwRI Project 14-4579, San Antonio, Texas, p. 65.
- Parasnis, D.S., 1973, Mining geophysics: Elsevier, Amsterdam, p. 395.

- Peters, L.J., and Bardeen J., 1932, Electrical prospecting in oil-fields: Physics, vol. 2, March 1932, pp. 103-122.
- Reford, M.S., 1980, History of geophysical exploration - Magnetic method: Geophysics, vol. 45, no. 11, pp. 1640-1658.
- Rodi, W.L., 1976, A technique for improving the accuracy of finite element solutions for magnetotelluric data: Geophys. J. R. astr. Soc., vol. 44, pp. 483-506.
- Scherman, S., 1978, Forarbeten for platsVal, berggrunds undersokningar: Karnbranslesakerhet Technical Report (in Swedish), vol. 60, Swedish Geological Survey, Stockholm, Sweden, p. 300.
- Sheriff, R.E., 1977, Limitations on resolution of seismic reflections and geologic detail derived from them: in Seismic Stratigraphy, American Association of Petroleum Geologists memoir no. 26, pp. 3-14, Tulsa, Oklahoma.
- Shuey, R.T. and Pasquale A.S., 1973, End corrections in magnetic profile interpretation: Geophysics, vol. 38, no. 3, pp. 362-371.
- Spiegel, R.J., Sturdivant V.R. and Owen T.E., 1980, Modeling resistivity anomalies from localized voids under irregular terrain: Geophysics, vol. 45, no. 7, pp. 1164-1183.
- Stoyer, C.H., Geoelectricity and geoelectromagnetics: Elsevier, Amsterdam, Holland, in press.
- Stoyer, C.H., 1974, Numerical solutions of the response of a two-dimensional earth to an oscillating magnetic dipole source with application to a groundwater field study: Ph. D. Thesis, Pennsylvania State University, p. 195.
- Stoyer, C.H. and Greenfield R.J., 1976, Numerical solutions of the response of a two-dimensional earth to an oscillating magnetic dipole source: Geophysics, vol. 41, no. 3, pp. 519-530.
- Talwani, M., Worzel J.L., and Landisman M., 1959, Rapid gravity computations for two-dimensional bodies with application to the Mendocino submarine fracture zone: J. of Geophysical Research, vol. 64, no. 64, pp. 49-60.

- Talwani, M. and Ewing M., 1960, Rapid computation of gravitational attraction of three-dimensional bodies of arbitrary shape: Geophysics, vol. 25, no. 1, pp. 203-225.
- Telford, W.M., Geldart L.P., Sheriff R.E. and Keys D.A., 1976, Applied Geophysics: Cambridge University Press, Cambridge, England, p. 860.
- Trorey, A.W., 1962, Theoretical seismograms with frequency and depth dependent absorption:/ Geophysics, vol. 27, no. 6, pp. 766-785.
- Tullos, F.N. and Reid A.C., 1969, Seismic attenuation of gulf coast sediments: Geophysics, vol. 34, no. 4, pp. 516-528.
- Widess, M.B., 1973, How thin is a thin bed?: Geophysics, vol. 38, no. 6, pp. 1176-1180.
- Zietz, I. and Pakisar L.C., 1957, Note on an application of sonar to the shallow reflection problem: Geophysics, vol. 22, no. 2, pp. 345-347.